AD NUMBER

AD873386

LIMITATION CHANGES

TO:

Approved for public release; distribution is unlimited.

FROM:

Distribution authorized to U.S. Gov't. agencies and their contractors; Critical Technology; JUL 1970. Other requests shall be referred to Air Force Materials Laboratory Wright-Patterson AFB, OH 45433. This document contains export-controlled technical data.

AUTHORITY

AFML ltr, 7 Dec 1972

AFML-TR-66-310
PART IV
VOLUME III

INTEGRATED RESEARCH ON CARBON COMPOSITE MATERIALS

VOLUME III
STRUCTURAL COMPONENT DEVELOPMENT

UNION CARBIDE CORPORATION
CARBON PRODUCTS DIVISION
-IN ASSOCIATION WITH-
CASE WESTERN RESERVE UNIVERSITY
BELL AEROSYSTEMS COMPANY, A TEXTRON COMPANY

PROGRAM SUPERVISORS

H.F. VOLK
H.R. NARA
D.P. HANLEY

TECHNICAL REPORT AFML-TR-66-310, PART IV, VOLUME III

JULY 1970

AIR FORCE MATERIALS LABORATORY
AIR FORCE SYSTEMS COMMAND
WRIGHT-PATTERSON AIR FORCE BASE, OHIO

NOTICES

When Government drawings, specifications, or other data are used for any purpose other than in connection with a definitely related Government procurement operation, the United States Government thereby incurs no responsibility nor any obligation whatsoever; and the fact that the Government may have formulated, furnished, or in any way supplied the said drawings, specifications or other data, is not to be regarded by implication or otherwise as in any manner licensing the holder or any other person or corporation, or conveying any rights or permission to manufacture, use, or sell any patented invention that may in any way be related thereto.

This document is subject to special export controls and each transmittal to foreign Governments or foreign Nationals may be made only with prior approval of the Nonmetallic Materials Division, MAN, Air Force Materials Laboratory, Wright-Patterson Air Force Base, Ohio 45433.

Copies of this report should not be returned unless return is required by security considerations, contractual obligations or notice on a specific document.

INTEGRATED RESEARCH ON CARBON COMPOSITE MATERIALS

Summary Technical Report

AFML-TR-66-310, Part IV

Volume III

Structural Component Development

Program Supervisors

H. F. Volk
H. R. Nara
D. P. Hanley

July 1970

FOREWORD

The work reported herein was performed under the sponsorship of the Advanced Research Projects Agency, Department of Defense, through a contract with the Air Force Materials Laboratory (MAN) AFSC, Wright-Patterson Air Force Base, Ohio, Contract No. AF 33(615)-3110, ARPA Order No. 719, Program Code No. 6D10. Mr. H. S. Schwartz (MAN) is the Air Force Program Manager.

The prime contractor is Union Carbide Corporation, Carbon Products Division; the subcontractors are Case Western Reserve University and Bell Aerosystems Company, a Textron Company. At the beginning of this reporting period, the program was administered by a committee composed of: J. C. Bowman (Chairman) and G. B. Spence (Program Supervisor) from Union Carbide; R. H. Thomas and L. A. Schmit (Program Supervisor) from Case Western Reserve University; and W. H. Dukes and F. M. Anthony (Program Supervisor) from Bell Aerosystems Company. During this reporting period, the Program Supervisors were changed to H. F. Volk (Union Carbide); H. R. Nara and T. P. Kicher, Associate Program Supervisor (Case Western Reserve University); and D. P. Hanley (Bell Aerosystems Company). Technical personnel participating in the program are indicated as authors of their portions of the report. The report was submitted by the authors May 1970.

This is Part IV of the report and covers work performed from July 1968 to June 1969. It is issued in three volumes. Volume I covers materials research; Volume II, structural mechanics; and Volume III, structural component development.

This technical report has been reviewed and is approved.

A. M. Lovelace
Director
Air Force Materials Laboratory

ABSTRACT

The final design of the representative fuselage component was determined, and the component was fabricated with treated "Thornel" 50 graphite-fiber, ERL 2256 epoxy matrix composites. The structure consists of a tapered cylindrical skin, 48 inches long with end diameters of 24 inches and 20 inches; the fiber lay-up orientation of the skin is (90°, ±15°, 90°). The skin is stiffened by 31 longitudinal stringers having (+10°, -10°, -10°, +10°) fiber orientation and by three segmented ring stiffeners consisting of a balsa wood core reinforced with panels of (0°, ±45°) orientation. The fuselage component structure was analyzed by the discrete element method; stresses, displacements, and margin of safety predictions were obtained for various loading conditions. Prior to component fabrication, several treated "Thornel" 50 panels were fabricated and tested in tension and compression; failure levels were well above design requirements. The 90° layers of the skin were constructed by wet-winding and the inner 15° layers by hand lay-up of pre-pregged sheet. The stringers and the ring stiffener panels were molded from pre-pregged sheet. Stringers and the ring stiffener panels were adhesively bonded to the component skin. Both ends of the component were reinforced with a lay-up of fiberglass tape and bonded to segmented aluminum rings for attachment of the component to the test stand. The NDT inspection of the component revealed defects consisting primarily of partial debonding of the stringers and ring-stiffeners from the skin. Extensive analysis indicated that the debonding very likely resulted from thermal degradation of the adhesive and from thermal stresses incurred during the final cure of the end attachments. Novel repair techniques for composite structures were established, and the component was successfully repaired. Detailed plans for the various response tests and the final destruct test of the component are also presented.

BLANK PAGE

TABLE OF CONTENTS

TABLE OF CONTENTS (Cont'd.)

TABLE OF CONTENTS (Cont'd.)

LIST OF ILLUSTRATIONS

LIST OF ILLUSTRATIONS (Cont'd.)

LIST OF ILLUSTRATIONS (Con't.)

LIST OF TABLES

LIST OF TABLES (Cont'd.)

LIST OF TABLES (Cont'd.)

SECTION I

INTRODUCTION

This report covers the fourth year's work of a program which represents a novel approach designed to fulfill three different, but clearly interdependent, needs of the Department of Defense: a materials need, a structural design capability need, and a need for more scientists and engineers trained in applied materials problems and advanced design methods. The Carbon Products Division of Union Carbide Corporation, Case Western Reserve University, and Bell Aerosystems Company have formed an Association to meet these needs.

The Association has formulated a broad program which includes the development of new materials, generation of advanced analyses and design methods, and education of graduate students. In brief, the major objectives are (1) to develop high modulus graphite fiber composites, (2) to extend the methods of structural mechanics, (3) to identify DOD applications toward which the program efforts should be directed, (4) to educate engineers capable of developing and using modern materials, and (5) to integrate materials research with the needs of the designer by extending the technique of structural synthesis to include material variables.

The primary responsibilities of Union Carbide Corporation, Carbon Products Division, are the development and production of composite materials and the measurement of those mechanical and thermal properties needed for the structural design work within the Association. The technical program at Union Carbide consists of: (1) materials research, a basic research program to develop new, improved composites of high modulus graphite fibers in both resin and metal matrices; (2) materials fabrication, an applied research program to produce materials for the joint research programs of the Association and to seek new ways of fabricating components which better utilize the superior properties of composite materials; (3) properties evaluation, the measurement of the mechanical and thermal properties of certain composites to provide data for the joint research programs of the Association; and (4) failure criteria, a basic research program to determine experimentally adequate failure criteria for anisotropic materials under multiaxial stress states and to find ways of representing the failure surface which can be used by the designer in practical calculation.

The work at Case Western Reserve University has two major objectives. The first objective is to advance the basic structural mechanics technology required for rational design with composite materials. Composite materials offer the structural

design engineer the prospect of being able ultimately to carry on simultaneously the design of the structural configuration and the material. Achieving this capability will require fundamental advances in structural synthesis as well as a substantially improved understanding of the behavior of composite materials. The goals of the structural mechanics research program at Case are (1) the quantitative formulation and efficient solution of the structural synthesis problem, including material variables, for elementary, but representative components fabricated from composite materials; (2) experimental stress analysis studies and theoretical investigations in micromechanics with the objective of improving the measurement and calculation of stiffness properties and failure mode criteria for composite materials; and (3) the development of improved analysis methods for anisotropic, nonlinear, and nonconservative materials. The second objective of the work at Case Western Reserve University is to develop new or improved graphite fiber-resin composites through materials research. At present, the knowledge of fiber surface morphology and the relation between fiber surface characteristics and interfacial adhesion to the resin system(s) is incomplete. A better understanding of these interfacial interactions will lead to improvements in presently used fiber resin composites and will ultimately permit the judicious selection of new resins and new fabrication methods, thus leading to a second generation of advanced composites. The materials research work at Case Western Reserve University has been initiated during the second half of the report period. The present report covers the program plans and some initial results.

The primary purposes of Bell Aerosystems Company's participation in this program are to interject user requirements into the applied materials research efforts; to apply, at the prototype design level, the advanced analytical procedures and improved understanding of material behavior which will result from the research; and to establish application-related property specifications for materials research activities. To attain these objectives, a six-part technical program is being performed by Bell: (1) application selection, the objective of which is to define representative configurations and environmental conditions which reflect DOD requirements; (2) recognition of failure modes, a task which involves the overall structural behavior such as elastic instability, deformation limits, and fracture and the material failure modes; (3) determination of the nature of and methods for the application of analytical tools needed to cope with the anisotropic, anelastic, and nonconservative material property behavior and the multiaxial stress distributions anticipated in structural configurations associated with the use of the subject materials; (4) structural synthesis, a task which involves the application of structural synthesis techniques at the practical level to define the most desirable material compositions within a

particular class of composites; (5) study of creative design concepts which will be required because of the complex material behavior of composites; (6) testing to verify the value of analysis procedures used to design composite materials and the components made from composite materials.

In contrast to the previous three Annual Reports,[1,2,3] which consisted of single volumes, the present report has been divided into three volumes. Volume I covers the effort on materials research; Volume II covers the work on structural mechanics, analysis, and optimization; and Volume III covers the design, fabrication, and testing of a representative subscale fuselage component. This division was made because particular projects might be of interest to a particular audience; this arrangement also made possible the reduction of the physical size of each volume. However, this introduction and the following Summary (Section II) are common to each volume.

SECTION II

SUMMARY

The activities of the Association formed by Union Carbide Corporation, Case Western Reserve University, and Bell Aerosystems Company are directed toward designing, fabricating, and evaluating a representative composite fuselage component; investigating selected critical problem areas in advanced composite technology; and involving students in an important new technology. The component activity serves as a hardware performance demonstration and also serves to reveal new, or to emphasize suspected, technological shortcomings. Investigations of these shortcomings and of other problems which clearly must be solved for the next generation of advanced composite applications form the basic, long range studies. Through knowledge of the total program and by participation in specific projects, the graduate students gain skill in advanced composite technology and become better informed concerning the nature of industrial research and development.

The experimental and theoretical work presented in this report covers materials research in the following areas: graphite fiber reinforced resin-matrix and metal-matrix composites, physical properties and design data studies of fiber composites, the mechanics of fiber composites, advanced analysis and synthesis, and fabrication and testing of a representative fuselage component. Although these projects are clearly related in their common objective of advancing the state of the art of composite materials, the diversity and physical volume of this work made it desirable to present the report in three volumes. Volume I covers materials research on graphite fiber, resin-matrix and metal-matrix composites; Volume II is concerned with the structural mechanics of composite materials; and Volume III covers the structural development of a representative, subscale fuselage component. The following paragraphs summarize the contents of each of the three volumes.

Volume I: Materials Research

Techniques were developed to study the interfacial region between fiber and resin in composite materials. The tools used were electron microscopy, electron diffraction, and laser excited Raman spectroscopy. The electron microscope was used in the study of epitaxial growth of polyethylene on graphite fiber surfaces (cleaned with boiling water) and on the 001 planes of graphite single crystallites. Electron diffraction results indicate that the crystals grown on the graphite single crystal surfaces are oriented so that the molecules stand upright on the substrate. A microsampling technique was developed for the Raman spectroscopy studies. By this technique, spectra of graphite fibers and graphite single crystals

could be obtained and compared. The spectra show bands at 1580 cm^{-1} and 1355 cm^{-1}. The relative intensity of the two bands is different for the various graphite samples, allowing differentiation among fibers of different origin. The spectra can be correlated with the presence of more or less graphitized surfaces.

Graphite-fiber, resin-matrix composites were prepared by *in situ* polymerization of ε-caprolactam (the monomer of nylon 6) on "Thornel" 25 fibers (cleaned with boiling water). The kinetics of this anionic polymerization of caprolactam, in which various latent catalysts were used, were investigated. With a number of catalysts, the presence or absence of water in the monomer was found to affect the catalysis of polymerization. However, since diethyl carbonate was found to catalyze the polymerization under both wet and dry conditions, this latent catalyst was used for the preparation of composites. These composites were examined by X-ray diffraction and electron microscopy. The examination showed the complete absence of voids and confirmed the original hypothesis that *in situ* polymerization would lead to greater wetting of the fibers by the polymer than that which resulted from using conventional methods and would therefore yield void-free composites.

The oriented crystallization and subsequent oriented solid state reaction of the monomers of nylon 66 (hexamethylene-diammonium adipate) and nylon 6 (6-aminocaproic acid) on "Thornel" 40 carbon fibers have been investigated. The reaction of these monomers, epitaxially crystallized on the carbon fiber substrate, yields cyclic dimer and cyclic trimer, respectively, whereas reaction in the absence of substrate under otherwise identical conditions yields the respective polymers. The strong and specific effect of surface interactions on these solid state reactions is clearly demonstrated. *In situ* polymerization of these cyclic materials and other monomers is being investigated.

Sophisticated equipment has been constructed to characterize the graphite fiber surfaces by measurements of adsorption from the gas phase and from solution. A highly sensitive balance capable of detecting a weight change of 1×10^{-6} grams in a 1-gram sample was designed and constructed for use in this study.

Graphite-fiber, nickel-matrix composites were fabricated by electrodepositing nickel uniformly around each filament and hot-pressing the precoated, prealigned filaments into fully densified composites. Previously, fabrication of large test specimens was limited by the relatively slow electrodeposition process. This problem was partially rectified by construction of equipment which can electrodeposit nickel continuously on two untwisted plies of "Thornel" yarn. Higher deposition rates were also obtained by applying current simultaneously to both ends of the yarn as it

enters and leaves the plating bath, but the nickel distribution was not uniform. The most uniform deposition of nickel around the filaments is achieved if cathodic contact is employed only at the entrance roller. The fabrication of larger specimens was extended to include uniaxial test bars up to three inches long and orthogonal plates up to three inches square. Short sections of tape approximately 0.010 inch thick were also prepared and will be used for further fabrication into laminates of complex geometry and configuration. A problem of adherence between the graphite mold surface and the tape after hot-pressing was overcome by using boron nitride at the interface. Three-inch square tape prepared by this process showed minor delaminations parallel to the fibers. Studies of the influence of fabrication variables (pressure, temperature, and time) on properties of the composite were extended to include 1250°C as a fabrication temperature. The average tensile strength (89,400 psi) and Young's modulus (33.6×10^6 psi) are consistent with previously established trends. The fiber morphology showed only slight change.

The elastic properties of unidirectional graphite-fiber, nickel-matrix composites were obtained by static, sonic, and ultrasonic methods. The values derived from each of these methods are in reasonable agreement. Experimental values of Young's modulus, shear modulus, and Poisson's ratio were correlated with predictions based on Whitney's micromechanics model for orthotropic filaments. All measured elastic properties, with the exception of the transverse modulus, can be reconciled with predicted values based on fiber and matrix properties. Stress-strain data were obtained on unidirectional specimens with fibers oriented at various angles to the tensile axis. Strain at failure when the fibers are parallel to the test axis is 0.4 percent. Deformation is considerably greater at slight angles ($\sim$15°) and much less at the highest test angles (>45°). Composites with 45 percent fibers are characterized by a sharply defined yield point at 12,000 psi and a secondary modulus. The secondary modulus is stress dependent. If the matrix contribution to the secondary modulus is assumed to be zero, the fiber modulus corresponds to 36.5×10^6 psi at low stresses, a value which gradually increases to 45×10^6 psi at 160,000 psi stress. The composite modulus in compression is 28.7×10^6 psi, appreciably less than the tensile modulus of 32.2×10^6 psi. Failure in compression occurs at 96,000 psi. The constituent behavior during a strain cycle experiment was analyzed from the known tensile and compression stress-strain curves. The linear thermal expansion was measured between room temperature and 1000°C and found to be 0.5×10^6/°C and 20×10^6/°C in the longitudinal and transverse directions, respectively. The composite is highly anisotropic and the thermal expansion is controlled by the thermal behavior of the graphite fiber. Cyclic behavior and plastic deformation of the matrix were also studied. Orthogonal laminates with 3-, 5-, and 7-ply configurations with orientations of 0°, 45°, and 90° were tested in tension to obtain the static modulus, stress-strain behavior, and

ultimate tensile strength. These properties correlated well with predictions based on uniaxial properties. This correlation indicates that, to a first approximation, microcracks caused by thermal expansion differences of the laminate layers do not decrease the composite strength and modulus properties. Attempts were made to correlate the tensile strength values obtained on three-inch long test specimens with data measured previously on one-inch bars. The three-inch specimens, either dog-boned or of the IITRI type, failed outside the gage section.

Volume II. Structural Mechanics

A finite element displacement analysis computer capability for the microstress analysis of fibrous composites has been developed. A specialized finite element containing a circular fiber in a finite elastic matrix is used as the basic analysis block. Several test cases have been examined to assess the accuracy of the capability.

The investigation of stress and strain concentration factors due to inclusions of various shapes in a physically nonlinear matrix has been continued. Emphasis was placed on developing a method, that may be extended to nonlinear solids, for solving linearly elastic inclusion problems. Some success has been achieved in this respect. The general solution of the elastic curvilinear inclusion problem has been found in the case of antiplane, or transverse, shear deformation. In the case of plane deformation, only the general functional form of solution for rigid curvilinear inclusion and cavity has been found.

The experimental methods and techniques necessary to study the plane strain fracture toughness of fiber composites as related to the void content have been developed. The effect of the width of the specimen on the fracture toughness has been determined. Work was also done in studying microscopically the effect of voids on the fracture of composites.

Examination of the fracture surfaces of cross-plied "Thornel" fiber tensile specimens provided indications for the fracture mechanism, which also accounts for the effect of specimen width on the tensile strength. Results of creep studies on unidirectional composites indicated that the matrix was in the plastic region for a significant period of time before failure.

The stress-strain behavior and fracture strength under uniaxial, torsional, and combined stresses have been determined for "Thornel" 50 graphite fiber, epoxy-matrix composites. The combined-stress tests were conducted on four-ply (orthogonal) hollow cylinders. Torsional properties were measured on both orthogonal and on uniaxial (hoop-wound) cylinders. Uniaxial tensile and compressive strengths

were determined on orthogonal plates. The experimental fracture strength was found to be lower than that predicted by several theories of fracture. This result is attributed mainly to a non-homogeneous structure of the test specimens and in some cases, to premature buckling failure.

Test techniques have been devised for adapting the scattered light method of photoelastic stress analysis to multi-layered fiber composites. A special polariscope has been designed and built to obtain the data from multilayered composite photo-elastic models. A computation scheme employing numerical methods has been devised to obtain the full stress tensor from the photo-elastic data and the stress relations of elasticity. The experi-mental and computational techniques have been tested by application to a homogeneous model: a sphere in compression under two self-equilibrating concentrated loads while imposing the constraints of the multilayered composite. The results obtained were compared with those obtained by other investigators, and the agreement is considered good under the constraints imposed on the problem.

An experimental study of the vibrations of laminated orthotropic plates has been completed. The experimental results were correlated with classical homogeneous plate theory. For unbalanced plates, the reduced flexural stiffness yielded values which indicated good correlation between theoretical and experi-mental results.

A program for the prediction of post-buckling strengths of composite plates which would increase the utility of composites in aircraft construction has been formulated. Classical methods of post-buckling analysis for isotropic metallic plates have been surveyed for possible extension to anisotropic nonhomgeneous com-posites.

An approximate solution for the eigenvalue problem for simply supported anisotropic plates has been suggested. The buckling mode takes the form of a finite series which satisfies the buckling equation throughout the field and the boundary conditions at a finite number of points. Better approximations can be achieved by carrying more terms in the series to satisfy boundary conditions at more points. If an infinite number of terms were used, the exact solution could be obtained. The solution technique is applicable to any type of boundary conditions.

The analysis of unbalanced cross-plied elliptic plates under uniform pressure has been extended to configurations where the principal axes of the material are skewed to the semi-major axis of the ellipse. The fully clamped boundary condition case has been solved in closed form.

A finite deflection discrete element analysis capability for predicting displacement and force distributions in sandwich plates and cylindrical structures with unbalanced laminated faces has been completed. Correlation of the results with published data and experiment results for "Thornel" fiber composites show excellent agreement.

Laminated fiber composite plate and shell configurations may be viewed as a collection of highly orthotropic lamina. If one assumes that the layup is not unidirectional, the lamina are highly heterogeneous through the thickness. An investigation has been initially aimed at critically assessing several basic assumptions upon which current laminated plate and shell theory rests.

A study of the accuracy of various shell theories when applied to anisotropic cylindrical shells is currently underway. Flugge's theory is accepted as a standard for comparison of several approximate theories. The range of validity of the various approximate theories will be determined.

A structural synthesis capability for stiffened fiber composite cylindrical shells has been developed. The design variables consist of both configuration and material parameters. The optimal design problem is formulated as a nonlinear mathematical programming problem. Numerical examples are discussed.

Volume III: Structural Component Development

The previous (third) annual report([3]) described work on the implementation of advanced structural analysis methods and the material and structural element evaluations leading to final design of a graphite-fiber, epoxy-resin composite fuselage section. Initial fabrication activities and a tentative test program plan for the fuselage component were also presented. Additional design work and analysis studies were completed during the present report period. A design solution was found for an interference fit problem concerned with insertion of the fiberglass block end buildups. The basic fuselage structure was analyzed by the discrete element method; stresses, displacements, and margin of safety predictions were obtained for four loading conditions. Influence of the stringer-ring-skin combination tie was studied with regard to the performance expected of the structure during test. Ring-to-skin bond loads due to Poisson effects were examined; these bond stresses should not cause problems during the fuselage component test.

Several treated "Thornel" 50 stiffened panel end attachment specimens were fabricated by using the final shell geometry and were tested. Ultimate strengths were 2710 and 3070 lb/in. in tension and compression, respectively; failures occurred in the gage sections. Effective elastic moduli of the specimens were

14.7 and 17.3 x 10^6 psi. The failure levels were well above design requirements and demonstrated stiffness and weight advantages over conventional metallic construction. Based on these design and analysis data and test results, fabrication of the fuselage component was begun.

The representative fuselage component was fabricated by using treated "Thornel" 50 graphite-fiber, ERL 2256 epoxy matrix composites. A tapered, cylindrical fuselage skin, 48 inches long with end diameters of 24 inches and 20 inches, was constructed by using a fiber lay-up orientation of (90°,±15°,90°). The 90° layers were wet-wound on a plaster mandrel, and the inner 15° layers were constructed by hand lay-up of prepregged sheet. Forty-five hat-shaped stringers, 50 to 52 inches long, were molded from prepregged sheet having a fiber orientation of (+10°,-10°,-10°,+10°), and their properties were measured on coupons cut from each end of the stringers. Thirty-one of these stringers were bonded to the fuselage skin by an adhesive consisting of 70 weight percent Araldite 6005 epoxy resin and 30 weight percent ZZL-0325 hardener. Segmented ring stiffeners, consisting of a balsa wood core reinforced with "Thornel"-fiber, epoxy-resin panels of (0°,±45°) orientation, were fabricated and also bonded to the fuselage skin. The ends of the fuselage component were reinforced with a lay-up of fiberglass tape. Segmented aluminum rings, designed and fabricated at Bell Aerosystems, were bonded to the fiberglass laminate. The function of the fiberglass lay-up and aluminum rings is to permit attachment of the fuselage component to the test stand. A weight analysis of the representative fuselage component was also prepared.

Inspection of the finished fuselage component by visual and mechanical techniques revealed stringer debonding, minor ring debonding, and cracks in the shell skin and ring-stiffener shear panels. These defects were more thoroughly characterized by other inspection techniques such as helium leak detection, a contact ultrasonic technique and an acoustic impact bond inspection method. Correlations of data obtained from the various nondestructive inspections were made.

Potential causes of the damage in the fuselage component have been studied in both experimental and analytical investigations with emphasis on the problem of stringer-to-skin debonding. Experimental studies examined possibilities of surface contamination which may have affected the bond strength, bond line thickness effects, possibility of adhesive embrittlement due to post-cure, and other potential causes such as fixturing expansion during component cure and air bubble entrapment within the adhesive. It was concluded that thermal embrittlement of the adhesive and thermal stresses in the bond-line probably contributed most to the observed debonding, although the influence of the other factors cannot be completely discounted. Analytical studies were also made of thermal

stresses due to elevated temperature exposures and of mechanical stresses due to radius of curvature mismatches between the stringers and shell skin. The thermal analysis suggests that stresses in the adhesive were sufficiently large and, in conjunction with end effects, peeling actions and possible adhesive embrittlement may have contributed significantly to the debonding. Predicted transverse stresses in the skin due to skin fabrication conditions also appeared significant and may be related to the observed skin cracks. Peel loads on the adhesive glue line due to the curvature mismatches between stringers and skin were found to be small and were not likely to have contributed to the stringer debonding.

Repair of the fuselage component was successfully accomplished. The stringers were rebonded to the skin using a room-temperature curing adhesive (Scotchweld 2216 clear). For this purpose, perforated polyethylene bladders were inserted into the stringers, filled with adhesive, and pressurized to force the adhesive to flow into the debonded areas. After the bonding was completed, the bladders were removed, thus minimizing the quantity of excess adhesive remaining in the stringer cavities. The ring stiffeners were rebonded to the skin by using an overlay of fiberglass tape prepregged with room-temperature-curing Scotchweld 2216 gray. The craze cracks in the skin were similarly repaired by patching with the same prepregged fiberglass tape. Prior to rebonding, both adhesive systems and the rebonding procedures were extensively evaluated by tensile, lap shear, and bond peel tests; compression tests on stringer stiffened plates were carried out, and practice bonding runs of full length stringers bonded to an aluminum mock-up of the component skin were made.

The shell loads for the component test evaluation have been revised to reflect the material change from untreated "Thornel" 40 to treated "Thornel" 50. The instrumentation plan for response and destructive testing of the component has been defined, and fixturing and test preparations have been made. Testing of the repaired component was scheduled for the fall of 1969.

SECTION III

COMPONENT DESIGN AND ANALYSIS STUDIES

Selection of a fuselage section for the representative fiber composite component was described in Section IV of the First Annual Report.[1] Section X of the Second Annual Report[2] described preliminary design of the fuselage section and development of analytical methods required for final design. Section IX of the Third Annual Report[3] described implementation of the advanced analysis methods and the material and structural element evaluations leading to the final design of the fuselage section. This report section describes work on final design of the component end attachments, shell stress analysis, and the shell behavior expected during test.

A. Design of End Attachments

(R. Higgins, E. Eckman, and D. P. Hanley, Bell Aerosystems)

During the fabrication of the fuselage component at Union Carbide Corporation, a problem arose concerning insertion of the fiberglass blocks on the inside of the small end of the shell. When the glass blocks were cut to the final 'in-place' dimensions, they did not fit into place, despite the clearances provided. This problem was attributed to the shell taper which resulted in a changing stringer spacing from end to end. The stringer spacing also changes radially, which affected the placement of the glass blocks.

A method was devised whereby the slots cut in the glass blocks to accept the stringers would be enlarged to account for the change in stringer spacing. A full-size layout of the glass blocks was prepared (shown in Figure 1), and the in-place stringer slots were positioned. It was assumed that one stringer slot of each of the four sections would be centered over a stringer. Adjacent slots would then be widened to accommodate the stringers during insertion. The dimensions of the widened slots were based on the difference between the in-place spacing and the spacings at the ends of the stringers. Those slots further away from the centered slot were made progressively wider on the side furthest from the middle slot. The slots were tapered and chamfered to minimize the gap between the glass blocks and the stringers when the latter were positioned.

The cuts between sections in the unslotted regions of the blocks were placed at an angle to avoid interference with adjacent blocks during insertion. This positioning, however, required that the blocks be placed in the component in the order given in Figure 1.

During this period, the aluminum end rings (each in four segments) for the component were designed (Bell Drawing No. 8506-150011), fabricated, and sent to Union Carbide Corporation for attachment to the shell.


M
G
F
E
D
C
B
A

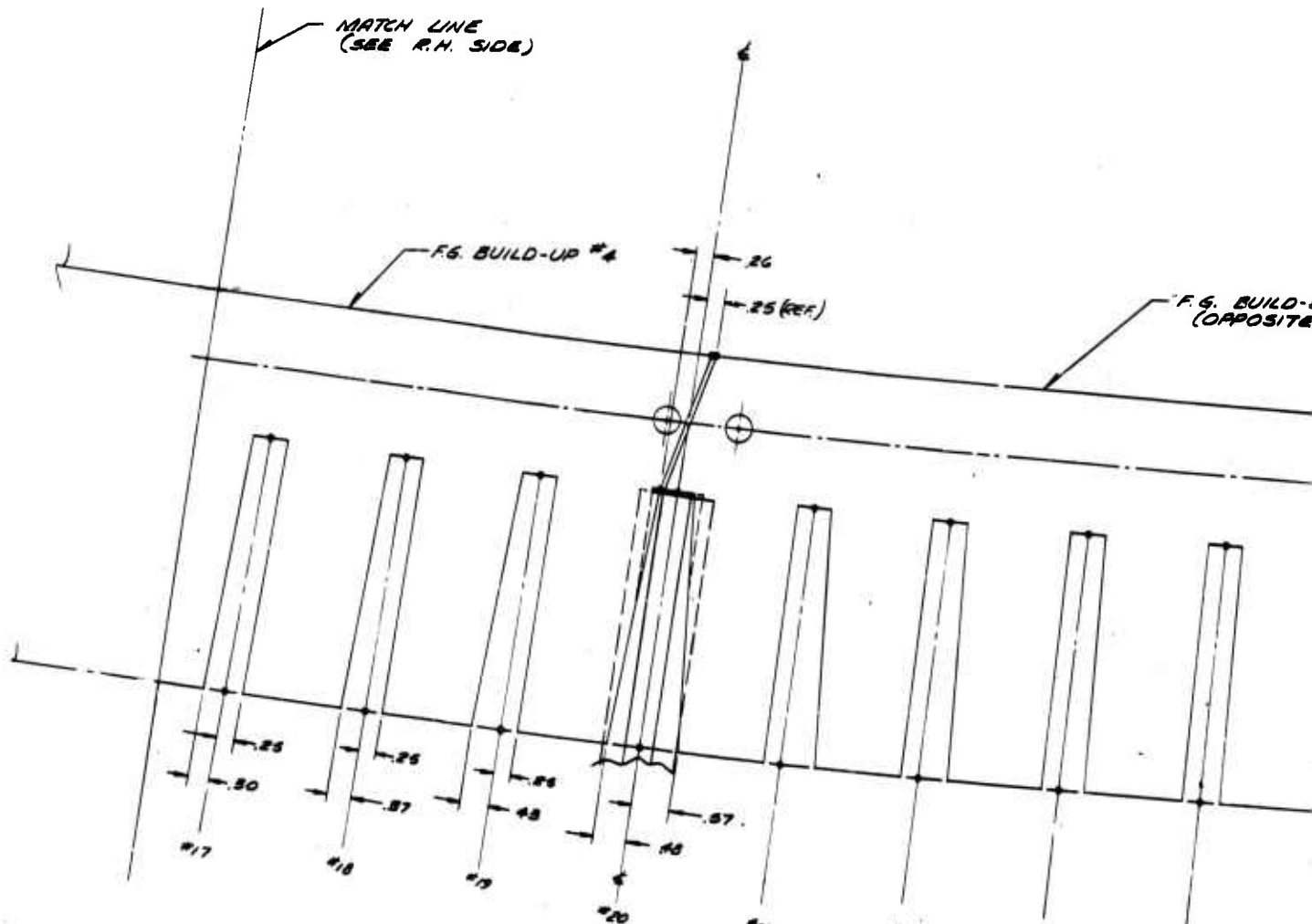
MATCH LINE
(SEE R.H. SIDE)
F.G. BUILD-UP #4
26
25 (REF.)
F.G. BUILD-UP
(OPPOSITE
25
50
26
87
24
48
18
67
#17
#18
#19
#20
#21
#22
#23
#24

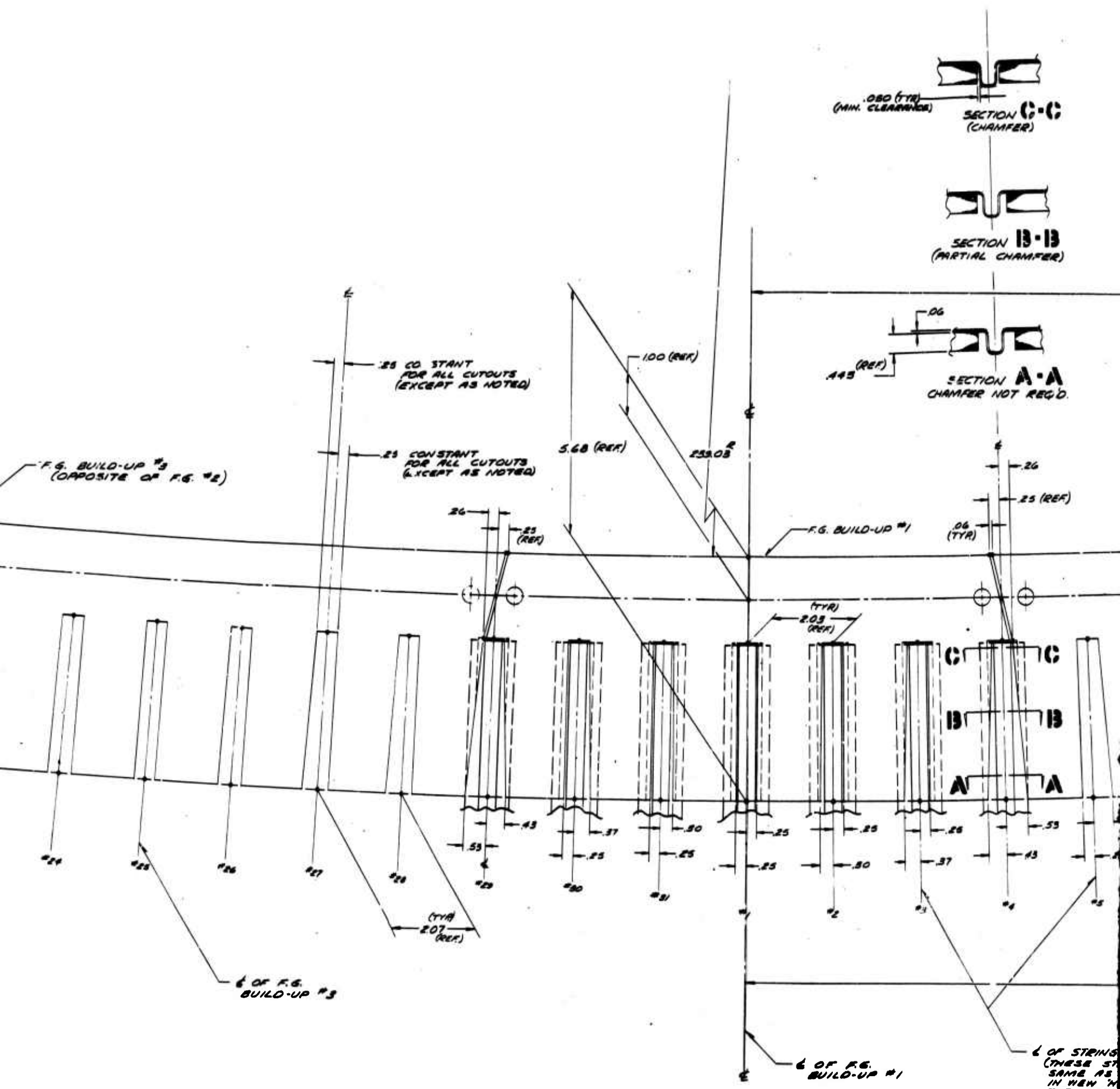
.080 (TYP.) (MIN. CLEARANCE)
SECTION C-C (CHAMFER)
SECTION B-B (PARTIAL CHAMFER)
.06
.445 (REF.)
SECTION A-A CHAMFER NOT REQ'D.
.25 CONSTANT FOR ALL CUTOUTS (EXCEPT AS NOTED)
.25 CONSTANT FOR ALL CUTOUTS (EXCEPT AS NOTED)
F.S. BUILD-UP #3 (OPPOSITE OF F.S. #2)
1.00 (REF.)
5.68 (REF.)
259.03
F.S. BUILD-UP #1
.26
.25 (REF.)
.06 (TYP.)
(TYP.) 2.03 (REF.)
(TYP.) 2.07 (REF.)
C
B
A
#24
#25
#26
#27
#28
#29
#30
#31
#1
#2
#3
#4
#5
6 OF F.S. BUILD-UP #3
6 OF F.S. BUILD-UP #1
6 OF STRING
(THESE ST
SAME AS
IN NEW 'M
THE FUSE

B

C-C
ER)

B-B
AMFER)

A-A
REQ'D.

ASSEMBLY ORDER FOR F.G. BUILD-UP
F.G. BUILD-UP #1
" " #2
" " #3
" " #4

31.21 (REF.)

MATCH LINE (SEE L.H. SIDE)

.26

.25 (REF)

℄ BOLT HOLES (REF)

F.G. BUILD-UP #2

℄

.26

.25 (REF)

F.G. BUILD-UP #4

C

B

A

.55 .46 .40 .31 .25 .25 .25 .25 .25 .25 .26 .25 .25 .48 .37 .30 .26

.13 .25 .25 .25 .25 .31 .40 .46 .53 .57 .25 .16 .26

#5 #6 #7 #8 #9 #10 #11 #12 #13 #14 #15 #16

℄ OF F.G. BUILD-UP #2

32.08 (REF.)

℄ OF STRINGERS (REF.)
(THESE STRINGER NO'S ARE THE SAME AS THE STRINGER NO'S. IN VIEW "H" ON SHEET #2 OF THE FUSELAGE DWG.)

C

ED NO.	NUMBER	APPLICATION	NEXT ASSY	USED ON

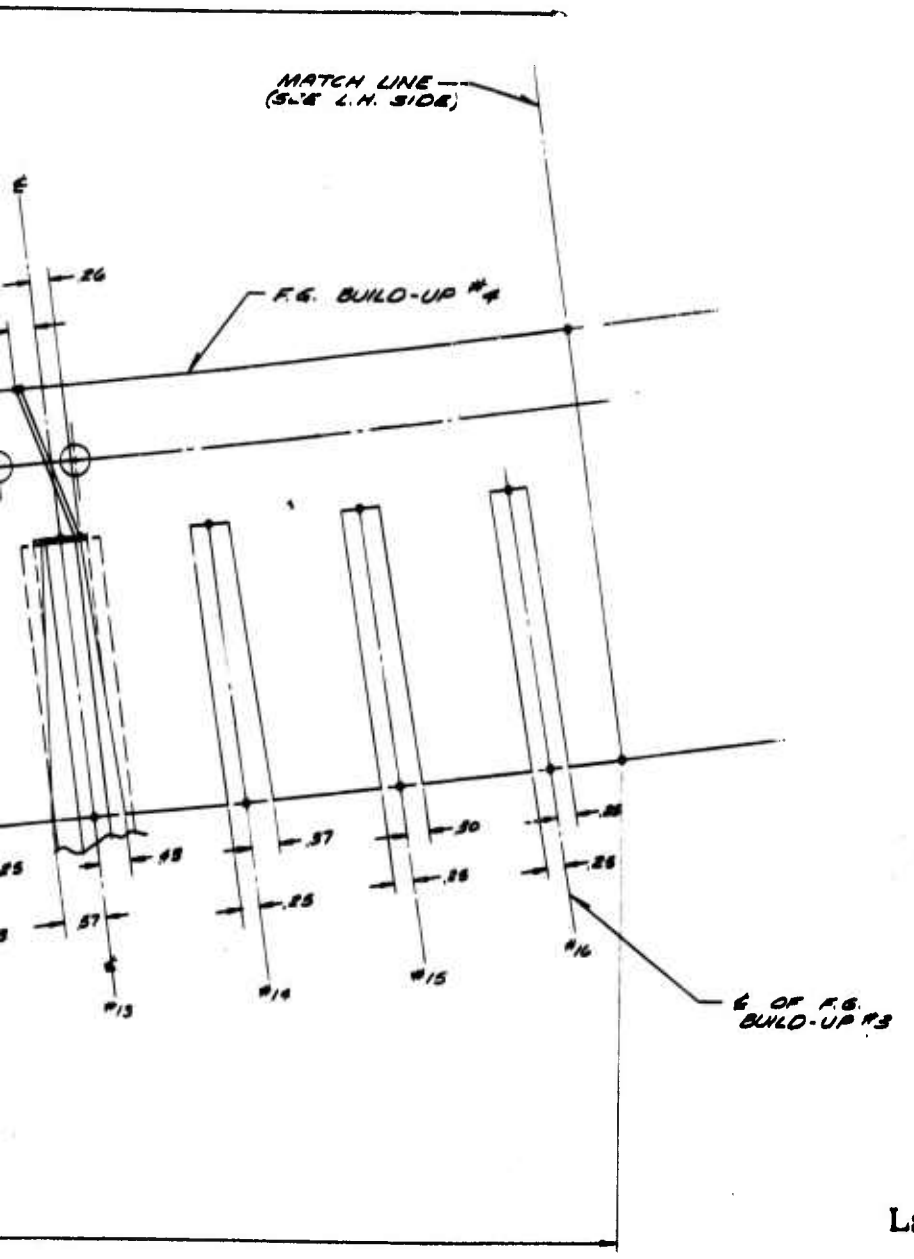

NOTE:
THIS L/O SHOWS F.G. BUILD-..
CUT INTO 4 PIECES WITH
NECESSARY CLEARANCES FOR
ASSEMBLY (AT .06 INSIDE OF
SHELL) FOR SMALL END OF FUSELAGE.

Figure 1.

Layout of Glass Buildup at Small End of Shell

PARTS LIST

LAYOUT
FLAT PATTERN OF
8306-13001D-17 F.G. BUILD-UP

J | 80070 | SK-1015-68

B. Shell Stress Analysis

(Dr. R. H. Mallett, D. L. Turner, and R. A. Elkin, Bell Aerosystems)

A linear elastic finite element structural analysis has been performed to determine static response of the shell to representative test load conditions. Nominal "Thornel"* 50 graphite fiber material properties were used. Test conditions were nearly identical to those proposed for a "Thornel" 40 component. The final shell stress analysis will employ revised loads and measured property data and the appropriate geometry for the treated "Thornel" 50 component.

1. Idealization and Loading

Structural idealization was based on the final design geometry (Figure 149 in Reference 3) and made use of planar and bending quadrilateral shell elements for skin and end reinforcement representation and frame elements for the stringers and rings. The idealized structure extends from the centerline of the support structure attachment bolts to the centerline of the loading structure attachment bolts and was considered built-in at the support structure end. The loading structure was represented by a two-inch thick steel bulkhead assembled from planar/bending triangular plate elements and located at the centerline of the appropriate attachment bolts.

Various simplifying and "lumping" techniques were used. Final idealization consisted of 561 elements with 171 grid points representing a 923 degree-of-freedom problem.

Stringer lumping was accomplished by retaining Stringers 1, 16, and 17 individually and lumping, in pairs, the remaining stringers with suitable circumferential relocation (see Figure 2).

The end attachment glass buildup, which has been analyzed in detail separately in Reference 3, was represented as circumferentially continuous shells laminated to the graphite composite skin. These rings represented the 'inter-stringer' blocks and the inner and outer glass buildups (Figure 3). This idealization is quite representative of the actual structure except for the absence of discontinuities in the inter-stringer blocks to accommodate the stringers. Computed material properties employed are given in Table I.

For analysis purposes, four loading conditions were considered:

(1) Vertical Shear

Vertical loads are supplied around the perimeter of the bulkhead, each carrying a sinusoidal load (zero at top and bottom) such that the maximum shear flow is ~ 180 lb/in. at the sides. This arrangement corresponds to a net load of 7350 lb.

*"Thornel" is a registered trademark of Union Carbide Corporation.

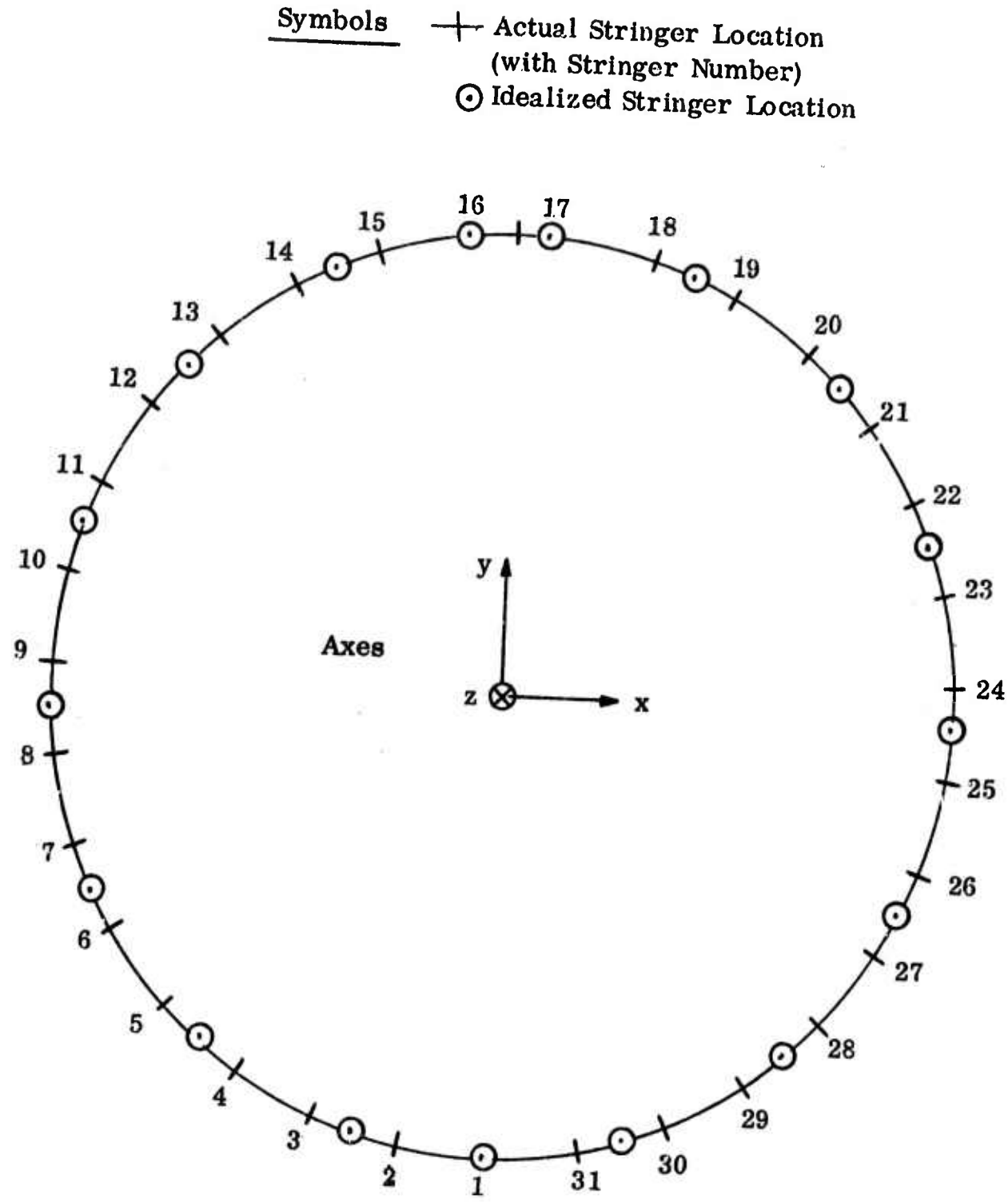

Figure 2. Schematic Cross Section of Model Fueslage Component Looking Toward Loaded End

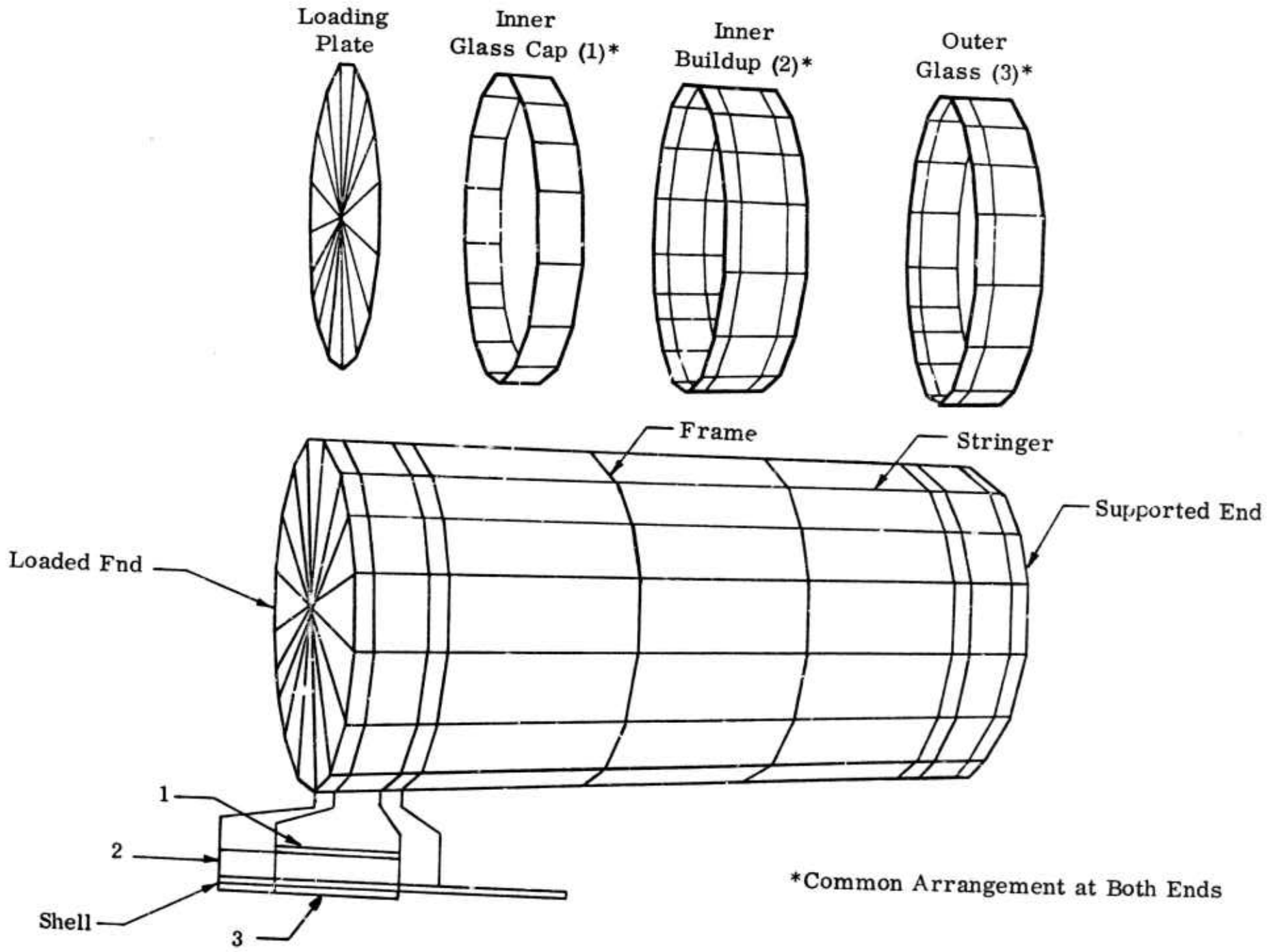

Figure 3. Fuselage Idealization

TABLE I

PREDICTED NOMINAL MATERIAL PROPERTIES

	Material	Properties*	
Skin	"Thornel" 50	E_1 = 11.65	ν_{12} = 0.083
	(90, ±15, 90°)	E_2 = 13.26	ν_{21} = 0.094
	V_F = 50%	G_{12} = 1.30	
Stringers	"Thornel" 50	E_1 = 29.82	ν_{12} = 0.929
	(±10, ∓ 10°)	E_2 = 1.30	ν_{21} = 0.040
	V_F = 65%	G_{12} = 1.71	
Buildup	Fiber glass (Pseudo-isotropic)	E_1 = 3.24	ν_{12} = 0.13
		E_2 = 3.24	ν_{21} = 0.13
		G_{12} = 0.81	

Frame† Data

AE	EI_Z	EI_Y	GJ_X
1.161	0.211	0.0566	0.0256

Stringer Properties

A	I_Z	I_Y	J_X
0.0657	0.00305	0.00444	0.00288

*Elastic Moduli are (10^6 psi)

Areas are ($in.^2$)

Rigidities are (10^6 psi)

† "Frame" refers to the four circumferential stiffening rings made rom balsa wood and reinfo.ced with graphite fiber, epoxy resin composite.

(2) Vertical Bending

Loads are applied around the perimeter of the bulkhead to provide a linear variation of axial load from top (tension) to bottom (equal compression), * the maximum load being ~1800 lb/in. of circumference. This load corresponds to a net moment of 576,000 in.-lb.

(3) Torsion

Transverse loads are applied around the perimeter of the bulkhead to generate a uniform tangential shear flow of ~ 180 lb/in. This load corresponds to a net torque of 114,600 in.-lb.

(4) Frame Load

A concentrated load of 80 lb is applied radially inward at the intersection of Frame 3 and Stringer 1.

2. Analytic Results

Reduction and interpretation of the computer program output are still in progress. Hence, the following discussion is restricted to summarizing the gross structure behavior for each of the four loading conditions.

In the course of this analysis, two sets of automated Margins of Safety were computed for the shell elements of the structure. The first set, termed hereafter 'Hill-Gross M.S.' considers each element as homogeneous and orthotropic and, basically, uses the X, Y, and T skin allowables for the (90, ±15, 90°) laminate. The second set is termed 'Hill-Laminate M.S.' and takes into account the individual lamina properties, layups, etc.; i.e., the basic ply X, Y, and T strengths are employed in conjunction with internal ply stress distributions. These two approaches were studied as a means of comparing computational procedures (the former method, 'Hill-Gross,' being somewhat faster) and analytical results. These comparisons are illustrated in Figures 4 (a) and (b) which present a side view of the structure with M.S. contours shown for each of the two criteria for Load Condition 1. The stringer and ring M.S.'s are the same in both cases by virtue of the problem formulation. The two criteria show the same general distribution patterns; however, the 'Hill-Laminate M.S.' method gives lower values for the skin. In the following discussions, only the 'Hill-Laminate M.S.' values are shown, since these are considered to have a more firm analytical base and are conservative with respect to failure predictions. Predicted allowable stress levels used for these M.S. calculations are given in Table II.

*Subsequent to this analysis, it was decided to reverse the direction of vertical bending load in the response and destruct tests. Thus, the top of the component will be in compression instead of tension.

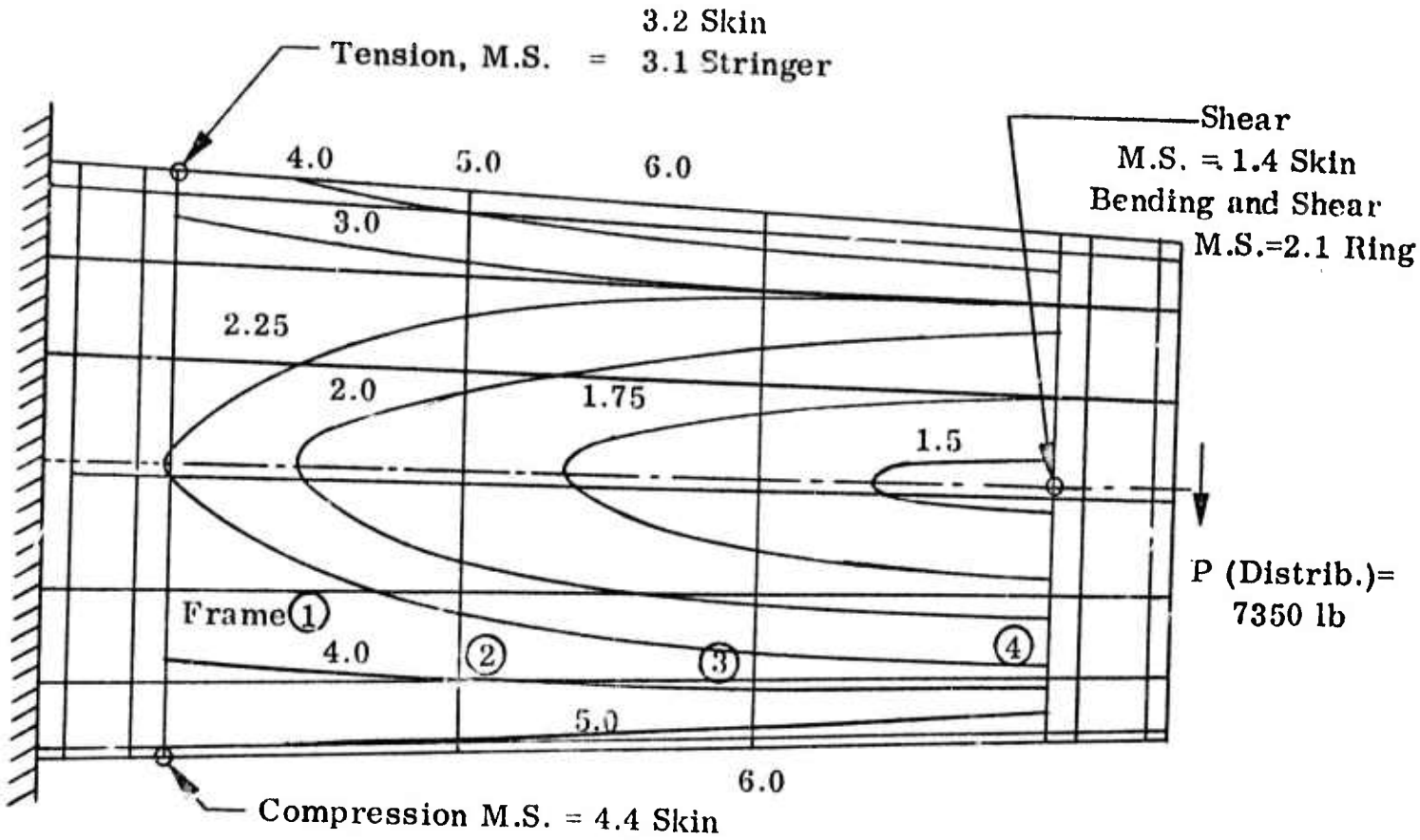

3.5 Stringer

Figure 4(a). Margin of Safety Contours - Hill-Gross

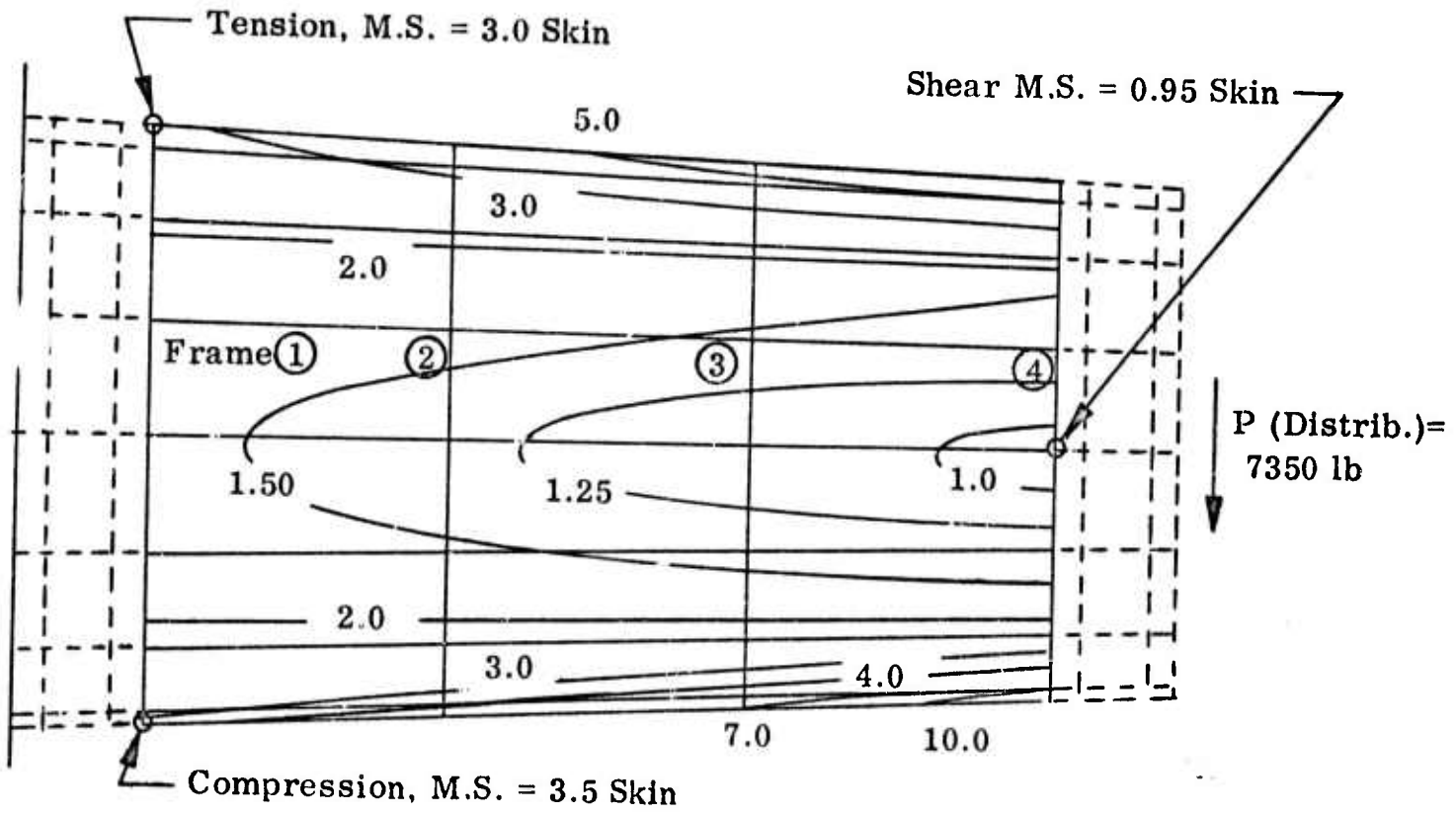

Figure 4(b). Margin of Safety Contours - Hill-Laminate

TABLE II

PREDICTED TREATED "THORNEL" 50 ALLOWABLE STRESSES*

'Hill-Gross Properties'

	X_T	X_C	Y_T	Y_C	T
Skin	30.3	34.6	32.5	36.8	11.0
Stringers	61.7	55.0	—	—	—
Buildup	43.7	41.6	43.7	41.6	14.0

'Hill-Laminate Properties'

	X_T	X_C	Y_T	Y_C	T
0° Ply	65	70	2.5	28	7.0

$E_L = 32.7$ $\quad \nu_{LT} = 0.290$

$E_T = 1.27$ $\quad \nu_{TL} = 0.011$

$G_{LT} = 0.83$ $\quad V_F = 65\%$

*Units are:

Stress (ksi) (ultimate)

Modulus (10^6 psi)

Figure 5, a contour plot of the computed margins of safety on the developed shell, shows more definitively than Figure 4 the gross shell behavior for Load Condition 1. As expected, tension governs the load-carrying capability of the upper surface, and the contours there serve to indicate the distribution of axial tension in the upper surface. Similarly, compression governs the lower surface. The influence of a higher allowable strength in compression than in tension is reflected in the higher M.S.'s shown at the bottom of the fixed end in comparison with those at the top.

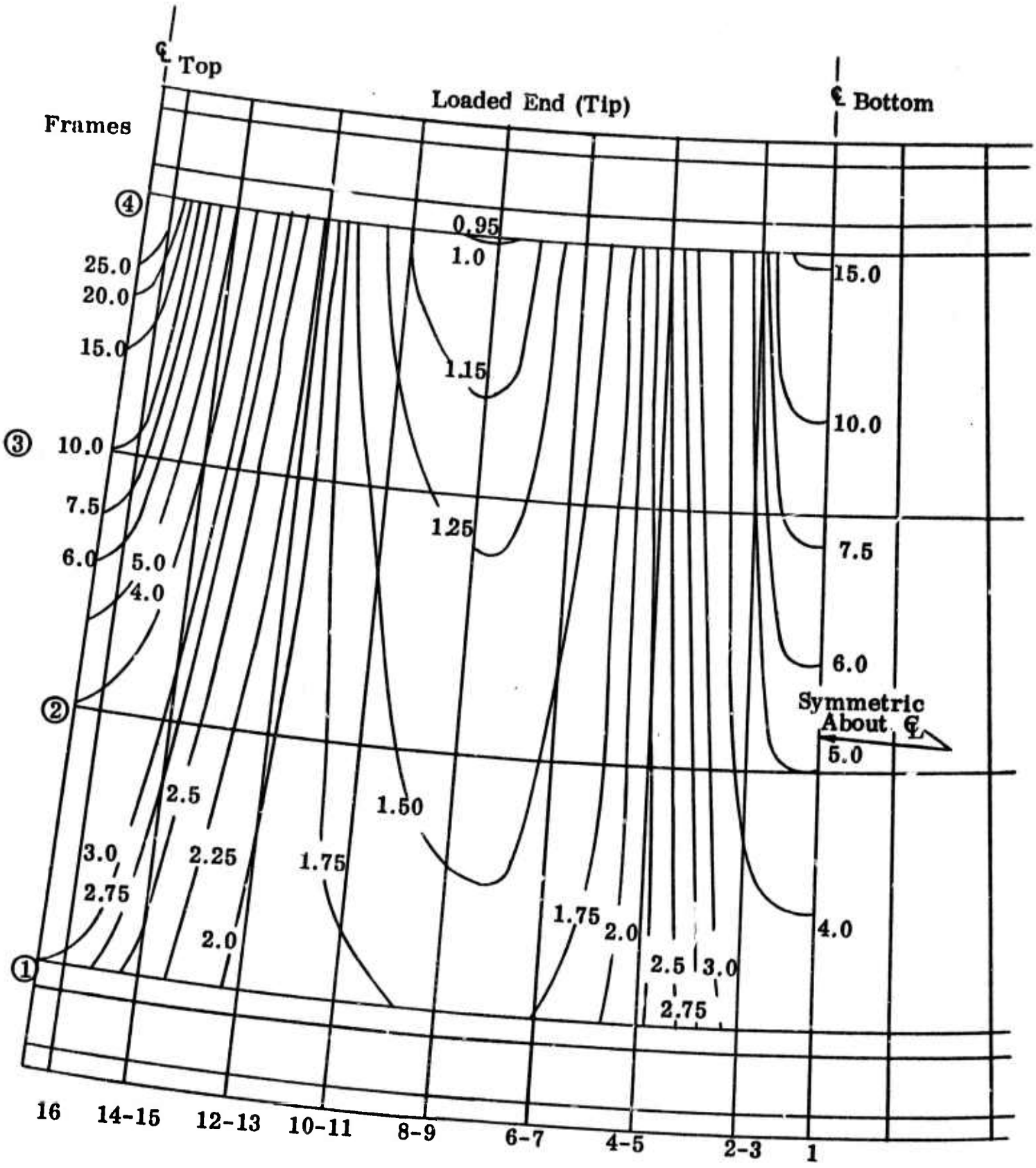

Figure 5. Margin of Safety Distribution (Developed Shell)
Load Condition 1 - Vertical Shear
"Hill - Laminate Method"

The side panels of the component (between Stringers 6-7 and 10-11) are governed by shear stresses, and the M.S. contours in these regions reflect the shear stress distribution. The influence of taper, as seen in Figure 5 serves (a) to give increasing M.S.'s from tip to root due to the shear stress reduction with increased diameter and (b) to cause elongation of the contour loops on the lower (compression) side due to the higher compression allowable.

Figures 6 and 7 show the axial and shear load distributions in the shell for Load Condition 1, and Figure 8 shows the vertical displacements. These data indicate that the structure, because of its rigidity, behaves essentially as a beam.

Figure 9 presents a margin of safety contour plot on the developed shell for Load Condition 2. As in Load Condition 1, tension governs the upper surface, and compression governs the lower surface. The influence of taper for this load condition increases the M.S.'s (all are positive) as the root is approached and results in closed contour loops. The effect of a higher compression allowable is seen both on the minimum M.S. at the loaded end upper surface and on the location of the transition region between tension and compression, which is shifted above the horizontal centerline.

Figures 10 and 11 give typical axial stress responses and the shell displacements, again indicating beam-type action.

The results of the analysis for Load Condition 3, torsion, showed no unexpected behavior of the structure. The margin of safety contour plot showed curves parallel to the developed frames with values ranging from 2.4 at Frame 1 to 1.6 at Frame 4. Shear stress distribution in the shell was found uniform with respect to radial position, being 133 lb/in. at Frame 1 and 166 lb/in. at Frame 4.Tangential displacements along the shell were linear with respect to stations along the Z-axis.

Results of analysis for Load Condition 4 showed that the structure response does not conform to simple beam theory. Figures 12 and 13 give the distribution of axial and shear stress at various cross sections of the shell for Load Condition 4. From the diagrams of Figure 12, the effect of load 'dumping' into stringers is evident (note the steps in the N_x plots). Further, near the fixed end, the stress distribution is not quite linear because of the load diffusion effect; however, with greater L/D proportions, this trend toward Mc/I would be expected. Figure 14 shows frame radial deformations. Finally Figures 15 (a, b, and c) show developed surface contour plots of axial, tangential, and shear loads.

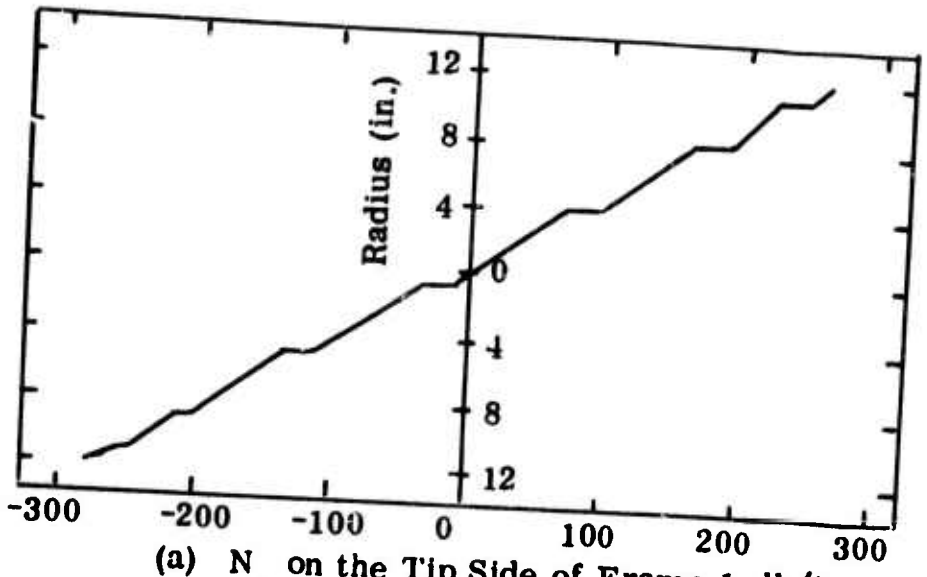

(a) N_x on the Tip Side of Frame 1, lb/in.

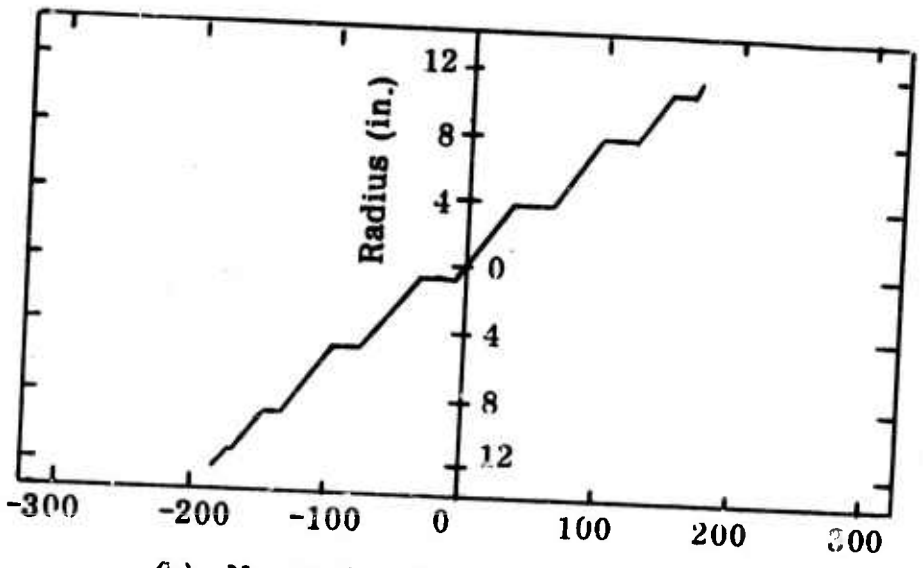

(b) N_x on the Tip Side of Frame 2, lb/in.

Figure 6. Axial Stress Distribution in Fuselage Shell-Load Condition 1

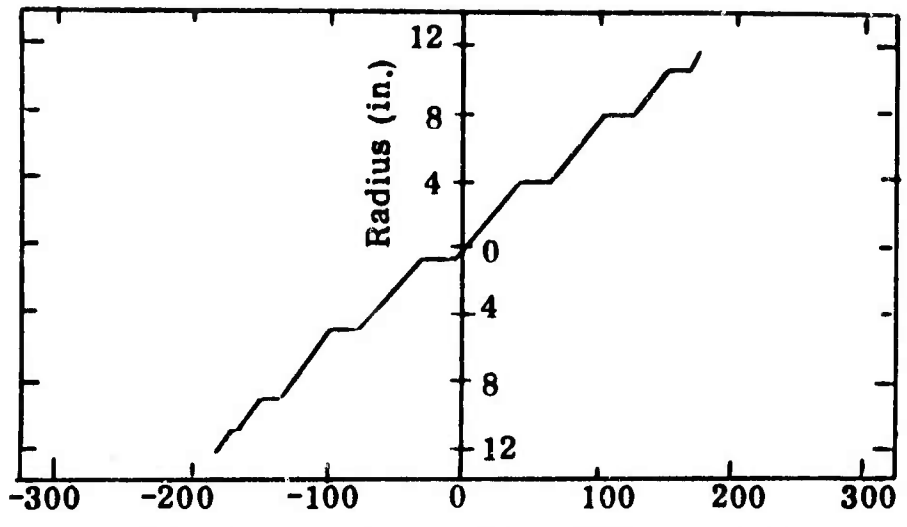

(c) N_x on the Root Side of Frame 3, lb/in.

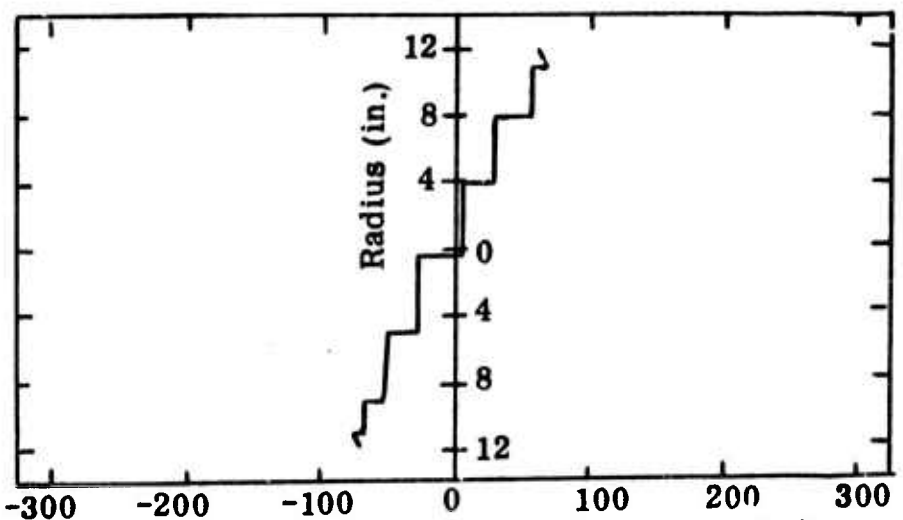

(d) N_x on the Root Side of Frame 4, lb/in.

Figure 6 (cont). Axial Stress Distribution in Fuselage Shell-Load Condition 1

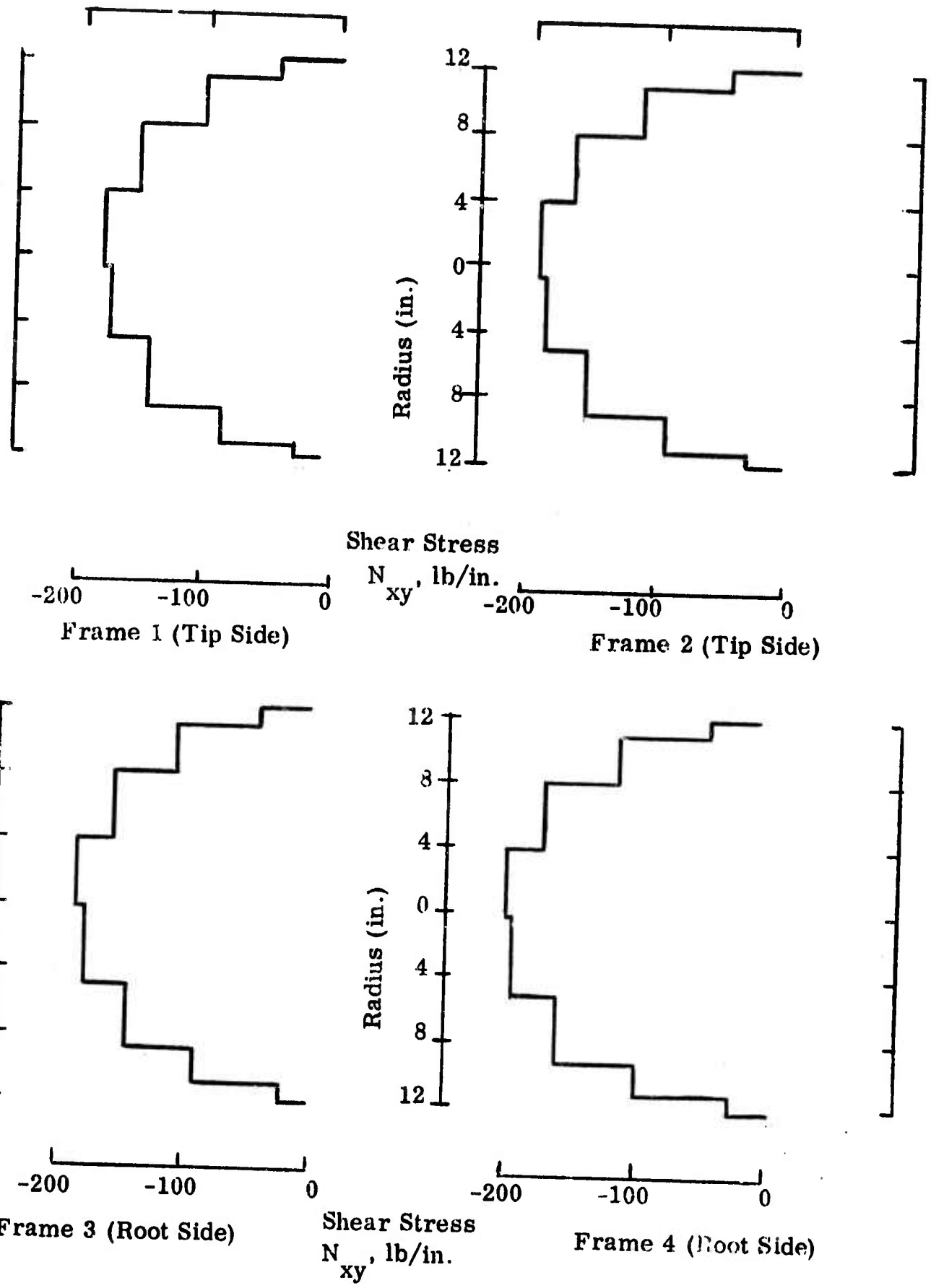

Figure 7. Shear Stress Distribution in Fuselage Shell-Load Condition 1

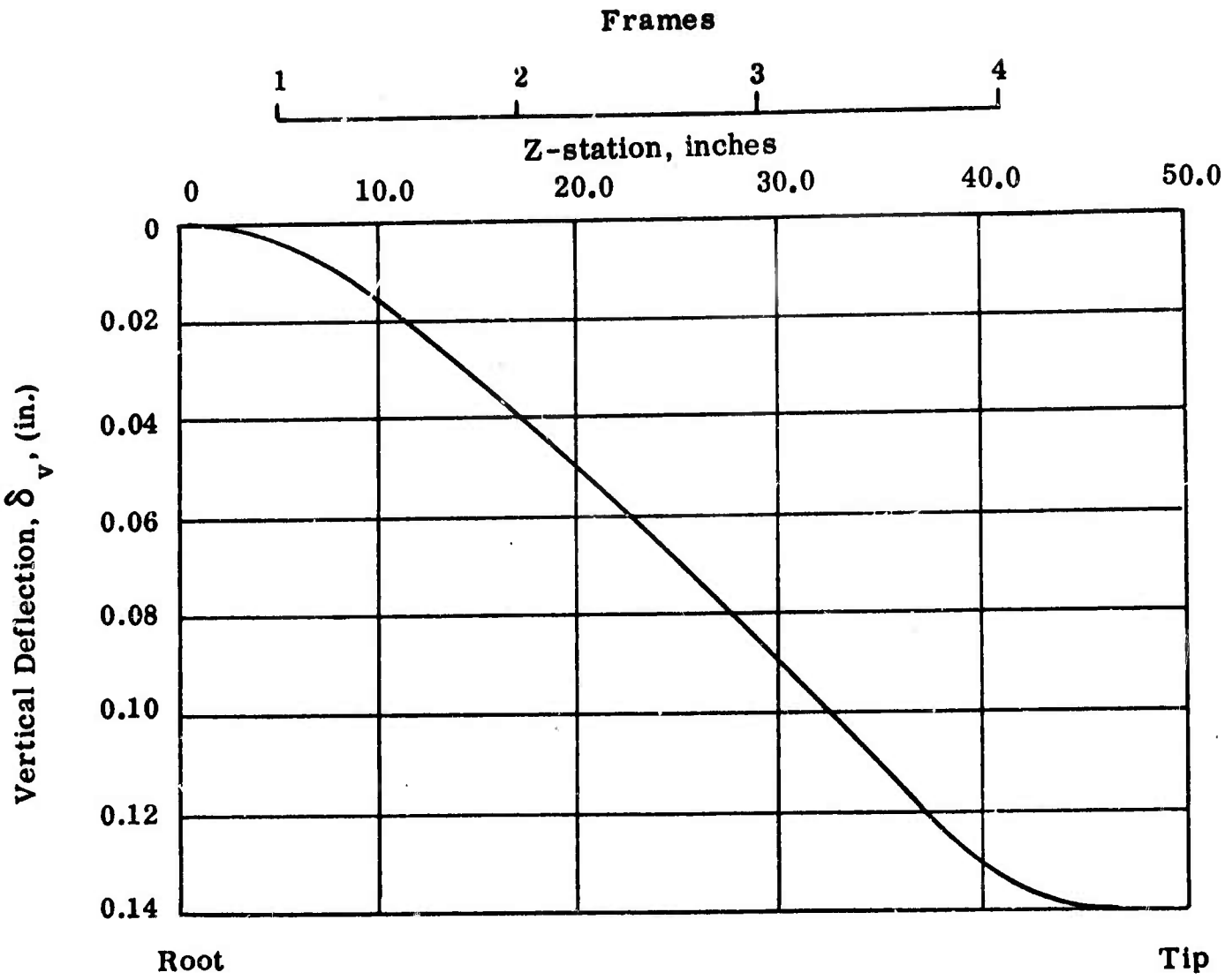

Figure 8. Vertical Displacements of Fuselage Shell-Load Condition 1

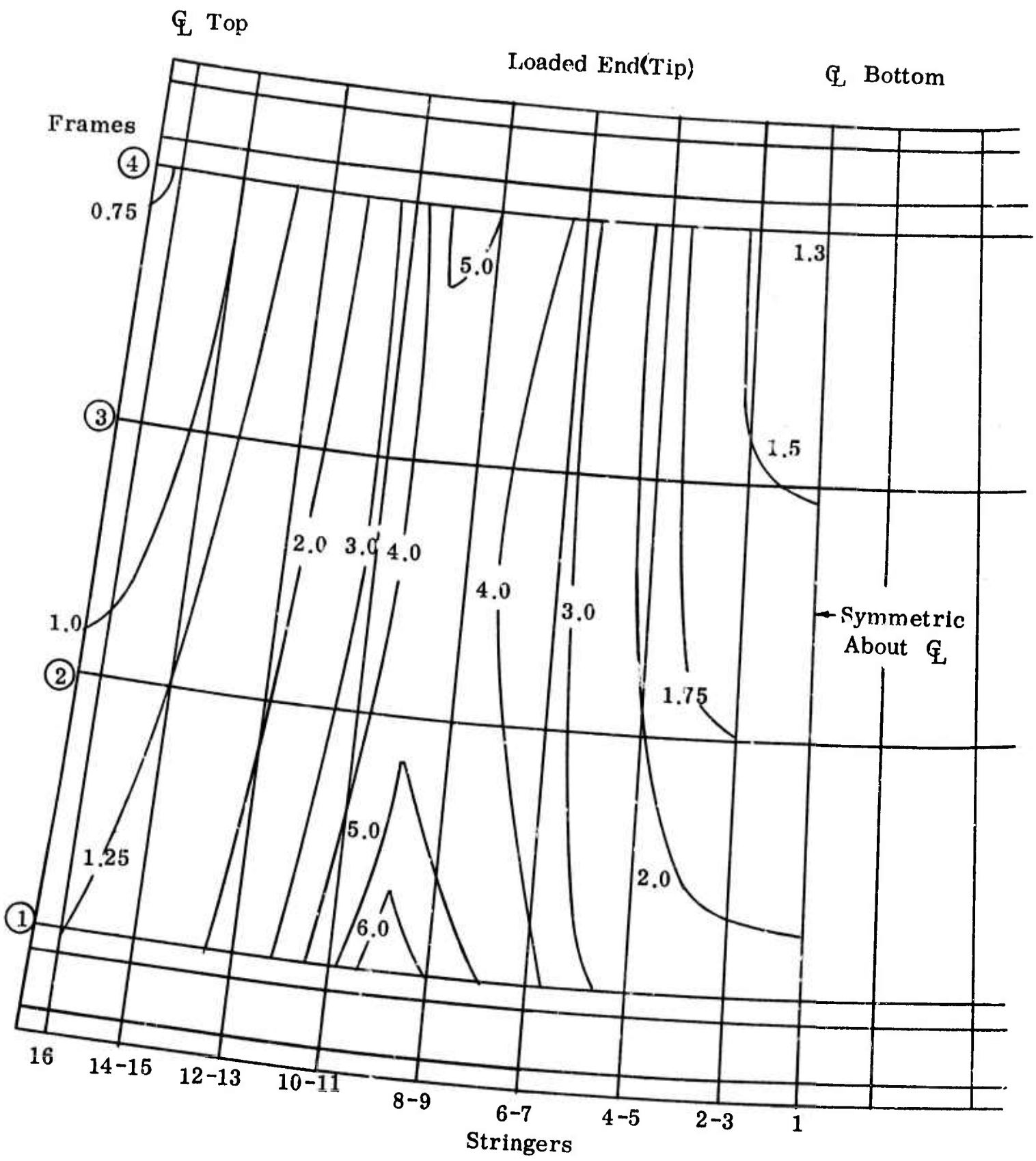

Figure 9. Margin of Safety Distribution (Developed Shell)
Load Condition 2 - Vertical Bending Moment
" Hill - Laminate Method"

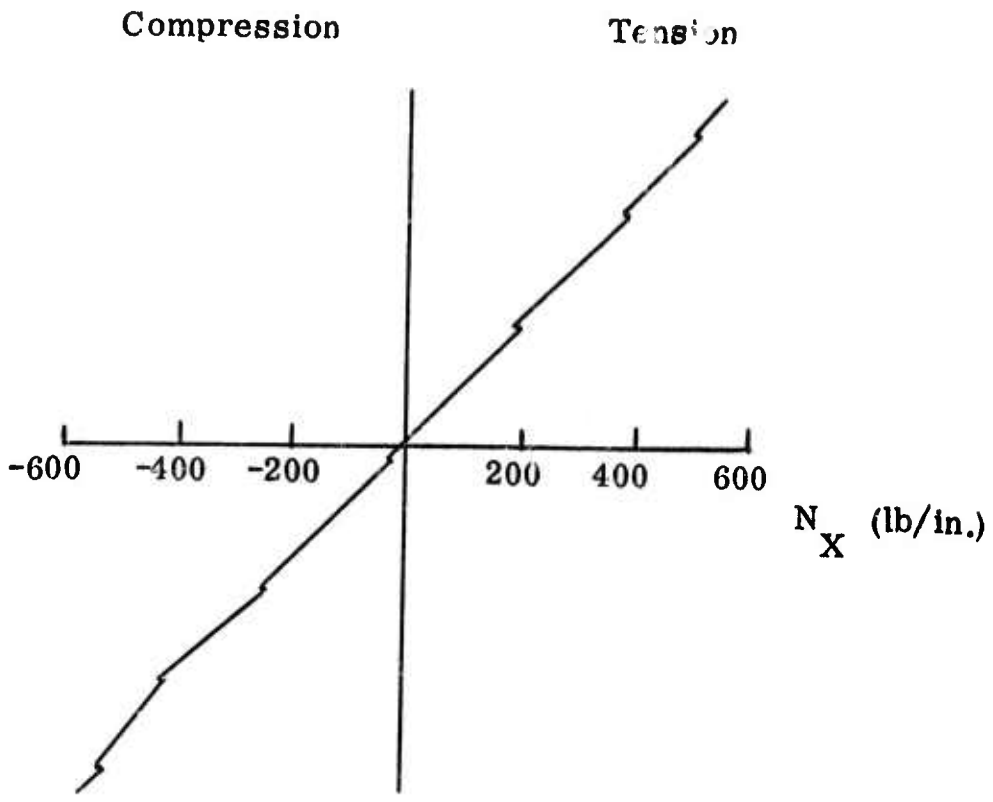

(a) Frame 1 (Tip Side)

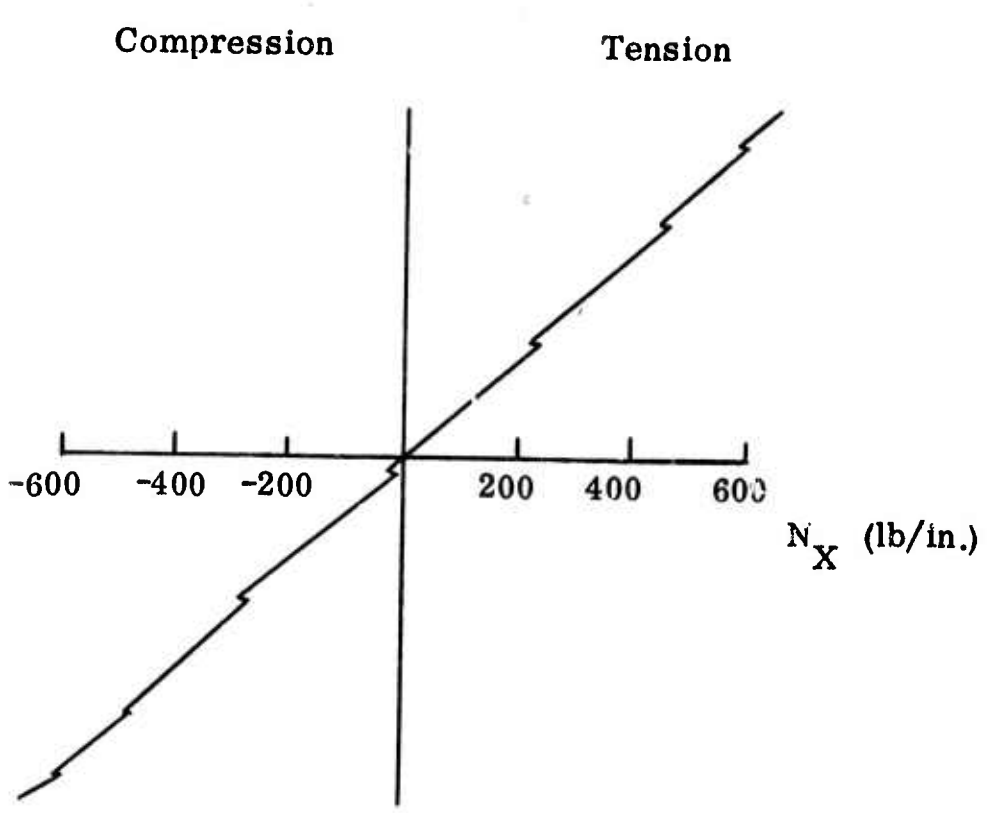

(b) Frame 4 (Root Side)

Figure 10. Axial Stress Distribution in Shell-Load Condition 2 - Vertical Moment

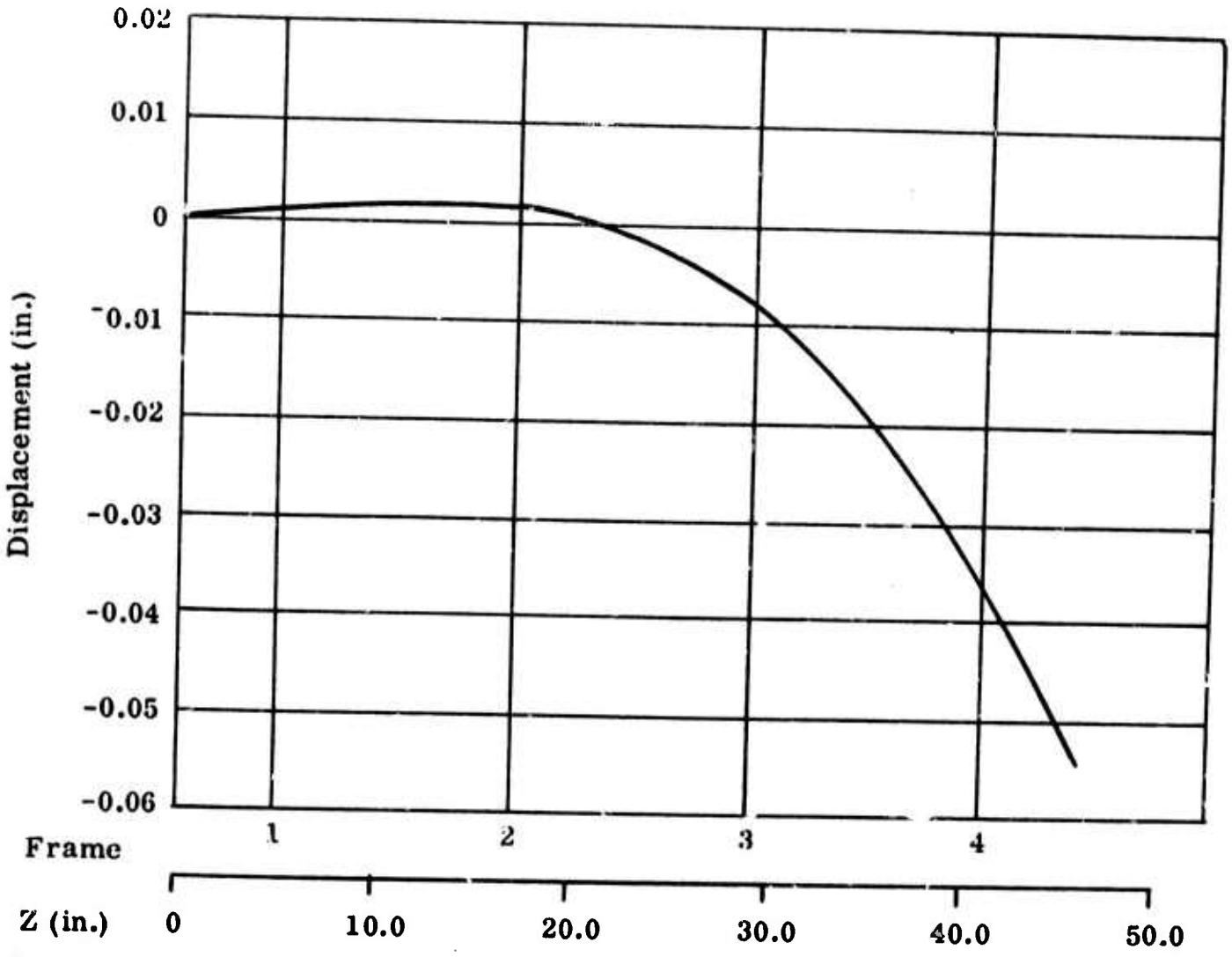

Figure 11. Vertical Displacement of Structure-Load Condition 2-Vertical Moment

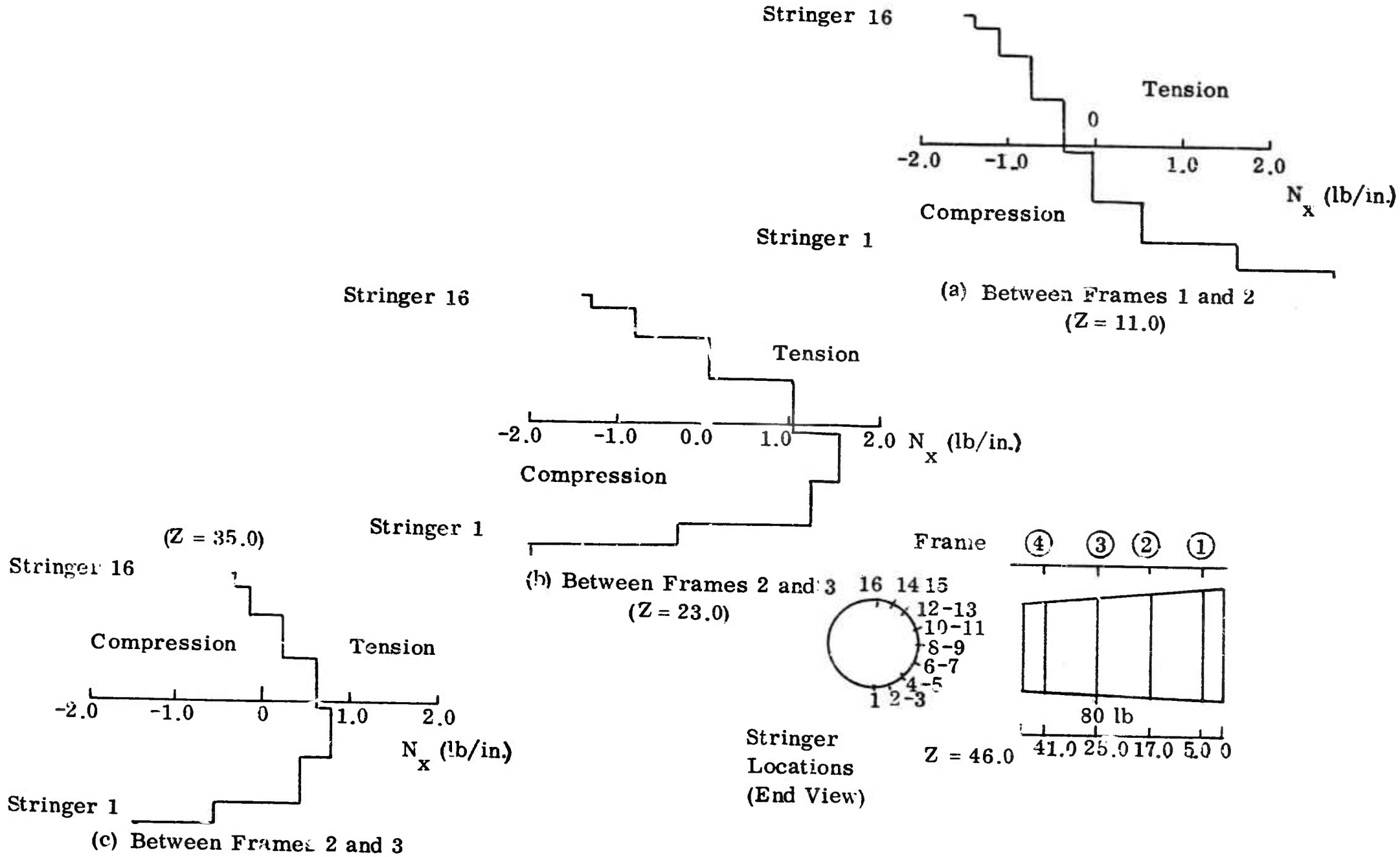

Figure 12. Axial Stress Distribution in Shell-Load Condition 4 - Local Vertical Load

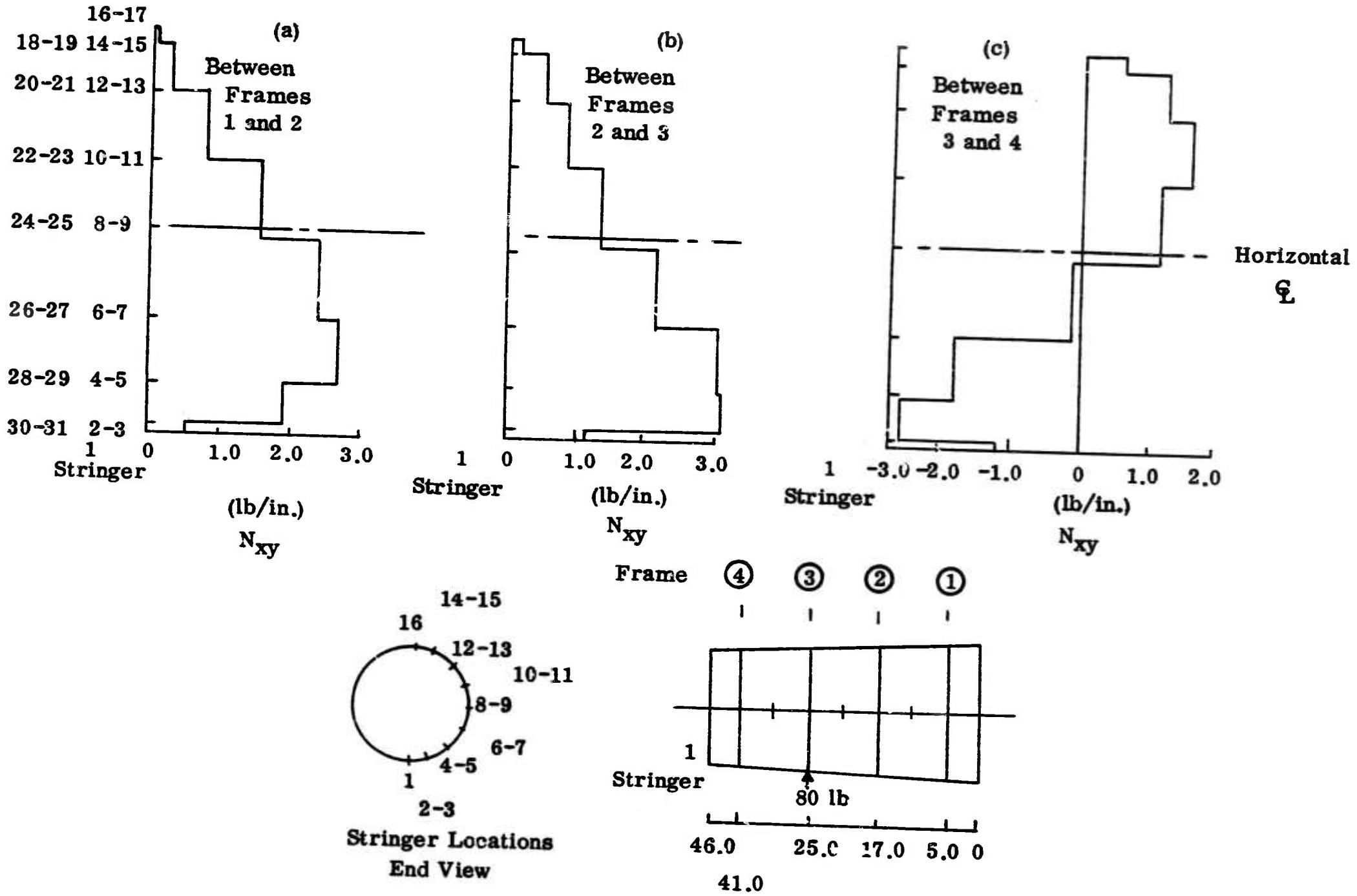

Figure 13. Shear Flow Distribution-Load Condition 4 - Local Vertical Load

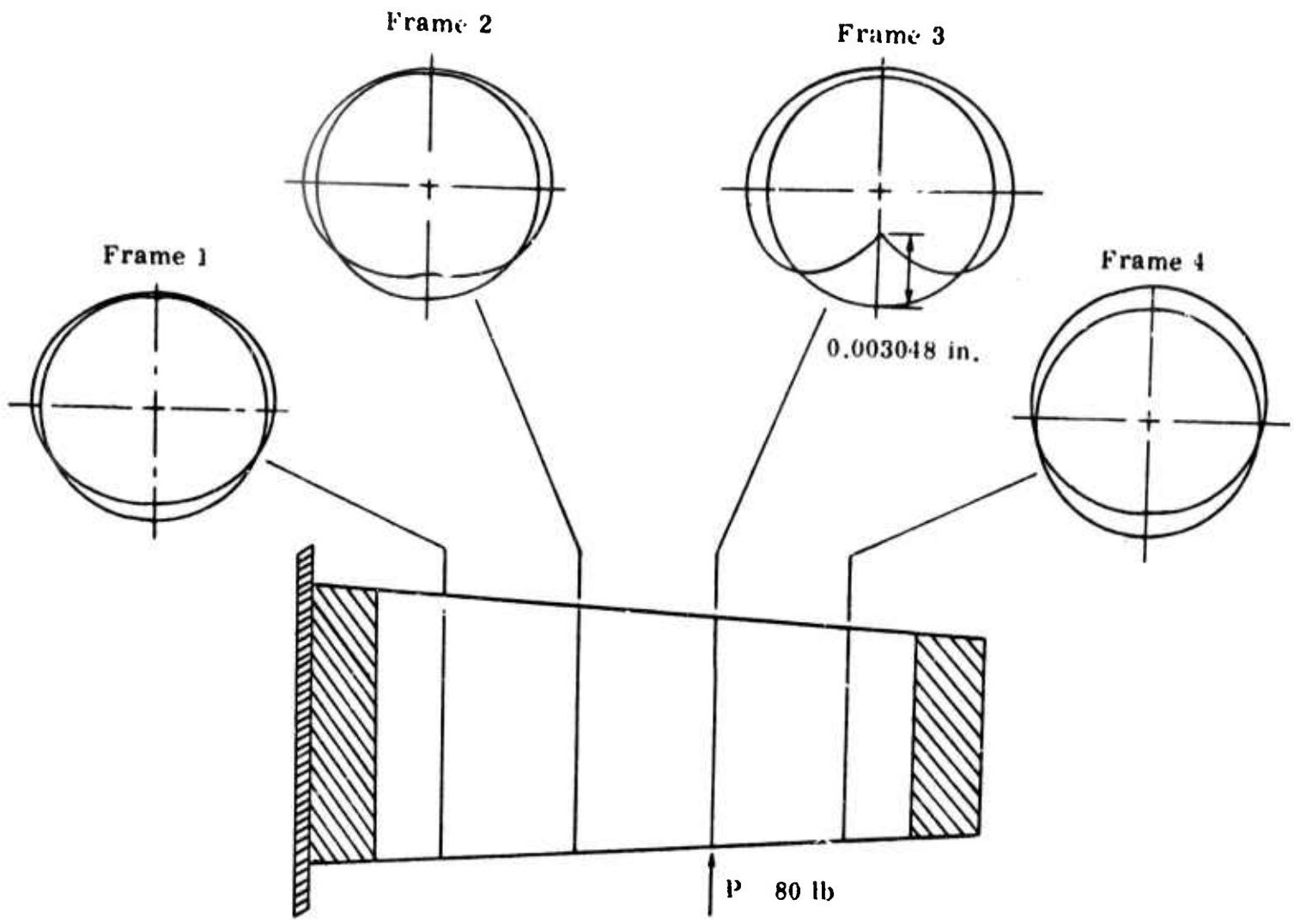

Figure 14. Frame Deflections with Local Applied Load

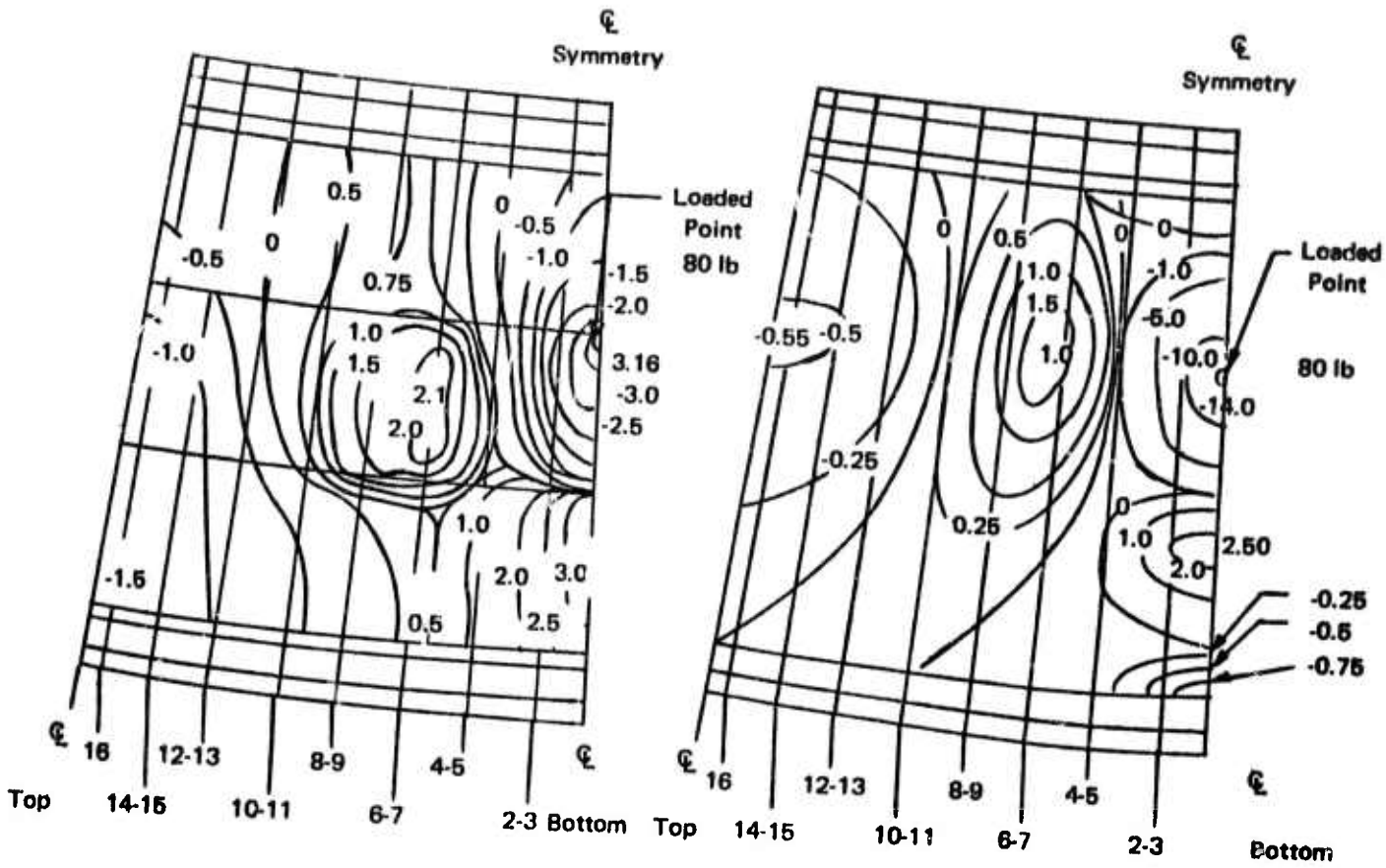

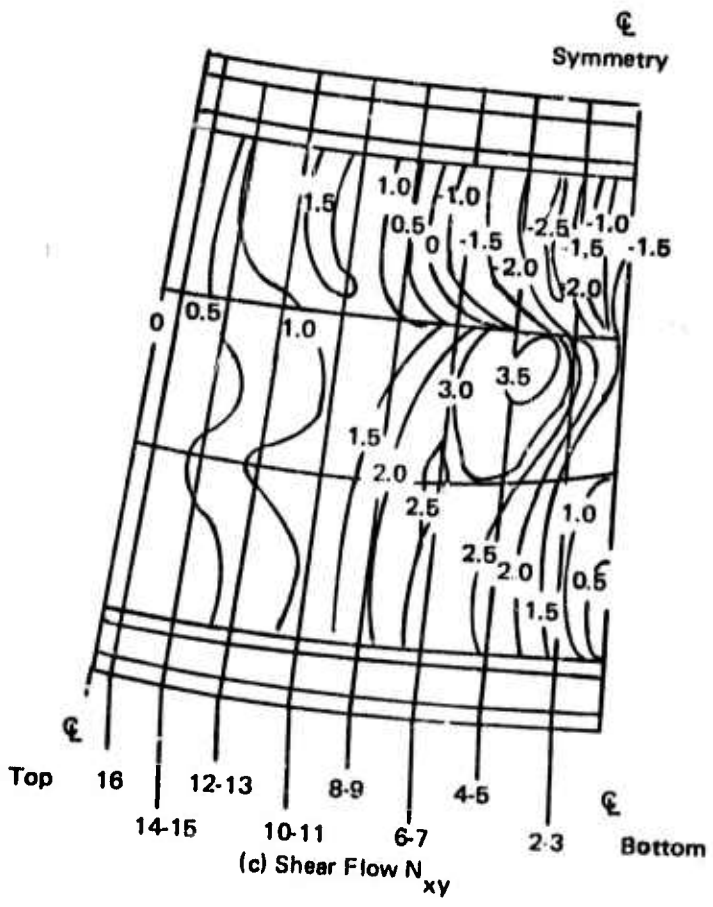

Figure 15. Stress Distributions for Load Condition 4

C. Anticipated Shell Behavior

(Dr. K. H. Sayers, D. L. Turner, and D. P. Hanley, Bell Aerosystems)

Several analytical investigations were conducted to determine the expected performance of the fuselage component during test. These studies primarily concerned structural integrity of the stringer/ring/skin combination tie. Some concern over this juncture region had been expressed because no clips join the rings to the stringers. The basic shell geometry and the selected ring design given in Figure 149 of Reference 3. The analytical investigations are reported in three areas: (1) shell buckling analyses considering various degrees of ring effectiveness with idealized stringer/ring/skin ties, (2) a discrete element buckling analysis of a critical shell section considering a realistic stringer/ring/skin tie, and (3) analysis of ring/skin bond loads due to Poisson effects.

Shell characteristics assumed nominal properties. Skin thickness was taken as 0.047 inch with a fiber volume content of 50%. Stringer properties were based on average measurements in the compression critical shell region (Stringer Nos. 14-19, shown in Figure 149(b) of Reference 3: 0.041 inch thickness, with V_F = 49%. Stringer cross-sectional area was 0.0803 in.^{2}. Ring geometry assumed 0.016 in./layer thickness with V_F = 50%.

1. Shell Buckling Analyses

Elastic properties of the various "Thornel" 50 shell elements were calculated by using values determined from previously given characteristics. These properties were then used in the NASA Program[4] to predict failure loads and buckling modes of a 33-in. diameter cylinder with various degress of ring effectiveness. Strength cut-offs were also calculated. Results are given in Table III.

TABLE III

RESULTS OF SHELL BUCKLING ANALYSES

-Failure Loads, N_x (lb/in.)-

Failure Mode	Present Ring Design	Ring Stiffnesses 50% of Present Design	No Rings
General Instability	21,500	17,700	1,900
Panel Buckling	6,010	6,010	1,900
Strength Cut-Off	3,010	3,010	3,010

Compared with results given in Section IX B of Reference 2, the high loads/inch in compression due to bending at which instabilities occur are due to: (a) the use of "Thornel" 50 properties instead of "Thornel" 25 and 40 properties used previously, and (b) actual stringer thicknesses greater than nominal (0.041 in. actual vs. 0.033 in.). The data in Table III show that general instability and panel buckling conditions could be more closely matched in the shell, thereby providing a somewhat lighter weight design, by using rings of reduced stiffness or by using fewer rings. For the present shell with rings, the panel buckling mode is critical; however, this load (6,010 lb/in.) is well above the strength cut-off (3,010 lb/in.).

The strength cut-off (therefore, the performance estimate) for the shell was determined as follows. Average stringer compression strength measured by Union Carbide on coupons cut from stringers 13 through 20 (see Section IV D) was 49,940 psi, reasonably close to the expected compression strength of 55,040 psi. Computed tensile strength of the stringer was 61,700 psi and was not critical, since it is greater than the stringer compression strength. Computed stringer modulus is 22.6×10^{-6} psi. Therefore the predicted failure strain is

$$\epsilon_{max} = \frac{49.95 \times 10^{3}}{22.6 \times 10^{6}} = 0.00221.$$

Initial skin buckling is not expected to occur, and the skin/stringer combination is stringer-critical in compression. Computed skin modulus is 11.65×10^{6} psi, and skin stress at stringer failure is $0.00221 \times 11.65 \times 10^{6} = 25,700$ psi. Hence, the expected load/inch at failure is

$$(N_x)_{ult} = 25,700 \times 0.047 + 49,950 \times 0.0803/2.23$$
$$= 3,010 \text{ lb/in.},$$

where 2.23 is the stringer pitch in inches.

Thus, the fuselage component would be expected to fail at a load of ~ 3,010 lb/in. due to the stringers reaching their ultimate compression strength near the top centerline of the shell. Since, however, the expected stringer tensile strength cut-off is close to the compression cut-off, there is some uncertainty as to which side will fail first. On the basis of the treated "Thornel" 50 end attachment specimen test which failed at 2,710 lb/in. (see Section IV B), failure on the tensile side is slightly favored.

Panel and general instability loads for the shell are well above the compressive strength cut-off loading, and, hence, the shell is not critical in either of these modes. With no rings at all, general instability would occur at 1,900 lb/in. From 1,900 lb/in. to 3,010 lb/in., the rings are being relied upon to prevent shell instability, their primary function. The presence of the rings raises the critical shell instability mode to 6,010 lb/in., almost twice the expected ultimate strength. Thus, very small column effects are expected during the shell destruct test.

2. Finite Element Analysis of Critical Shell Segment

A single stringer segment of the fuselage component has been idealized to enable a linear elastic finite element general instability analysis to be conducted.

Idealization was based on the geometry given in Figure 149(b) of Reference 3. The idealized segment (of Stringer Numbers 16 or 17), assembled from planar/bending quadrilateral shell elements, represents a single stringer segment of the structure extending between Frames 1 and 4 (Figure 16) . The root end was considered built-in, the tip end being subjected to boundary conditions such that when loaded in compression it behaves as if it were built-in, i.e., rotations were not permitted. Longitudinal segment edges carry symmetric boundary conditions.

The ring frame segments were represented by sandwich plate elements lying in the radial/tangential mid-plane of the ring, with "reduced" frame elements (no torsional or radial bending stiffness) representing the "inner cap" of the ring frame (see Figure 16). The structure between frames was represented by three sets of shell and stringer elements. The resulting idealization consists of 110 elements with 96 grid points representing a 404 degree-of-freedom system. This system is condensed to a 316 degrees-of-freedom model for the instability eigenvalue problem. Numerical results from the analysis are expected in the next report period.

3. Local Ring/Skin Bond Loads

Analysis of local ring/skin bond loads was performed with reference to a 22-inch diameter cylinder loaded in direct compression. The ring/skin bond load at an axial load level corresponding to shell failure was estimated as follows. Failure strain given previously is

$$\epsilon_{Axial} = 0.00221 \text{ at } N_x = 3{,}010 \text{ lb/in.}$$

Circumferential strain is

$$\epsilon_{Circum} = \nu_{12}\ \epsilon_{Axial} = 0.083 \times 0.00221 = 0.000183.$$

If no rings were present, the increase in shell radius would be

$$\delta = \epsilon_{Circum} \times R = 0.000183 \times 11.021 = 0.00202 \text{ in.}$$

The presence of the rings means that the combined structure will have a lesser radius increase, Δ. Circumferential compression will be developed in the skin and tension in the rings. If one considers only membrane effects, the radius increase is

$$\Delta = \frac{\ell t\, E_{Circum}\, \delta}{\ell t\, E_{Circum} + (EA)_{Ring}} = 0.00174 \text{ in.},$$

Note: Hatched areas indicate sandwich plate elements representing ring frame segments.

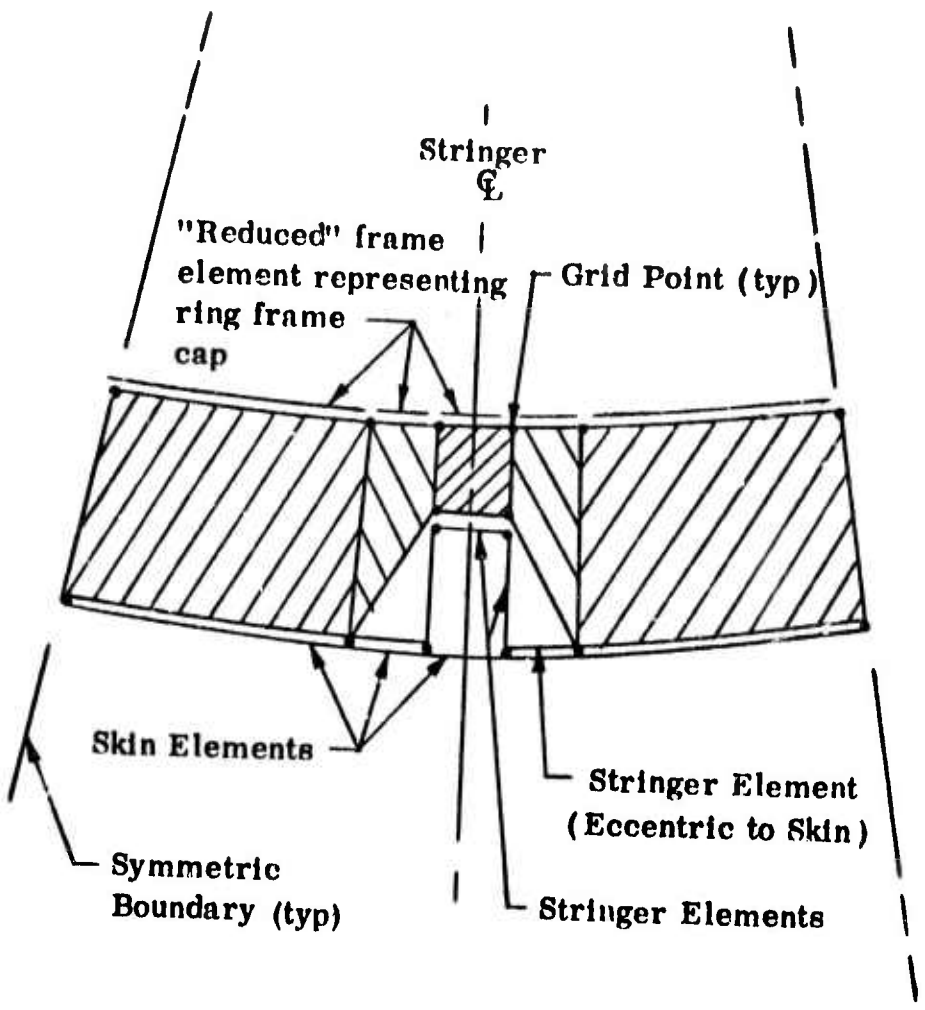

Stringer Segment Cross Section at Typical Frame showing Element Breakdown

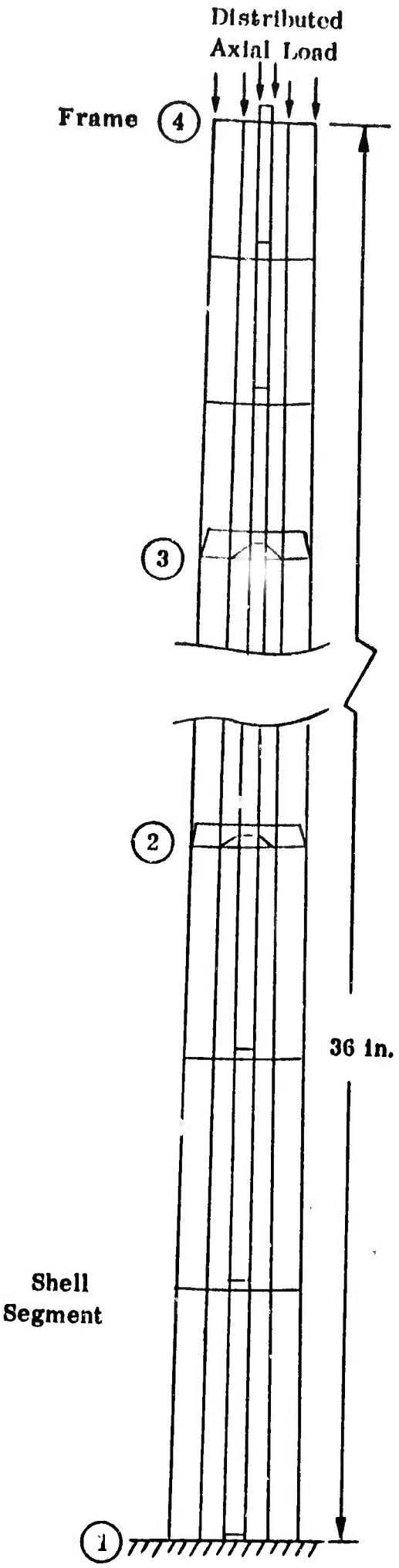

Figure 16. Idealization and Typical Cross Section for Instability Analysis

where

ℓ = 12.0 in. (ring spacing),

t = 0.047 in. (skin thickness),

$E_{Circum} = 13.26 \times 10^6$ lb/in.^{2} (circumferential skin modulus), and

$(EA)_{Ring} = 1.16 \times 10^6$ lb (ring circumferential stiffness).

The circumferential skin and ring direct stresses induced by this effect are very low. The associated load/ring is

$$P = 1.16 \times 10^6 \times \frac{0.00174}{11.021} = 184 \text{ lb.}$$

Hence, ring interaction loading normal to the ring-to-skin joint is

$$w = \frac{P}{R} = \frac{184}{11.02} = 16.6 \text{ lb/in.}$$

The loading per inch of bond line is

$$w' = \frac{16.6}{2} \times \frac{2.23}{1.13} = 16.4 \text{ lb/in.}$$

The above load accounts both for the fact that there are two bond lines and for the interruption due to the stringer cutouts in the rings.

The peel tests (Table LXV in Reference 3) gave peel bond loads/inch from 13.2 to 28.6 lb/in. (average 20.1 on five tests). These tests used untreated "Thornel" 40 laminates, and fractures were characterized by failures in the short transverse direction of the laminates themselves. The treated "Thornel" 50 laminates currently being used have higher tensile transverse strengths; hopefully, the peel strengths will also be improved. Additionally, in the peel tests, considerable skin bending was involved; very little skin bending is expected during the shell tests.

The estimates of the skin-to-ring bond loadings due to Poisson effects are within the lower part of the range of values obtained in previous peel tests. The latter were somewhat severe tests which were conducted with and used untreated "Thornel" 40 samples. With the type of loading expected in the treated "Thornel" 50 shell test, higher bond strengths are anticipated.

SECTION IV

TESTS OF PANELS AND STRINGERS

Tests to establish data for the design and analysis studies of the fuselage component were reported in Sections IX E through J of the Third Annual Report.[3] Data were obtained from tests of coupons cut from flat panels and stringers and from tests of stiffened panels with and without glass-reinforced plastic and aluminum end-attachment buildup. During this period, the graphite fiber used was changed from "Thornel" 40 to a "Thornel" 50 fiber treated to improve composite shear strength. Improvements were continually being made in the treatment process, and each treatment was given a separate letter designation. Treatments A, B, and C were investigated prior to the start of the fuselage component fabrication. The fuselage component was fabricated almost entirely from fibers which received Treatments D or E.

In this section, additional design data and quality control test results are reported. End-attachment test specimens with a modified design were fabricated and tested. Tests were made on coupons cut from flat panels made with fibers which received the final treatment (Treatment E) in order to obtain additional data on the material used in the fuselage component. Results are reported on various tests carried out on the fuselage component stringers. The section concludes with a summary of the quality control tests that were made to evaluate the experimentally treated yarn used in this program.

A. Fabrication of End-Attachment Test Specimens
(A. A. Pallozzi, Union Carbide)

The original end-attachment design for the fuselage component was described in Section IX C of the Third Annual Report;[3] Figure 151 of the Third Annual Report shows the design of the end-attachment test specimens used to evaluate the attachment concept. Tests of one tension specimen and one compression specimen (see Section IX H of the Third Annual Report) indicated the need for introducing loads into the cap and sides of the stringers as well as into the flanges. The design was modified by adding glass-reinforced plastic (GRP) laminates over the stringer caps; the modified design is shown in the final fuselage component drawing (Figure 149 (b) of the Third Annual Report).

So that both the modified design and the treated "Thornel" 50 fiber used in the component might be evaluated, two end-attachment test specimens were fabricated. The fabrication procedure was similar to that described in Section IX D-3 of the Third Annual Report, except for the modified design and

the use of treated "Thornel" 50 fiber. In the tensile specimen, six layers of Narmco-550 adhesive glass fiber prepreg* (style 181 glass cloth) were used to cover the stringer caps; eight layers were used for the compressive test specimen.

The lay-up configuration, dimensions, and physical properties of the end-attachment test specimens are listed in Table IV. The tensile end-attachment specimen was made with Treatment C fibers, and the compression specimen utilized primarily Treatment E fibers. The compressive strengths of stringer specimens cut from the ends of two of the stringers used on the tensile specimen were in the upper part of the range of values obtained for stringers made with treated fibers.

Weight analyses of the two end-attachment test specimens are given in Table V. Properties of the fibers used in the end-attachment test specimens are given in Section IV E. Both specimens were tested by Bell Aerosystems, as discussed in the next section.

TABLE V

WEIGHT ANALYSIS FOR END-ATTACHMENT TEST PANELS

Item	Weight (lb) Panel No. SP50-3	Panel No. SP50-4
Plate and Stringers	0.371	0.446
Glass Buildup 0.050 in. Thick	.175	.134
GRP Laminate & Prepreg Buildup 0.420 in. Thick	1.213	1.232
Glass Layers Over Stringer Caps	.159	.231
Aluminum End Plates	.796	.870
Material Removed in Drilling Holes for Fasteners	---	- .092
Fasteners	---	.583
Total Weight	2.71*	3.40

*Panel SP50-3 was shipped without fasteners.

*Product of Whittaker Corporation, Narmco Materials Division.

TABLE IV

DIMENSIONS AND PHYSICAL PROPERTIES
OF END-ATTACHMENT TEST SPECIMENS

Stiffened Panel No.	Part No.	Lay-up (deg)	Density ρ (lb/in.^{3})	Area A (in.^{2})	Ply Thick. $\bar{t}$ (10^{-3}in.)	Fiber Content V_f (v/o)	Void Content V_v (v/o)	Young's Mod. E (10^6psi)	AE (10^6lb)	Coupon Compression σ (10^3psi)	Fiber Treatment No.
SP50-3 Tension Specimen											
	P50-212	90,15	.0487	.227	10.2	42	4	---	---	---	C
	H50-213	10,10	.0515	.0764	9.8	56	3	19.8	1.51	57.	C
	H50-214	10,10	.0508	.0761	9.8	55	4	21.2	1.61	53.	C
	H50-215	10,10	.0510	.0763	9.8	54	3	19.3	1.47	---	C
SP50-4 Compression Specimen											
	P50-223	90,15	.0533	.260	11.8	55	0	---	---	---	D & E
	H50-262	10,10	.0522	.0880	11.3	56	2	23.0	2.03	---	E
	H50-264	10,10	.0520	.0890	11.4	56	2	22.9	2.04	---	E
	H50-263	10,10	.0522	.0886	11.4	55	2	23.1	2.05	---	E

Notes:
(a) P50 and H50 denote plates and hat-shaped stringers made from a treated "Thornel" 50 fiber and ERL 2256/MPDA epoxy resin.
(b) Lay-up
90,15 → (90°,15°,-15°,90°)
10,10 → (10°,-10°,-10°,10°)

B. Tests of End-Attachment Specimens
(Dr. K. H. Sayers and D. P. Hanley, Bell Aerosystems)

Two stiffened panels with built-up ends were tested in tension and compression to evaluate a modification which was made in the end-attachment design for the fuselage component. A description of this modification and of the panel fabrication is given in Section IV A. The tests also served to evaluate further the increase in performance due to the use of a treated "Thornel" 50 fiber.

1. Tension Panel

The first specimen was tested in tension at load increments of 100 lb; gages were read during load-holds. A very slight amount of cracking was heard above a load of 8000 lb, probably due to loading of the fiber glass as evidenced by slight discontinuities in the output of gages mounted on the buildup. Ultimate failure occurred suddenly at 15,000 lb after approximately 15 sec at that load. This load corresponded to a load per inch of panel width of $(N_x)_{ult} = 2710$ lb/in.

Examination of strain gage data showed that panel bending was greatly reduced compared with the previous "Thornel" 40 tensile test and was comparable with that observed in tests of the various compression panels (overstraining on skin side). The gage outputs showed that, near their ends, the stringers were loading as intended. All gage outputs remained linear (no creep was observed). Figure 17 shows typical measured strain distributions.

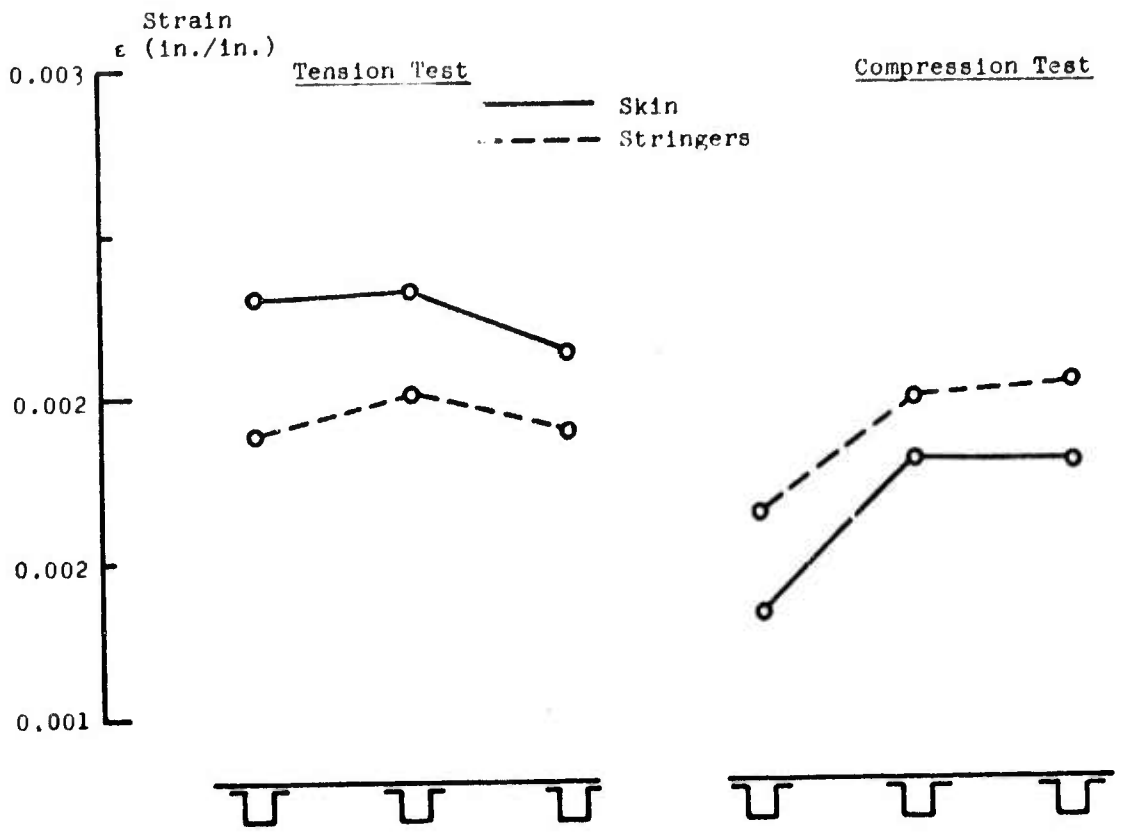

Figure 17. Treated "Thornel" 50 Panel Strains at P = 14,000 lb

Failures of both the skin and stringers in the tension test (Figure 18) appeared to be of the tensile type (not the shear type observed before). Some slight "stepping" was observed, although the "steps" were smaller than those seen in the compression tests.

Results of the tension panel failure analysis are given in Table VI. Calculations based on the assumption that strains at the fracture were the same as those at the panel center show that the average stringer tensile stress at failure was 46,200 psi and that of the skin 19,500 psi. These values are significantly less than the values expected for coupons cut from flat panels with the same fiber content and fiber properties as those of the stringers and skin on the stiffened panel (62,000 psi for the stringer lay-up and 30,000 psi for the skin lay-up, based on data given in Section IV C). Analytically predicted strengths are 64,000 psi for the stringers and 25,000 psi for the skin. Although it is not known with certainty whether the stringers or the skin failed first, it is more probable that failure first occurred in the stringers. Possible causes of lower-than-expected stringer strength are nonuniformities due to composite fabrication, non-uniform stress loading of the stringers, and internal microcracks in the stringers.

TABLE VI

ANALYSIS OF TREATED "THORNEL" 50 TENSION TEST

Panel Number SP50-3

N_x (ult) = 2710 lb/in.

Element	t (in.)	V_F (%)	E (Computed) (psi)	Average Failure Strain ε (in./in.)	Estimated Stress at Failure (psi)
Skin	0.041	42	9.8×10^6	0.00242	19,500
Stringers	0.039	55	25.1×10^6	0.00224	46,200

	Overall Panel Stiffness, P/ε (lb)	E_{eq} (psi)
Computed	7.97×10^6	17.5×10^6
Test	$15{,}000/0.00242 = 6.20 \times 10^6$*	13.6×10^6*
	$15{,}000/0.00224 = 6.70 \times 10^6$**	14.7×10^6**

*Based on strain in skin.

**Based on strain in stringer.

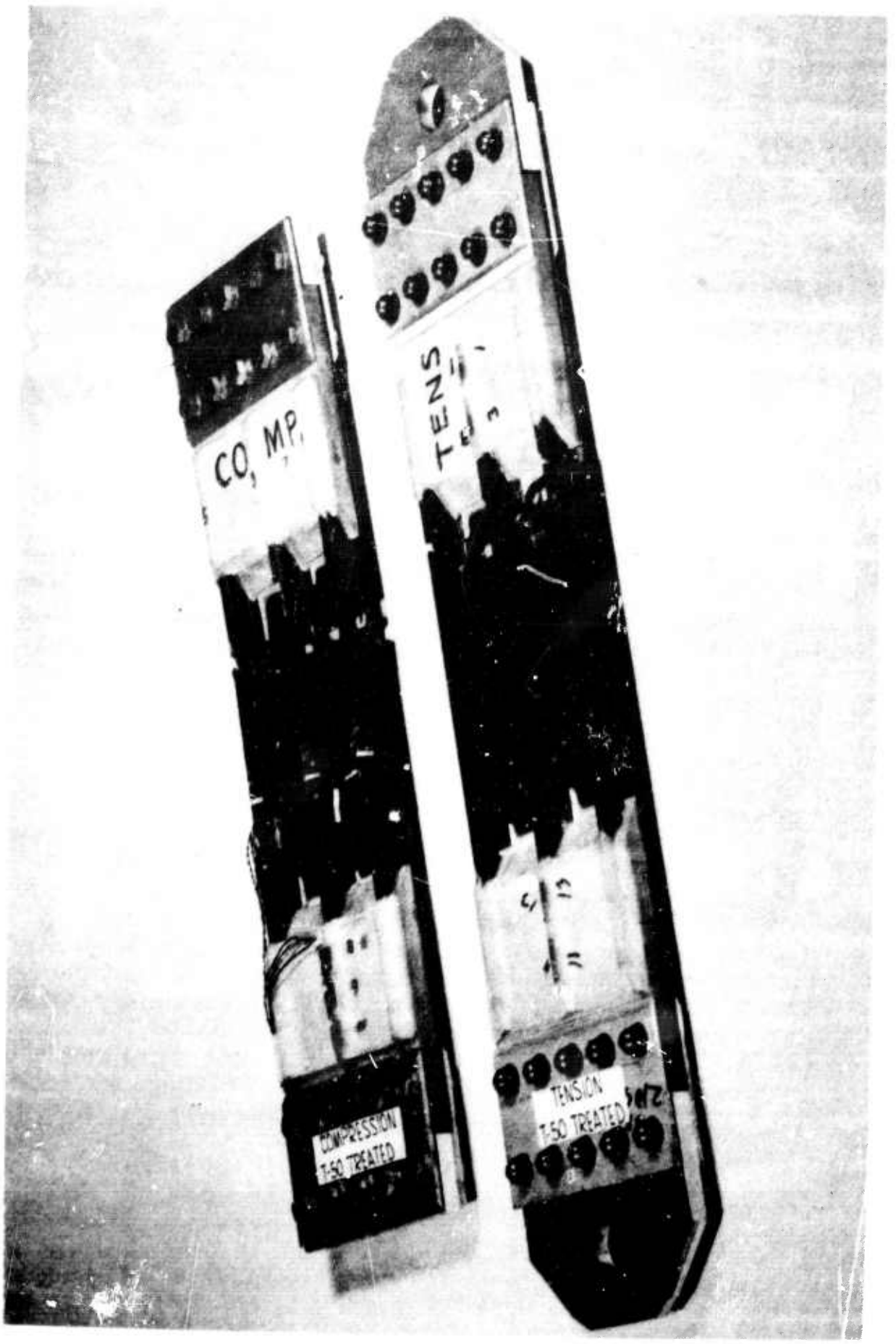

Figure 18. Treated "Thornel" 50 End-Attachment Specimens After Test.

The equivalent modulus of the tension panel, computed on the basis of a nominal 50 million psi modulus fiber, is 17.5 (in units of million psi). Because of eccentricities in loading, the strains in the skin and stringers were unequal. If one makes the assumption that the average panel strain is given by

$$\varepsilon = \frac{(A_{st}\ E_{st}\ \varepsilon_{st})\ \varepsilon_{st} + (A_{sk}\ E_{sk}\ \varepsilon_{sk})\ \varepsilon_{sk}}{A_{st}\ E_{st}\ \varepsilon_{st} + A_{sk}\ E_{sk}\ \varepsilon_{sk}}, \qquad \text{(IV B-1)}$$

where "st" denotes the stringers and "sk" denotes the skin, the actual panel modulus is estimated to be

$$E = \frac{P}{(A_{st} + A_{sk})\,\varepsilon} = 14.4 \times 10^6 \text{ psi}, \qquad \text{(IV B-2)}$$

based on calculated values of E_{st} and E_{sk} and measured values of the other quantities. The difference between this value and the computed modulus of 17.5 can be accounted for by the fact that the modulus of the fibers used in the panel was only 42.4 (see Section IV E). Thus, the computed panel modulus, based on the measured fiber modulus, is 17.5 x 42.4/50 = 14.9, a value which is only 3 percent greater than the estimated actual panel modulus. The computed stringer modulus, based on the measured fiber modulus, is 25.1 x 42.4/50 = 21.3, which is 6 percent greater than the average measured stringer modulus of 20.1.

2. Compression Panel

Since, in the tension test, the panel skin strained more than the stringers did, two extra layers of glass fiber prepreg were draped over the stringer caps and the GRP laminate block in the fabrication of the compression specimen. The specimen was tested in compression with 500 lb load increments, the gages again being read during load-holds. The amount of panel bending was similar to that observed in the tension test, although reversed in sign and direction (overstraining on stringer side), as may be seen in Figure 17. Therefore, in the fuselage shell component fabrication, only one extra layer of glass prepreg was used in the end buildup.

No cracking was heard during this compression test. The skin buckled prior to failure. Initial skin buckling occurred at approximately 12,500 lb or an $(N_x)_{I.B.}$ = 2250 lb/in. Ultimate failure, near the center of the panel, occurred at a load of 17,000 lb, corresponding to 3070 lb/in. The failure mode appeared similar to that of the tension panel (Figure 18).

Results of the compression panel failure analysis are given in Table VII. The calculated stringer and skin stresses at failure were 45,000 and 17,600 psi. The strength of the stringers was near the average for stringers made with treated fibers. The strengths expected for coupons cut from flat panels with the same fiber content and fiber properties as those of the stringers and skin on the stiffened panel are 64,000 psi for the stringer lay-up and 35,000 psi for the skin lay-up, based on data given in Section IV C. Analytically predicted strengths are 53,200 psi for the stringers and 32,900 psi for the skin. Comparison of these numbers with stresses in the stiffened panel at failure indicates that the stringers failed first.

TABLE VII

ANALYSIS OF TREATED "THORNEL" 50 COMPRESSION TEST

Panel Number SP50-4

N_x (I.B.) ~ 2250 lb/in. N_x (ult) = 3070 lb/in.

Element	t (in.)	V_F (%)	E (Computed) (psi)	Average Failure Strain ε (in./in.)	Estimated Stress at Failure (psi)
Skin	0.047	55	12.6×10^6	0.00188	17,600
Stringers	0.045	56	25.6×10^6	0.00236	45,000

	Overall Panel Stiffness, P/ε (lb)	E_{eq} (psi)
Computed	10.1×10^6	19.2×10^6
Test	17,000/0.00188 = 9.04×10^6*	17.2×10^6*
	17,000/0.00236 = 7.20×10^6**	13.7×10^6**

*Based on strain in skin.

**Based on strain in stringer.

The computed equivalent modulus of the compression panel is 19.2 (in units of million psi) based on the nominal fiber modulus of 50; the computed panel modulus is 17.7 based on the average measured moduli of the fibers in the skin and stringers

(45.4 and 46.6, respectively). The actual panel modulus has been estimated from measured strains of the stringers and skin at a load level of 8500 lb, prior to initial buckling, and at the ultimate load of 17,000 lb, well into the post-buckled condition. At a load of 8500 lb, the estimated panel modulus is 15.7; in the post-buckled condition at 17,000 lb load, the estimated panel modulus is 14.5, a decrease of 8 percent. The reason that the estimated panel modulus (15.7) prior to initial buckling is 11 percent less than the modulus (17.7) computed with the actual fiber moduli is not known. These results, together with the tension panel results, suggest that the stiffened panel is several percent stiffer in tension than in compression. However, in both cases, the equivalent panel modulus can be computed within approximately 10 percent provided the calculations are based on true (rather than design) panel dimensions, fiber contents, and fiber moduli. The average stringer modulus measured by a sonic resonant vibration test is 23.0. This value is only 4 percent less than the value of 23.9 computed with the actual stringer fiber modulus.

C. Tests of Flat Panels

(I. Mackay, Dr. D. G. Proctor, and Dr. G. B. Spence, Union Carbide)

Basic mechanical property data were reported in Section IX F of the Third Annual Report([3]) for "Thornel" 50/ERL 2256 composites made with fibers which had received experimental treatments to improve the composite shear strength. Properties were given for a unidirectional lay-up, the (90°,15°,-15°,90°) skin lay-up, and the (10°,-10°,-10°,10°) stringer lay-up. During this period, the fiber treatment process was being modified and improved. For plates made with fibers which received Treatment B, the tensile strength was less than the compressive strength in all three lay-up configurations. A less severe treatment (Treatment C) was developed. Measurements made on the 7-ply (0°) plate P50-211 made with this fiber indicated a much better balance between tensile and compressive properties, but the tensile strength was still slightly less than the compressive strength. A slightly less severe treatment was introduced (Treatment D); later, changes were made to improved uniformity (Treatment E). Almost all of the fibers used in the stringers and skin of the fuselage component received either Treatment D or Treatment E.

As a final evaluation of the fibers used in the component, plates were made with fibers which received Treatment E; the resin system was Union Carbide's ERL 2256/MPDA. Physical and mechanical properties measured on coupons cut from flat panels with the unidirectional, skin, and stringer lay-up configurations are listed in Tables IX, X, and XI. An explanation of the notation and units used in these tables is given in Table VIII. Test procedures were the same as those described in previous reports.([1],[2],[3])

TABLE VIII

SYMBOLS AND UNITS USED IN TABLES OF COMPOSITE PROPERTIES

Symbol	Item and Unit
Est. Compr.	Estimated compressive properties. See text for explanation.
Sp. No.	Specimen number
Str. No.	Stringer number
Str. Loc.	Location of stringer in the fuselage component
Treat.	Treatment--experimental fiber treatments were labeled alphabetically
A	Specimen cross-sectional area ($in.^2$)
AE	Cross-sectional area times modulus (10^6lb)
E_{son}	Young's modulus determined from sonic resonant frequency (10^6psi)
E_{sta}	Young's modulus determined from a static test with strain gages (10^6psi)
ℓ/t	Span to depth ratio in short beam shear test
M_f	Fiber mass content in composite (percent)
t	Ply thickness (10^{-3}in.)
V_f	Fiber volume content in composite (percent)
V_v	Void volume content in composite (percent)
ε	Fracture strain (percent)
ρ	Density ($lb/in.^3$)
σ	Fracture strength (10^3psi)
τ_{SBS}	Short beam shear strength by 3-point flexural test (10^3psi)
DIM	Specimen destroyed in machining or mounting
NB	Not broken--specimen was compressed until restraining cap hit side fixture
C0	Compressive specimen oriented in 0° direction
C90	Compressive specimen oriented in 90° direction
FC	Fiber content specimen
S0	Short beam shear specimen oriented in 0° direction
T0	Tensile specimen oriented in 0° direction
T90	Tensile specimen oriented in 90° direction

TABLE IX

DIMENSIONS AND PROPERTIES OF THORNEL COMPOSITES WITH 8-PLY (0°) LAY-UP

Plate No. & Treat.	Sp. No.	ρ	t	E_{son}	E_{sta}	ν	σ	ε	Notes
P50-220 E	T0-1	.0521	11.1	25.6	26.0	0.34	62	0.22	
	T0-2	.0522	11.1	25.8	---	---	76	---	
	T0-3	.0532	10.9	26.6	---	---	75	---	
	T0-4	.0530	10.8	25.8	---	---	89	---	
	T90-1	.0534	10.2	0.96	0.94	.012	2.4	0.26	
	C0-1	.0527	10.8	25.6	25.4	---	---	---	
	C0-2	.0525	10.8	25.1	---	---	71	---	
	C0-3	.0528	10.8	25.9	---		81	---	
	C90-1	.0531	10.4	0.95	0.94	0.011	---	---	
	C90-5	.0534	9.6	0.97	---	---	>13	---	NB
	C90-6	.0535	9.6	0.97	---	---	>19	---	NB

Sp. No.	ρ	t	M_f	V_f	V_v	Location
FC-1	.0528	---	64.56	56.8	0.9	Bottom
FC-2	.0527	---	65.28	57.4	1.2	Top

Sp. No.	ℓ/t	τ_{SBS}	Sp. No.	ℓ/t	τ_{SBS}
S0-1	5.0	5.58	S0-8	5.1	6.00
S0-2	5.0	5.66	S0-9	5.2	6.10
S0-3	5.0	5.76	S0-10	5.2	5.84
S0-4	5.0	5.81	S0-11	5.2	5.73
S0-5	5.0	5.91	S0-12	5.1	5.95
S0-6	5.0	5.96		---	---
S0-7	5.1	5.78	Avg.	5.1	5.84

See Table VIII for explanation of symbols and units.

TABLE X

DIMENSIONS AND PROPERTIES OF "THORNEL" COMPOSITES
WITH (90°,15°,-15°,90°) LAY-UP

Plate No. & Treat.	Sp. No.	ρ	t	E_{son}	E_{sta}	ν	σ	ε
P50-221 E	T0-1	.0517	11.2	9.8	9.8	0.081	32	0.33
	T0-2	.0516	11.5	9.5	---	---	30	---
	T0-3	.0517	11.7	9.8	---	---	34	---
	T0-4	.0510	12.1	9.9	---	---	34	---
	T90-1	---	12.9	---	11.3	0.084	44	0.35
	T90-2	---	12.8	---	---	---	38	---
	C0-1	.0512	12.8	9.5	10.2	0.076	---	---
	C0-2	.0511	12.1	10.0	---	---	30	---
	C0-3	.0510	13.0	9.1	---	---	29	---
	C0-4	.0513	12.2	10.0	---	---	36	---
	C0-5	.0509	13.1	9.0	---	---	27	---
	C90-1	.0510	12.7	11.5	11.6	.077	---	---
	C90-2	.0509	12.7	11.3	---	---	40	---
	C90-3	.0508	13.4	11.2	---	---	39	---
	C90-4	.0509	13.3	11.1	---	---	41	---

Sp. No.	ρ	t	M_f	V_f	V_v	Location
FC-1	.0503	---	54.52	46.4	2.0	Bottom
FC-2	.0511	---	58.53	50.7	1.5	Top

See Table VIII for explanation of symbols and units.

TABLE XI

DIMENSIONS AND PROPERTIES OF "THORNEL" COMPOSITES WITH (10°,-10°,-10°,10°) LAY-UP

Plate No. & Treat.	Sp. No.	ρ	t	E_{son}	E_{uta}	ν	σ	ε	Notes
P50-222 E	T0-1	.0525	9.4	24.2	24.1	1.03	65	0.25	
	T0-2	.0518	9.8	24.1	---	---	65	---	
	T0-3	.0519	9.9	24.0	---	---	64	---	
	T0-4	.0519	10.1	23.7	---	---	71	---	
	T90-1	.0532	9.7	0.94	---	---	---	---	DIM
	T90-2	.0523	10.0	0.95	---	---	---	---	DIM
	C0-1	.0524	9.1	23.4	25.2	1.16	---	---	
	C0-2	.0524	9.4	24.2	---	---	71	---	
	C0-3	.0530	9.5	24.8	---	---	66	---	
	C0-4	.0532	9.5	25.6	---	---	67	---	
	C0-5	.0530	9.7	25.1	---	---	77	---	
	C90-1	.0530	10.0	0.97	1.01	0.029	---	---	
	C90-2	.0528	10.1	0.99	---	---	25	---	
	C90-3	.0529	10.2	1.01	---	---	26	---	
	C90-4	.0528	10.3	1.02	---	---	22	---	

Sp. No.	ρ	t	M_f	V_f	V_v	Location
FC-1	.0527	---	70.75	62.1	3.1	Left side
FC-2	.0526	---	69.03	60.4	2.8	Center

Sp. No.	ℓ/t	τ_{SBS}
S0-1	5.0	6.20
S0-2	5.0	6.64
S0-3	4.9	6.22
S0-4	5.0	6.36
S0-5	5.0	6.53
S0-6	4.9	6.17
Avg.	5.0	6.35

See Table VIII for explanation of symbols and units.

For each lay-up (plates P50-220, 221, and 222), the tensile and compressive strengths in the zero-degree direction were essentially equal; thus, the desired balance between tensile and compressive properties was achieved for flat panels. Compared with the present panels, the earlier panels (with fiber Treatment B) had higher shear strength and lower tensile strengths for both the unidirectional and the angle-ply configurations. The compressive strengths for fibers with Treatments B and E were approximately equal, contrary to the expectation that the compressive strength would increase with increasing shear strength (i.e., with better fiber-matrix bonding). Both fiber treatments increased the compressive strength of free-standing stringers by 40 percent or more compared with the strength of stringers made with untreated fibers.

The measured skin and stringer properties strongly support properties predicted previously at Bell Aerosystems for use in their preliminary shell stress analysis (see Section III B). The predicted skin and stringer strengths, given in Table II, were based on unidirectional laminate properties which were essentially those for plate P50-211 made with Treatment C fibers. The measured and predicted skin and stringer strengths are in reasonable agreement, except, perhaps, for a somewhat higher measured stringer compressive strength than that predicted. As expected, measured and predicted elastic properties agree within a few percent if the differences in fiber properties and resin content are taken into account.

D. Tests of Stringers

(I. Mackay, Dr. D. G. Proctor, and Dr. G. B. Spence, Union Carbide)

The thirty-one stringers for the fuselage component were selected from a total of forty-five stringers on the basis of various quality control tests. In addition, the arrangement of the thirty-one stringers around the fuselage shell was governed by the stringer properties. The test methods and results for all forty-five stringers are discussed in Section IV D-1. The criteria for selecting and arranging the thirty-one stringers and a summary of their properties are given in Section IV D-2.

1. Properties of Forty-Five Stringers

Each stringer was originally over 50 inches long. A stringer coupon approximately two inches long was cut from each end and tested in compression by the test procedure described in Section IX F-2 of the Third Annual Report.[3] Also, a specimen for fiber volume content was cut from one end. The central section was trimmed to a length of 43.92 inches.

The stringer properties are listed in Table XII. The first column of this table gives the stringer number that was assigned sequentially as the stringers were made. If the stringer was used in the fuselage component, the stringer location, as shown on the fuselage component drawing in Figure 149(a) in the Third Annual Report, is also listed in the first column. The second column lists the specimen number: C0-1 and C0-2 denote the two compressive strength coupons and the three-digit number denotes the central 44-inch stringer section. The density ρ was determined from the ratio of the mass to the volume; the volume was measured by water immersion. The average cross-sectional area A was calculated from the specimen volume divided by the specimen length. The average ply thickness $\bar{t}$ was obtained by dividing the cross-sectional area A by 4 x 1.951, where 4 is the number of plies and 1.951 inch is the perimeter length of the stringer. The sixth column lists the sonic Young's modulus E_{son}, calculated from the longitudinal resonant vibration of the 44-inch long stringer; and the next column lists the AE_{son} product.

The eighth and ninth columns give the compressive strength and strength-to-density ratio for each coupon. The ultimate fracture strain in compression (tenth column) was calculated from the formula

$$\varepsilon = \sigma/E = P/AE, \qquad \text{(IV D-1)}$$

where P is the ultimate load. Two assumptions were made. First, since previous work had shown that the stress-strain curve for stringers is nearly linear, it was assumed that the sonic modulus could be used in place of the secant modulus at failure. Also, previous work had shown that the AE product varies much less along the length of a stringer than does either A or E individually. Therefore, the second assumption was made that (AE_{son}) for the coupon could be replaced by (AE_{son}) for the 44-inch stringer, as listed in column seven.

The last two columns in Table XII give an estimated compressive fracture strain and specific strength for the 44-inch long stringer. The estimates were obtained in the following way. The cross-sectional areas of the two coupons cut from the ends of a stringer were often significantly larger than the cross-sectional area of the middle 44-inch long part. Also, the compressive strength and fracture strain tended to decrease with decreasing cross-sectional area. The average trend of fracture strain versus cross-sectional area was used to reduce the average fracture strains of each pair of coupons by an amount proportional to the difference between the cross-sectional area of the coupons and that of the middle 44-inch part. The estimated specific strength was calculated from the estimated fracture strains and the measured Young's modulus and density of the middle 44-inch long stringer part.

TABLE XII

STRINGER PROPERTIES

Str. No. & Str. Loc.	Sp. No.	ρ	A	$\bar{t}$	E_{son}	AE_{son}	Coupon Compr. σ	Coupon Compr. σ/ρ	Coupon Compr. ε	Est. Str. Compr. ε	Est. Str. Compr. σ/ρ
H50-220	CO-1	.0516	.099	12.7	---	---	59.9	1.16	.336	---	---
---	220	.0514	.100	12.8	17.6	1.76	---	---	---	.33	1.13
	CO-2	.0508	.114	14.6	---	---	50.8	1.00	.329	---	---
H50-225	CO-1	.0510	.130	16.7	---	---	56.9	1.12	.378	---	---
---	225	.0514	.112	14.4	17.5	1.96	---	---	---	.33	1.12
	CO-2	.0513	.132	16.9	---	---	55.0	1.07	.371	---	---
H50-223	CO-1	.0507	.100	12.8	---	---	51.7	1.02	.302	---	---
---	223	.0513	.097	12.4	17.2	1.72	---	---	---	.30	1.01
	CO-2	.0515	.099	12.7	---	---	54.3	1.06	.313	---	---
H50-216	CO-1	.0521	.083	10.6	---	---	51.3	.98	.273	---	---
17	216	.0518	.083	10.6	19.3	1.60	---	---	---	.28	1.02
	CO-2	.0518	.085	10.9	---	---	53.5	1.03	.284	---	---
H50-219	CO-1	.0521	.082	10.5	---	---	50.7	.97	.254	---	---
15	219	.0523	.082	10.5	19.8	1.63	---	---	---	.27	1.00
	CO-2	.0521	.084	10.8	---	---	53.7	1.03	.278	---	---
H50-221	CO-1	.0514	.100	12.8	---	---	43.5	.85	.266	---	---
19	221	.0518	.089	11.4	18.3	1.63	---	---	---	.27	.94
	CO-2	.0520	.092	11.8	---	---	49.0	.94	.277	---	---
H50-232	CO-1	.0515	.076	9.7	---	---	51.7	1.00	.276	---	---
16	232	.0515	.073	9.4	19.5	1.43	---	---	---	.26	.98
	CO-2	.0515	.074	9.5	---	---	53.2	1.03	.274	---	---
H50-218	CO-1	.0525	.085	10.9	---	---	52.1	.99	.262	---	---
---	218	.0527	.085	10.9	19.7	1.69	---	---	---	.26	.97
	CO-2	.0500	.122	15.6	---	---	31.0	.62	.224	---	---
H50-224	CO-1	.0518	.087	11.1	---	---	47.4	.92	.270	---	---
18	224	.0521	.079	10.1	19.2	1.52	---	---	---	.26	.96
	CO-2	.0516	.087	11.1	---	---	50.3	.98	.287	---	---
H50-238	CO-1	.0517	.068	8.7	---	---	52.0	1.01	.244	---	---
21	238	.0520	.072	9.2	20.3	1.46	---	---	---	.25	.98
	CO-2	.0515	.076	9.7	---	---	54.6	1.06	.284	---	---

TABLE XII (Cont'd.)
STRINGER PROPERTIES

Str. No. & Str. Loc.	Sp. No.	ρ	A	$\bar{t}$	E_{son}	AE_{son}	Coupon Compr. σ	Coupon Compr. σ/ρ	Coupon Compr. ϵ	Est. Str. Compr. ϵ	Est. Str. Compr. σ/ρ
H50-240	C0-1	.0516	.076	9.7	---	---	53.4	1.04	.279	---	---
20	240	.0520	.073	9.4	19.7	1.45	---	---	---	.25	.95
	C0-2	.0527	.069	8.8	---	---	50.5	.96	.241	---	---
H50-229	C0-1	.0525	.072	9.2	---	---	53.1	1.01	.248	---	---
14	229	.0525	.076	9.7	20.5	1.55	---	---	---	.24	.94
	C0-2	.0522	.073	9.4	---	---	42.0	.80	.197	---	---
H50-244	C0-1	.0519	.071	9.1	---	---	47.3	.91	.233	---	---
13	244	.0522	.072	9.2	20.2	1.45	---	---	---	.24	.93
	C0-2	.0516	.071	9.1	---	---	48.5	.94	.239	---	---
H50-230	C0-1	.0525	.070	9.0	---	---	52.1	.99	.253	---	---
8	230	.0530	.069	8.8	20.9	1.44	---	---	---	.23	.91
	C0-2	.0525	.075	9.6	---	---	47.3	.90	.246	---	---
H50-228	C0-1	.0526	.070	9.0	---	---	45.4	.86	.221	---	---
24	228	.0527	.071	9.1	20.3	1.44	---	---	---	.23	.88
	C0-2	.0523	.076	9.7	---	---	49.8	.95	.263	---	---
H50-259	C0-1	.0504	.093	11.9	---	---	38.7	.77	.234	---	---
31	259	.0514	.083	10.6	18.7	1.55	---	---	---	.23	.84
	C0-2	.0513	.078	10.0	---	---	47.4	.92	.239	---	---
H50-243	C0-1	.0526	.071	9.1	---	---	49.7	.95	.222	---	---
27	243	.0525	.071	9.1	21.5	1.53	---	---	---	.22	.90
	C0-2	.0519	.077	9.9	---	---	43.4	.84	.219	---	---
H50-227	C0-1	.0519	.080	10.3	---	---	49.9	.96	.269	---	---
23	227	.0531	.070	9.0	21.2	1.49	---	---	---	.22	.88
	C0-2	.0525	.074	9.5	---	---	51.9	.99	.256	---	---
H50-235	C0-1	.0532	.063	8.1	---	---	47.6	.89	.196	---	---
30	235	.0517	.074	9.5	20.7	1.53	---	---	---	.22	.88
	C0-2	.0516	.072	9.2	---	---	47.5	.92	.222	---	---
H50-255	C0-1	.0515	.071	9.1	---	---	56.0	1.09	.274	---	---
3	255	.0520	.070	9.0	20.6	1.45	---	---	---	.22	.87
	C0-2	.0509	.078	10.0	---	---	43.0	.85	.232	---	---

TABLE XII (Cont'd.)

STRINGER PROPERTIES

Str. No. & Str. Loc.	Sp. No.	ρ	A	$\bar{t}$	E_{son}	AE_{son}	Coupon Compr. σ	Coupon Compr. σ/ρ	Coupon Compr. ε	Est. Str. Compr. ε	Est. Str. Compr. σ/ρ
H50-222	CO-1	.0519	.086	11.0	---	---	43.8	.84	.232	---	---
7	222	.0523	.080	10.3	20.2	1.62	---	---	---	.22	.85
	CO-2	.0525	.084	10.8	---	---	45.2	.86	.235	---	---
H50-253	CO-1	.0522	.074	9.5	---	---	46.6	.89	.214	---	---
2	253	.0528	.074	9.5	21.6	1.61	---	---	---	.21	.86
	CO-2	.0517	.075	9.6	---	---	45.9	.89	.213	---	---
H50-252	CO-1	.0516	.075	9.6	---	---	49.6	.96	.266	---	---
29	252	.0524	.067	8.6	20.8	1.40	---	---	---	.21	.83
	CO-2	.0509	.074	9.5	---	---	46.3	.91	.246	---	---
H50-254	CO-1	.0520	.077	9.9	---	---	48.3	.93	.218	---	---
---	254	.0533	.075	9.6	23.0	1.71	---	---	---	.20	.86
	CO-2	.0516	.084	10.8	---	---	52.3	1.01	.256	---	---
H50-236	CO-1	.0515	.072	9.2	---	---	45.9	.89	.237	---	---
6	236	.0525	.064	8.2	22.1	1.40	---	---	---	.20	.84
	CO-2	.0526	.066	8.5	---	---	51.5	.98	.242	---	---
H50-241	CO-1	.0522	.068	8.7	---	---	42.8	.82	.200	---	---
9	241	.0530	.068	8.7	21.3	1.46	---	---	---	.20	.80
	CO-2	.0535	.064	8.2	---	---	48.1	.90	.212	---	---
H50-248	CO-1	.0515	.072	9.2	---	---	47.5	.92	.239	---	---
26	248	.0525	.068	8.7	21.1	1.44	---	---	---	.20	.80
	CO-2	.0520	.065	8.3	---	---	39.8	.77	.179	---	---
H50-249	CO-1	.0515	.072	9.2	---	---	42.6	.83	.225	---	---
---	249	.0540	.066	8.5	20.7	1.36	---	---	---	.20	.77
	CO-2	.0515	.068	8.7	---	---	40.6	.79	.203	---	---
H50-237	CO-1	.0513	.073	9.4	---	---	39.7	.77	.198	---	---
5	237	.0521	.069	8.8	21.3	1.47	---	---	---	.19	.78
	CO-2	.0519	.071	9.1	---	---	44.8	.86	.216	---	---
H50-239	CO-1	.0518	.071	9.1	---	---	44.4	.86	.216	---	---
28	239	.0525	.068	8.7	21.5	1.47	---	---	---	.19	.78
	CO-2	.0508	.071	9.1	---	---	44.1	.87	.214	---	---

TABLE XII (Cont'd.)

STRINGER PROPERTIES

Str. No. & Str. Loc.	Sp. No.	ρ	A	$\bar{t}$	E_{son}	AE_{son}	Coupon Compr. σ	Coupon Compr. σ/ρ	Coupon Compr. ε	Est. Str. Compr. ε	Est. Str. Compr. σ/ρ
H50-231	CO-1	.0526	.070	9.0	---	---	35.1	.67	.162	---	---
11	231	.0529	.070	9.0	21.1	1.49	---	---	---	.19	.76
	CO-2	.0512	.075	9.6	---	---	48.3	.94	.243	---	---
H50-242	CO-1	.0520	.070	9.0	---	---	39.9	.77	.189	---	---
10	242	.0523	.071	9.1	20.8	1.47	---	---	---	.19	.76
	CO-2	.0519	.071	9.1	---	---	50.5	.97	.245	---	---
H50-245	CO-1	.0521	.069	8.8	---	---	51.6	.99	.234	---	---
25	245	.0534	.071	9.1	21.3	1.51	---	---	---	19	.76
	CO-2	.0513	.076	9.7	---	---	33.1	.65	.167	---	---
H50-247	CO-1	.0517	.074	9.5	---	---	47.0	.91	.243	---	---
1	247	.0519	.073	9.4	19.7	1.43	---	---	---	.19	.72
	CO-2	.0514	.075	9.6	---	---	33.8	.66	.178	---	---
H50-233	CO-1	.0512	.078	10.0	---	---	51.3	1.00	.292	---	---
---	233	.0536	.061	7.8	22.3	1.37	---	---	---	.18	.75
	CO-2	.0516	.076	9.7	---	---	51.1	.99	.285	---	---
H50-257	CO-1	.0528	.071	9.1	---	---	52.0	.99	.251	---	---
4	257	.0527	.068	8.7	21.8	1.48	---	---	---	.18	.74
	CO-2	.0523	.068	8.7	---	---	39.6	.76	.181	---	---
H50-261	CO-1	.0517	.085	10.9	---	---	48.1	.93	.271	---	---
22	261	.0523	.074	9.5	20.5	1.51	---	---	---	.18	.70
	CO-2	.0509	.079	10.1	---	---	34.6	.68	.181	---	---
H50-234	CO-1	.0512	.067	8.6	---	---	41.4	.81	.189	---	---
---	234	.0519	.068	8.7	21.7	1.48	---	---	---	.17	.71
	CO-2	.0515	.066	8.5	---	---	32.8	.64	.146	---	---
H50-260	CO-1	.0524	.076	9.7	---	---	42.6	.81	.205	---	---
12	260	.0524	.072	9.2	21.8	1.57	---	---	---	.17	.71
	CO-2	.0517	.076	9.7	---	---	40.1	.78	.193	---	---
H50-256	CO-1	.0527	.061	7.8	---	---	40.0	.76	.172	---	---
---	256	.0530	.061	7.8	23.4	1.42	---	---	---	.16	.71
	CO-2	.0526	.060	7.7	---	---	35.8	.68	.151	---	---
H50-246	CO-1	.0522	.067	8.6	---	---	39.6	.76	.187	---	---
---	246	.0529	.063	8.1	22.5	1.42	---	---	---	.15	.64
	CO-2	.0521	.066	8.5	---	---	31.7	.61	.148	---	---

TABLE XII (Cont'd.)
STRINGER PROPERTIES

Str. No. & Str. Loc.	Sp. No.	ρ	A	$\bar{t}$	E_{son}	AE_{son}	Coupon Compr. σ	Coupon Compr. σ/ρ	Coupon Compr. ε	Est. Str. Compr. ε	Est. Str. Compr. σ/ρ
H50-251	C0-1	.0520	.065	8.3	---	---	44.8	.86	.215	---	---
---	251	.0525	.063	8.1	21.4	1.36	---	---	---	.15	.61
	C0-2	.0519	.063	8.1	---	---	30.5	.59	.142	---	---
H50-258	C0-1	.0530	.059	7.6	---	---	38.4	.72	.146	---	---
---	258	.0530	.064	8.2	24.1	1.55	---	---	---	.14	.64
	C0-2	.0526	.062	7.9	---	---	31.6	.60	.126	---	---
H50-226	C0-1	.0520	.078	10.0	---	---	27.2	.52	.146	---	---
---	226	.0543	.061	7.8	23.7	1.45	---	---	---	.14	.61
	C0-2	.0528	.071	9.1	---	---	40.9	.77	.199	---	---
H50-250	C0-1	.0512	.067	8.6	---	---	36.8	.72	.185	---	---
---	250	.0533	.061	7.8	22.2	1.34	---	---	---	.14	.58
	C0-2	.0516	.067	8.6	---	---	34.8	.68	.173	---	---

See Table VIII for explanation of symbols and units.

The estimated numbers are probably still slightly high due to the use of the average cross-sectional area rather than the minimum cross-sectional area; however, this error is thought to be less than five percent.

Through an oversight, the fiber content samples were submitted for HNO_3 digestion before their density was obtained. The use of an estimated density causes an uncertainty of approximately two units, i.e., a typical value is $V_f = 50 \pm 2$ percent. Table XIII lists the fiber volume contents of a coupon cut from each of the forty-five stringers. Because of the variation in cross-sectional area, the fiber volume content of the 44-inch long stringer will probably be, in many cases, a few percentage points higher than that of the coupon.

TABLE XIII

FIBER VOLUME CONTENT OF STRINGERS

Stringer Number	Fiber Volume (percent)	Stringer Number	Fiber Volume (percent)	Stringer Number	Fiber Volume (percent)
H50-216	43	H50-232	48	H50-247	50
-218	36	-233	48	-248	55
-219	46	-234	47	-249	53
-220	38	-235	52	-250	53
-221	40	-236	54	-251	55
-222	44	-237	51	-252	49
-223	44	-238	52	-253	51
-224	48	-239	51	-254	57
-225	44	-240	45	-255	44
-226	49	-241	53	-256	55
-227	52	-242	50	-257	55
-228	55	-243	56	-258	55
-229	50	-244	55	-259	50
-230	53	-245	57	-260	55
-231	51	-246	58	-261	52

2. Selection of Stringers for the Fuselage Component

Several factors were taken into consideration in selecting the set of thirty-one stringers from the original set of forty-five stringers. One criterion was a large fracture strain. Therefore,

the stringer data were arranged according to decreasing estimated compressive fracture strains. The resulting sequence is that used in Table XII. Stringers with excessively high (over 1.70 x 10^6 lb) or excessively low (under 1.40 x 10^6 lb) AE products were eliminated in order to achieve AE values as uniform as possible. Additional and sometimes conflicting requirements included large values of compressive specific strength, large cross-sectional area, uniform wall thickness, and high fiber tensile strength.

The stringers to be subjected to high tension and compression stresses in the final ultimate strength test of the component were specially chosen. This procedure was justified on the basis that, with more fabrication experience, the average properties of stringers made in the future will equal or excel the best properties of the present set of stringers. The stringers in the top quadrant of the component will be subjected to the greatest compressive stresses. These eight stringers were selected first from the set of thirty-one stringers on the basis of high compressive fracture strain, high compressive specific strength, and large and uniform cross-sectional area. The stringers in the bottom quadrant of the component will be subjected to the highest tensile stresses. These seven stringers were selected next on the basis of high fiber tensile strength and large and uniform cross-sectional area. The remaining sixteen stringers were placed in the left and right quadrants. Within each quadrant, the stringers were arranged to balance, to the extent possible, the AE products.

The properties of the thirty-one stringers selected for the fuselage component are summarized in Table XIV in the sequence in which the stringers were placed around the component. Stringer Position 1 is at the bottom of the cylinder and will be subjected to the largest tensile stress during the final test of the component. Stringers 16 and 17 are at the top of the component and will be subjected to the largest compressive stress during the final test. In addition to the data reported, wall thickness measurements were made at seven points around the stringer perimeter and at five stations along the stringer length of the stringers in the top and bottom quadrants to check on wall thickness uniformity.

The average coupon compressive strength of the six stringers which will be located in the highest compressive stress field during the final test of the component (Positions 14 through 19) is 49,900 psi. This value is 10 percent higher than the stringer ultimate strength of 45,000 psi achieved in the test of the end-attachment compression panel (Table VII). The average fiber tensile strength of the seven stringers which will be located in the highest tensile stress field is lower than the tensile strength of the fibers used in the end-attachment tension panel. These results, together with the fact that the tensile end-attachment panel failed at a lower load than that for the compression panel and the fact that the tensile strength was less than the compressive strength

of coupons from the (10°,-10°,-10°,10°) panel (see Table XI), suggest that the fuselage stringer strengths will be approximately 45,000 and 50,000 psi in tension and compression, respectively. Consequently, the predicted stringer allowables given in Table II will be reduced in future shell stress analyses.

TABLE XIV

SUMMARY OF STRINGER PROPERTIES
FOR FUSELAGE COMPONENT

Str. Loc.	Str. No.	Est. Compr. ε	Est. Compr. σ/ρ	Measured AE	Measured E	Measured E_{bon}	Coupon Compr. σ	Fiber Tensile σ	Fiber Shear τ
Bottom Quadrant									
29	H50-252	.21	.83	1.40	8.6	20.8	48.0	199	5.68
30	-235	.22	.88	1.53	9.5	20.7	47.6	186	5.74
31	-259	.23	.84	1.55	10.6	18.7	43.0	193	5.60
1	-247	.19	.72	1.43	9.4	19.7	40.4	199	5.68
2	-253	.21	.86	1.61	9.5	21.6	46.2	190	5.95
3	-255	.22	.87	1.45	9.0	20.6	49.5	193	5.60
4	-257	.18	.74	1.48	8.7	21.8	45.8	193	5.60
Left Quadrant									
5	-237	.19	.78	1.47	8.8	21.3	42.2	186	5.74
6	-236	.20	.84	1.40	8.2	22.1	48.7	186	5.74
7	-222	.22	.85	1.62	10.3	20.2	44.5	170	5.51
8	-230	.23	.91	1.44	8.8	20.9	49.7	177	6.56
9	-241	.20	.80	1.46	8.7	21.3	45.4	168	6.96
10	-242	.19	.76	1.47	9.1	20.8	45.2	177	6.35
11	-231	.19	.76	1.49	9.0	21.1	41.7	177	6.58
12	-260	.17	.71	1.57	9.2	21.8	41.4	193	5.60
Top Quadrant									
13	-244	.24	.93	1.45	9.2	20.2	47.9	173	6.55
14	-229	.24	.94	1.55	9.7	20.5	47.6	177	6.56
15	-219	.27	1.00	1.63	10.5	19.8	52.2	170	6.51
16	-232	.26	.98	1.43	9.4	19.5	52.4	186	5.74
17	-216	.28	1.02	1.60	10.6	19.3	52.4	169	6.33
18	-224	.26	.96	1.52	10.1	19.2	48.8	176	6.50
19	-221	.27	.94	1.63	11.4	18.3	46.2	170	6.51
20	-240	.25	.95	1.45	9.4	19.7	52.0	168	6.96
Right Quadrant									
21	-238	.25	.98	1.46	9.2	20.3	53.3	186	5.74
22	-261	.18	.70	1.51	9.5	20.5	41.4	193	5.60
23	-227	.22	.88	1.49	9.0	21.2	50.9	177	6.44
24	-228	.23	.88	1.44	9.1	20.3	47.6	177	6.47
25	-245	.19	.76	1.51	9.1	21.3	42.4	171	6.69
26	-248	.20	.80	1.44	8.7	21.1	43.6	199	5.68
27	-243	.22	.90	1.53	9.1	21.5	46.6	170	6.77
28	-239	.19	.78	1.47	8.7	21.5	44.2	186	5.74

See Table VIII for explanation of symbols and units.

E. Tests of Treated Graphite Fibers

(I. Mackay, Dr. D. G. Proctor, and Dr. G. B. Spence, Union Carbide)

Two quality control tests were used to evaluate the treated yarn for the test panels and fuselage component. The tests were the strand test for fiber tensile strength and modulus and the torsion rod test for composite shear strength. The test methods are described in Section IV E-1. The fiber properties are listed in Section IV E-2 and discussed in Section IV E-3.

1. Test Methods

The tensile strength and modulus of the treated "Thornel" 50 fibers were determined from a strand test with a 9.2 inch gauge length. Each yarn evaluation consisted of testing five individual strands which had been impregnated with ERL 2256/MPDA epoxy resin and cured. In conjunction with the strand test, the fiber density and cross-sectional area were also measured.

The torsion rod test was selected in order to provide a test that would always give a shear failure. For each yarn evaluation, one composite rod approximately 0.15 inch in diameter and 5 inches long was fabricated with resin system ERL 2256/MPDA. The fiber content of the rods was not measured, but the number of yarns per rod was chosen to give a nominal fiber volume of 50 percent. The composite Young's modulus was obtained from the longitudinal resonant frequency of the 5-inch rod. The rod was then cut in half, and each half tested separately in static torsion to obtain two values of the composite shear strength.

A more extensive discussion of the strand and torsion tests is given in Sections V A and V B of the Third Annual Report. Detailed test procedures are given in Reference 5.

2. Summary of Yarn Properties

The "Thornel" 50 graphite yarn was treated in one-half pound (nominal) lots. One strand, torsion, and density evaluation was made at the beginning of each lot and, also, at the end of each lot. Thus, for each lot of yarn, the following data were obtained: ten individual values each of strand tensile strength and Young's modulus, four individual values of composite torsional shear strength, and two individual values each of composite Young's modulus and fiber density.

The plates, stringers, and fuselage skin were each made from several lots of yarn, usually from six lots. For each yarn property, five statistical parameters were calculated to characterize

the average value for all lots of yarn in the composite and to give two different measures of the spread of the values. The five parameters are:

(1) Avg. of Yarn Maxs. - the average of the largest individual value measured on each lot of yarn;

(2) Max. of Yarn Avgs. - the largest of the average value for each lot of yarn;

(3) Avg. of Yarn Avgs. - the average of the average value for each lot of yarn, equal to the average of all individual values for all lots of yarn in the composite;

(4) Min. of Yarn Avgs. - the smallest of the average value for each lot of yarn; and

(5) Avg. of Yarn Mins. - the average of the smallest individual value measured on each lot of yarn.

The summary of experimentally-treated "Thornel" 50 yarn properties is given in Table XV. In this table, the nomenclature is the same as that used elsewhere in this report; for example, "P50-211" denotes plate number 211 made with "Thornel" 50 and "H50-212" denotes hat-shaped stringer number 212 made with "Thornel" 50. The stringers used to stiffen flat panels and those used for the fuselage component are listed sequentially in the order in which they were fabricated. The table concludes with the properties of the yarn used in the fuselage component skin.

The composite items listed in Table XV were made from fifty-seven lots of yarn. The average yarn properties (the average of the individual lot yarn averages) for all fifty-seven lots are given in Table XVI; standard deviations are also listed.

3. Discussion of Yarn Properties

a. All Lots of Treated Yarn

The average Young's modulus of all lots of experimentally-treated "Thornel" 50 yarn is 43.8×10^6 psi (see Table XVI), as determined by a strand tensile test. This value does not mean that the yarn has a lower modulus than that specified for "Thornel" 50 because the modulus of "Thornel" 50 yarn is certified on the basis of a single-filament test. Comparative testing by Union Carbide has indicated that the modulus determined by a single-filament test is approximately 7.5×10^6 psi higher than that determined by the strand test used in this program. Thus, the average modulus of the yarn used in this program would have been approximately 51.3×10^6 psi if measured by a single-filament test, a value slightly higher than the average for "Thornel" 50. The average strand tensile strength of the yarn used in this program is 180,000 psi, and the composite

shear strength is 6,100 psi. Since the void content of the torsion rods was several percent, the true composite shear strength is probably several hundred psi higher than 6,100 psi.

TABLE XV

SUMMARY OF EXPERIMENTALLY TREATED "THORNEL" 50
YARN PROPERTIES FOR EACH COMPOSITE PART

Composite Part	Strength (10^3 psi) Strand Tensile	Strength (10^3 psi) Composite Torsion	Young's Modulus (10^6 psi) Strand	Young's Modulus (10^6 psi) Comp. Rod	Yarn Density (g/cm^3)
USED IN P50-211,212					
AVG. OF YARN MAXS.	231.	7.20	43.6	21.8	
MAX. OF YARN AVGS.	288.	7.58	43.7	22.0	
AVG. OF YARN AVGS.	208.	6.78	42.4	21.8	1.64
MIN. OF YARN AVGS.	149.	5.97	41.2	21.7	
AVG. OF YARN MINS.	176.	6.34	41.5	21.8	
USED IN P50-220					
AVG. OF YARN MAXS.	224.	6.47	47.6	23.0	
MAX. OF YARN AVGS.	229.	6.53	49.1	24.0	
AVG. OF YARN AVGS.	184.	5.95	45.5	22.7	1.66
MIN. OF YARN AVGS.	147.	5.39	42.6	22.2	
AVG. OF YARN MINS.	142.	5.46	43.9	22.3	
USED IN P50-221,223 FOR 15 DEGREE PLIES					
AVG. OF YARN MAXS.	228.	5.84	46.5	23.0	
MAX. OF YARN AVGS.	260.	6.40	48.6	24.0	
AVG. OF YARN AVGS.	192.	5.45	45.4	22.7	1.66
MIN. OF YARN AVGS.	164.	3.64	42.6	22.0	
AVG. OF YARN MINS.	153.	5.11	43.9	22.4	
USED IN P50-221,223 FOR 90 DEGREE PLIES					
AVG. OF YARN MAXS.	219.	6.37	44.2	22.4	
MAX. OF YARN AVGS.	220.	5.86	44.2	23.0	
AVG. OF YARN AVGS.	176.	5.65	42.1	22.1	1.61
MIN. OF YARN AVGS.	124.	5.44	37.8	21.2	
AVG. OF YARN MINS.	133.	4.81	39.5	21.7	

Continued

TABLE XV (CONTINUED)

Composite Part	Strength (10^3 psi) Strand Tensile	Strength (10^3 psi) Composite Torsion	Young's Modulus (10^6 psi) Strand	Young's Modulus (10^6 psi) Comp. Rod	Yarn Density (g/cm³)
USED IN H50-222					
AVG. OF YARN MAXS.	240.	5.69	47.4	23.2	
MAX. OF YARN AVGS.	260.	6.40	48.6	24.0	
AVG. OF YARN AVGS.	200.	5.22	46.4	22.9	1.66
MIN. OF YARN AVGS.	164.	3.64	44.0	22.2	
AVG. OF YARN MINS.	160.	4.83	44.8	22.6	
USED IN H50-212,213,214,215					
AVG. OF YARN MAXS.	231.	7.20	43.6	21.8	
MAX. OF YARN AVGS.	288.	7.58	43.7	22.0	
AVG. OF YARN AVGS.	208.	6.78	42.4	21.8	1.64
MIN. OF YARN AVGS.	149.	5.97	41.2	21.7	
AVG. OF YARN MINS.	176.	6.34	41.5	21.8	
USED IN H50-216					
AVG. OF YARN MAXS.	207.	6.85	46.6	24.0	
MAX. OF YARN AVGS.	178.	7.20	48.4	25.2	
AVG. OF YARN AVGS.	169.	6.33	44.8	23.6	1.66
MIN. OF YARN AVGS.	160.	5.44	41.7	22.6	
AVG. OF YARN MINS.	134.	5.69	43.2	23.1	
USED IN H50-218,219,220,221,222,223					
AVG. OF YARN MAXS.	208.	7.10	47.2	24.0	
MAX. OF YARN AVGS.	178.	7.20	48.4	25.2	
AVG. OF YARN AVGS.	170.	6.51	45.4	23.5	1.65
MIN. OF YARN AVGS.	160.	5.76	42.9	22.6	
AVG. OF YARN MINS.	132.	5.78	43.8	23.1	

Continued

TABLE XV (CONTINUED)

Composite Part	Strength (10^3 psi) Strand Tensile	Strength (10^3 psi) Composite Torsion	Young's Modulus (10^6 psi) Strand	Young's Modulus (10^6 psi) Comp. Rod	Yarn Density (g/cm^3)
USED IN H50-224,225					
AVG. OF YARN MAXS.	218.	7.24	46.0	24.1	
MAX. OF YARN AVGS.	205.	7.20	48.4	25.2	
AVG. OF YARN AVGS.	176.	6.50	44.6	23.5	1.65
MIN. OF YARN AVGS.	160.	5.90	40.8	21.7	
AVG. OF YARN MINS.	131.	5.71	42.5	22.9	
USED IN H50-226,227					
AVG. OF YARN MAXS.	221.	7.27	46.7	24.2	
MAX. OF YARN AVGS.	205.	7.20	48.4	24.5	
AVG. OF YARN AVGS.	177.	6.44	45.3	23.7	1.68
MIN. OF YARN AVGS.	160.	5.90	40.8	21.7	
AVG. OF YARN MINS.	133.	5.65	43.2	23.2	
USED IN H50-228					
AVG. OF YARN MAXS.	218.	7.23	46.1	24.1	
MAX. OF YARN AVGS.	205.	7.20	46.6	24.5	
AVG. OF YARN AVGS.	177.	6.47	44.7	23.6	1.67
MIN. OF YARN AVGS.	160.	5.90	40.8	21.7	
AVG. OF YARN MINS.	131.	5.85	42.4	23.0	
USED IN H50-229,230					
AVG. OF YARN MAXS.	214.	7.29	46.4	24.4	
MAX. OF YARN AVGS.	205.	7.20	46.8	25.4	
AVG. OF YARN AVGS.	177.	6.56	45.0	23.9	1.68
MIN. OF YARN AVGS.	160.	5.90	40.8	21.7	
AVG. OF YARN MINS.	135.	5.96	42.9	23.4	

Continued

TABLE XV (CONTINUED)

Composite Part	Strength (10^3 psi) Strand Tensile	Strength (10^3 psi) Composite Torsion	Young's Modulus (10^6 psi) Strand	Young's Modulus (10^6 psi) Comp. Rod	Yarn Density (g/cm^3)
USED IN H50-231					
AVG. OF YARN MAXS.	214.	7.31	46.0	24.3	
MAX. OF YARN AVGS.	205.	7.20	46.8	25.4	
AVG. OF YARN AVGS.	177.	6.58	44.7	23.8	1.67
MIN. OF YARN AVGS.	160.	5.90	40.8	21.7	
AVG. OF YARN MINS.	134.	5.93	42.9	23.3	
USED IN H50-232,233,234,235,236,237,238,239					
AVG. OF YARN MAXS.	210.	6.27	46.0	23.0	
MAX. OF YARN AVGS.	190.	6.08	46.6	22.8	
AVG. OF YARN AVGS.	186.	5.74	42.9	22.6	1.65
MIN. OF YARN AVGS.	176.	5.58	41.4	22.4	
AVG. OF YARN MINS.	158.	5.40	39.0	22.2	
USED IN H50-240,241					
AVG. OF YARN MAXS.	205.	7.45	45.3	23.3	
MAX. OF YARN AVGS.	178.	8.98	46.6	24.4	
AVG. OF YARN AVGS.	168.	6.96	43.6	23.0	1.68
MIN. OF YARN AVGS.	163.	5.44	41.2	20.8	
AVG. OF YARN MINS.	137.	6.59	41.7	22.7	
USED IN H50-242					
AVG. OF YARN MAXS.	207.	6.86	45.6	23.1	
MAX. OF YARN AVGS.	190.	8.98	46.6	24.4	
AVG. OF YARN AVGS.	177.	6.35	43.3	22.8	1.66
MIN. OF YARN AVGS.	163.	5.44	41.2	20.8	
AVG. OF YARN MINS.	148.	5.99	40.4	22.5	

Continued

TABLE XV (CONTINUED)

Composite Part	Strength (10^3 psi) Strand Tensile	Strength (10^3 psi) Composite Torsion	Young's Modulus (10^6 psi) Strand	Young's Modulus (10^6 psi) Comp. Rod	Yarn Density (g/cm^3)
USED IN H50-243					
AVG. OF YARN MAXS.	199.	7.14	43.7	22.4	
MAX. OF YARN AVGS.	184.	8.98	44.9	23.8	
AVG. OF YARN AVGS.	170.	6.77	41.7	22.0	1.64
MIN. OF YARN AVGS.	163.	5.44	39.6	20.8	
AVG. OF YARN MINS.	141.	6.43	39.7	21.6	
USED IN H50-244					
AVG. OF YARN MAXS.	201.	6.91	43.0	21.8	
MAX. OF YARN AVGS.	184.	6.96	42.6	22.0	
AVG. OF YARN AVGS.	173.	6.55	41.0	21.3	1.60
MIN. OF YARN AVGS.	166.	6.12	39.6	20.8	
AVG. OF YARN MINS.	144.	6.25	38.8	20.9	
USED IN H50-245					
AVG. OF YARN MAXS.	200.	7.05	43.4	22.1	
MAX. OF YARN AVGS.	184.	8.98	44.9	23.8	
AVG. OF YARN AVGS.	171.	6.69	41.4	21.7	1.62
MIN. OF YARN AVGS.	163.	5.44	39.6	20.8	
AVG. OF YARN MINS.	142.	6.36	39.4	21.3	
USED IN H50-246,247,248,249,250,251,252					
AVG. OF YARN MAXS.	246.	6.25	45.3	23.0	
MAX. OF YARN AVGS.	229.	5.86	47.2	24.0	
AVG. OF YARN AVGS.	199.	5.68	44.2	22.3	1.65
MIN. OF YARN AVGS.	186.	5.39	40.4	21.4	
AVG. OF YARN MINS.	147.	5.12	42.8	21.7	

Continued

TABLE XV (CONTINUED)

Composite Part	Strength (10^3 psi) Strand Tensile	Strength (10^3 psi) Composite Torsion	Young's Modulus (10^6 psi) Strand	Young's Modulus (10^6 psi) Comp. Rod	Yarn Density (g/cm^3)
USED IN H50-253					
AVG. OF YARN MAXS.	224.	6.42	46.0	22.8	
MAX. OF YARN AVGS.	229.	6.42	47.2	24.0	
AVG. OF YAPN AVGS.	190.	5.95	44.8	22.3	1.66
MIN. OF YARN AVGS.	170.	5.39	40.4	21.4	
AVG. OF YARN MINS.	153.	5.45	43.5	21.9	
USED IN H50-254					
AVG. OF YARN MAXS.	203.	6.59	46.7	22.6	
MAX. OF YARN AVGS.	193.	6.42	46.5	22.4	
AVG. OF YARN AVGS.	182.	6.21	45.4	22.3	1.67
MIN. OF YARN AVGS.	170.	6.00	44.2	22.2	
AVG. OF YARN MINS.	159.	5.78	44.3	22.1	
USED IN H50-255,256,257,258,259,260,261					
AVG. OF YARN MAXS.	231.	5.91	48.5	23.4	
MAX. OF YARN AVGS.	208.	6.20	49.6	23.4	
AVG. OF YARN AVGS.	193.	5.60	47.2	23.0	1.67
MIN. OF YARN AVGS.	172.	5.15	45.9	22.6	
AVG. OF YARN MINS.	154.	5.30	45.8	22.5	
USED IN H50-262,263,264					
AVG. OF YARN MAXS.	209.	6.33	47.8	23.2	
MAX. OF YARN AVGS.	195.	6.40	49.1	24.0	
AVG. OF YARN AVGS.	178.	5.93	46.6	22.9	1.66
MIN. OF YARN AVGS.	164.	5.62	44.0	22.2	
AVG. OF YARN MINS.	146.	5.56	45.1	22.6	

Continued

TABLE XV (CONTINUED)

Composite Part	Strength (10^3 psi) Strand Tensile	Strength (10^3 psi) Composite Torsion	Young's Modulus (10^6 psi) Strand	Young's Modulus (10^6 psi) Comp. Rod	Yarn Density (g/cm^3)
USED IN FUSELAGE SKIN FOR 15 DEGREE PLIES					
AVG. OF YARN MAXS.	199.	6.75	44.8	22.6	
MAX. OF YARN AVGS.	193.	7.24	46.5	22.6	
AVG. OF YARN AVGS.	179.	6.34	43.4	22.1	1.65
MIN. OF YARN AVGS.	170.	5.66	39.8	21.2	
AVG. OF YARN MINS.	153.	5.94	42.2	21.7	
USED IN FUSELAGE SKIN FOR 90 DEGREE PLIES					
AVG. OF YARN MAXS.	200.	6.45	44.8	22.7	
MAX. OF YARN AVGS.	220.	6.75	45.4	23.2	
AVG. OF YARN AVGS.	164.	5.85	42.0	22.3	1.63
MIN. OF YARN AVGS.	124.	5.34	37.3	21.2	
AVG. OF YARN MINS.	119.	5.24	38.3	21.9	

TABLE XVI

AVERAGE PROPERTIES OF ALL LOTS OF EXPERIMENTALLY TREATED "THORNEL" 50 YARN

Property	Average Value	Standard Deviation
Strand Young's Modulus (10^6 psi)	43.8	2.8
Strand Tensile Strength (10^3 psi)	180.	27.
Torsion Rod:		
Shear Strength (10^3 psi)	6.1	0.8
Composite Young's Mod. (10^6 psi)	22.6	1.0
Composite Shear Mod. (10^6 psi)	.635	.032
Yarn Density (lb/in.^{3})	.0596	.0014
Yarn Cross-Section Area (10^{-5} in.^{2})	6.96	.23

Test results reported in previous sections on stiffened panels indicate that the load-carrying capability of the fuselage component made with the treated fibers will be several tens-of-percent higher than that of a component made with untreated fiber. Therefore, the use of a fiber with the best experimental treatment available at the time of component fabrication was fully justified, in spite of an undesirable loss in fiber tensile strength. Since that time, major improvements in fiber treatments have been made; the present commercially available "Thornel" 50S treated fiber has tensile and shear strengths much higher than those of the experimentally-treated yarn used in the fuselage component.

The strand test for fiber modulus and strength was introduced just prior to the start of the treated fiber testing program. The Young's modulus of the torsion rods was determined from the longitudinal resonant frequency in order to assess the modulus translation efficiency. The modulus translation efficiency, η_f, was calculated for each rod in the following way. The fiber volume

content of each rod was calculated from the measured cross-sectional area of the yarn:

$$V_f = A_f/A_r. \qquad \text{(IV E-1)}$$

where

A_f = area of 128 yarns in rod
= 128 x average area of one yarn and

A_r = area of rod = 0.01767 $in.^2$

The modulus translation efficiency was calculated from the formula

$$\eta_f = [E_c - (1-V_f)\ E_m]/V_f E_f, \qquad \text{(IV E-2)}$$

where

E_c = modulus of the composite rod

E_m = modulus of the matrix = 0.6 x 10^6 psi, and

E_f = strand modulus of the yarn.

The number of yarns per rod (128) was chosen to give a nominal fiber volume content of 50 percent, the average fiber content for the fifty-seven lots of yarn was 50.4 percent, with a standard deviation of 1.7 percent. The average modulus translation efficiency was 101.3 percent with a standard deviation of 3.8 percent. Modulus translation efficiencies of greater than 100 percent have subsequently been found in other studies at Union Carbide. These results indicate that the modulus value given by the strand test was lower than the true fiber modulus. An investigation of thestrand test, conducted after the fiber treatment evaluation program was completed, has shown the need for a machine compliance correction. The effect of the correction is to increase the uncorrected strand modulus by an amount which increases with increasing fiber modulus.

The shear modulus of the torsion rods was calculated from the torsional resonant frequency with the expectation that voids and other defects which would lower the shear strength would also lower the shear modulus. However, no correlation between shear modulus and shear strength was found, and the data are not reported.

b. Unidirectional Plates

Composite tests have indicated that the translation efficiency for strength, as well as modulus, is close to 100 percent for unidirectional plates made from one uniform lot of treated "Thornel" fiber. In this program, the two unidirectional plates

(numbers P50-211 and P50-220) were each made from six lots of yarn which showed considerable variability from lot-to-lot. In order to see how composite properties would correlate with fiber properties when there is lot-to-lot variation, the Young's modulus and tensile strength for these plates were predicted with the rule-of-mixtures formulas:

$$E_c = \eta_f V_f E_f + (1-V_f) E_m, \qquad \text{(IV E-3)}$$

$$\eta_f = 1.013,$$

and

$$\sigma_c = [V_f + (1-V_f)\, E_m/E_f]\, \sigma_f. \qquad \text{(IV E-4)}$$

The predictions were made with the yarn properties listed in Table XV under the headings of "Avg. of Yarn Avgs.", "Min. of Yarn Avgs.", and "Avg. of Yarn Mins." The predicted values are compared with measured data in Table XVII. The average measured tensile moduli appear to be in better agreement with values predicted from "Avg. of Yarn Avgs." properties than with values predicted with either type of minimum yarn properties. The reverse is true for tensile strength, but the results do not indicate whether failure was initiated by one weak yarn (low value of "Min. of Yarn Avgs.") or by collective action of weak spots in all yarns (low value of "Avg. of Yarn Mins.")

TABLE XVII

COMPARISON OF PREDICTED RULE-OF-MIXTURES PROPERTIES WITH MEASURED PROPERTIES OF UNIDIRECTIONAL PLATES

Yarn Property Used in Calculation	Plate P50-211 (V_f = 48%)		Plate P50-220 (V_f = 57%)	
	Young's Modulus	Tensile Strength	Young's Modulus	Tensile Strength
Avg. of Yarn Avgs.	20.9	101	26.5	106
Min. of Yarn Avgs.	20.3	73	24.9	85
Avg. of Yarn Mins.	20.5	86	25.6	82
Measured Avgs.	21.1*	67*	26.0*	76**

*From Table XLIX of Reference 3.

**From Table IX of this report.

Units: Modulus -10^6 psi; Strength -10^3 psi

The short-beam shear strengths at approximately 5/1 span-to-depth ratio for plates P50-211 and P50-220 are within a few hundred psi of the torsion shear strength based on "Avg. of Yarn Avgs." properties. However, if the torsion shear strengths had not been reduced by the high void content of the rods, the short-beam shear strength might have been in better agreement with one of the torsion strengths based on minimum yarn properties.

c. Plates and Stringers with (±10°, ∓10°) Lay-Up

So that a comparison can be made more easily of the yarn properties for the thirty-one fuselage stringers with the yarn properties for the panels, some of the data given in Table XV have been averaged for the seven or eight stringers in each quadrant of the fuselage component. These average properties and the standard deviations are given in Table XVIII. The yarn in the bottom stringers, which were chosen for high yarn tensile strength, has 13,000 to 19,000 psi higher tensile strength than that for the top stringers. The top stringers were selected on the basis of high stringer compressive strain; since high stringer compressive strain requires high shear strength, it is not surprising that the top stringers were made with yarn with the highest torsional shear strength (6460 psi for top stringers compared with the average value of 6040 psi for the remaining stringers).

The yarn in the bottom fuselage stringers had approximately the same tensile and shear strengths as those for the yarn in the (10°,-10°,-10°,10°) plate P50-222 used for coupon tests. (One yarn with low shear strength was used accidentally in P50-222.) However, the values 193 and 5.69 x 10^3 psi for the average tensile and shear strengths of the yarn in the bottom stringers are 7 and 16 percent less than the corresponding values for the yarn in the stringers on the end-attachment panel SP50-3 tested in tension. Calculations made at Bell Aerosystems indicate the 16 percent loss in yarn shear strength should cause less than one percent loss in stringer tensile strength. Therefore, on the basis of yarn properties, the tensile strength of the bottom stringers is expected to be only a few percent less than the value of 46,200 psi calculated from the end-attachment panel tensile test.

The tensile strength of the yarn in the top fuselage stringers is approximately 13 percent less than that for the yarn in plate P50-222 and is nearly the same as that for the yarn in the stringers on the end-attachment panel SP50-4 tested in compression. The shear strength of the yarn in the top fuselage stringers is 5 to 10 percent greater than that for the yarn in plate P50-222 and in the stringers in panel SP50-4. Therefore, on the basis of yarn properties, the compressive strength of the top fuselage stringers should be a few percent greater than the value of 45,000 psi calculated from the panel compression test. This prediction is supported by the coupon compression tests for these eight stringers which gave an average compressive strength of 49,900 psi.

TABLE XVIII

AVERAGE PROPERTIES OF EXPERIMENTALLY-TREATED"THORNEL" 50 YARN IN FUSELAGE COMPONENT STRINGERS

Yarn Property	Strand Tensile Strength (10^3 psi)	Composite Torsion Strength (10^3 psi)	Strand Young's Modulus (10^6 psi)
Bottom Quadrant - 7 Stringers (Numbers 29-31, 1-4)			
Avg. of Yarn Avgs.	193(4)	5.69(.12)	45.4(1.7)
Min. of Yarn Avgs.	176(6)	5.31(.16)	42.9(2.6)
Avg. of Yarn Mins.	152(4)	5.28(.12)	43.6(2.3)
Left Quadrant - 8 Stringers (Numbers 5-12)			
Avg. of Yarn Avgs.	179(8)	6.26(.46)	44.4(1.4)
Min. of Yarn Avgs.	166(7)	5.59(.24)	42.0(1.6)
Avg. of Yarn Mins.	144(10)	5.79(.40)	41.9(2.2)
Top Quadrant - 8 Stringers (Numbers 13-20)			
Avg. of Yarn Avgs.	174(6)	6.46(.32)	44.1(1.4)
Min. of Yarn Avgs.	163(5)	5.74(.22)	41.4(1.0)
Avg. of Yarn Mins.	138(9)	5.90(.35)	42.0(1.9)
Right Quadrant - 8 Stringers (Numbers 21-28)			
Avg. of Yarn Avgs.	182(10)	6.14(.46)	43.8(1.8)
Min. of Yarn Avgs.	170(9)	5.55(.24)	41.2(1.9)
Avg. of Yarn Mins.	146(10)	5.69(.46)	41.4(2.3)
All Thirty-One Stringers			
Avg. of Yarn Avgs.	182(10)	6.15(.46)	44.4(1.7)
Min. of Yarn Avgs.	169(8)	5.56(.26)	41.8(2.0)
Avg. of Yarn Mins.	145(10)	5.68(.42)	42.2(2.3)

Numbers in parentheses are standard deviations

d. Plates and Fuselage Skin With (90°,±15°,90°) Lay-Up

The properties of the (90°,±15°,90°) laminate in the zero-degree direction depend mainly on the properties of the yarn in the ±15° plies; and better quality yarn was selected for these plies than for the 90° plies. For the ±15° plies, the tensile strength of the yarn in the fuselage skin is, roughly, 10 percent less than that of the same plies in panel P50-221 and in the skin of the end-attachment panels. The shear strength of the yarn in the ±15° plies in the fuselage skin is within the range of values for the same plies in the end-attachment and flat panels.

SECTION V

FABRICATION OF REPRESENTATIVE FUSELAGE COMPONENT

The design developed by Bell Aerosystems Company for the representative fuselage component was shown in Figure 149(a) and 149(b) in Section IX B of the Third Annual Report.[3] Section IX K of that report discusses the initial component fabrication activities on material for the stiffening rings, on the mandrel for the skin, and on the design of the stringer mold. In this section, the final fabrication activities are described. The section begins with a brief overview of the entire fabrication procedure.

A. Summary of Component Fabrication

(Dr. J. M. Criscione, Dr. G. B. Spence, and A. A. Pallozzi, Union Carbide)

The component was assembled by adhesively bonding stringers, stiffening rings, and end attachments to a tapered cylindrical skin. Prior to the component assembly, a set of forty-five stringers was molded; thirty-one of these stringers were selected for the component on the basis of quality control test results. Also, the four balsa-core rings were fabricated in a separate operation.

The skin was made on a plaster mandrel by a combination of wet winding the inner and outer 90° plies and hand lay-up of prepreg for the middle 15° plies. Before the skin was removed from the mandrel, a 50-mil thick buildup of glass reinforced plastic (GRP) was added at each end, and the outer aluminum rings were bonded to the GRP. These outer end attachments served to stabilize and protect the ends of the thin skin during the remainder of the fabrication operations.

The stringers were bonded to the inner surface of the skin in seven sets of four stringers at a time and a final set of three stringers. Next, the four balsa-core rings were bonded to the inner surface of the skin by inserting the rings from the large end of the tapered shell.

The inner end attachment was added in several steps. Five layers of GRP adhesive prepreg were applied at each end with strips that extended between and on top of the stringer flanges. Next, pre-molded slotted GRP blocks were bonded to the shell with the adhesive prepreg. The inner aluminum rings were bonded to the GRP blocks.

Bolts were added through the aluminum rings to keep the adhesive joints under compression and to provide a back-up

method of loading the component in the event of bond failure. A fairing material was added in front of the outer aluminum rings to simulate an aerodynamic surface.

Each of these operations is described in more detail in the following sections.

B. Fabrication of Hat-Shaped Stringers

The fabrication procedure used to form the hat-shaped stringers was given in Sections IX D-1 and IX K-4 of the Third Annual Report.[3] In brief, prepreg broadgoods were prepared with the experimentally treated "Thornel" 50 fiber and the ERL 2256†/MPDA epoxy resin system. Strips approximately 3.5 x 52 inches were cut at 10° and laid up to form a four ply (10°,-10°,-10°,10°) stringer preform. Approximately ten weight percent of resin was removed from the preform in a separate operation in order not to have a large resin flow in the mold that might have caused fiber wash. The preform was placed on a heatable surface, covered with bleeder cloth, and vacuum bagged (see Section IX D-1 of Reference 3 for details). The bleed out was accomplished by holding the preform under atmospheric pressure for one-half hour at 122°F (50°C).

The stringers were formed in the mold shown in Figures 19 and 20. Dimensional drawings of this mold were given in Figures 207 and 208 of Reference 3. Figure 19 is a photograph of the steel male section of the mold; the base is 4 inches wide by 54 inches long. The flange area of the mold has an 11.5-inch radius of curvature to ensure good contact between the stringer flange and the fuselage skin in the areas where the highest stresses will occur during the final testing of the component. Figure 20 shows the female mold section consisting of silicone rubber (RTV-60) contained within a steel chase. Both halves of the mold were heated by means of the heated platens of the press. More closely controlled heating of the male mold section was accomplished with a series of cartridge-type electrical heaters located in the mold base. Two temperature controllers were used to regulate the heating of each end of the mold; a multipoint recorder was used to monitor the temperature at four points along the mold. At the end of the cure cycle, the press platens were cooled with circulating water. In addition, cooling water was circulated through the ends of the steel section of the mold, as shown in Figure 19. Figure 21 shows the mold in the closed position with the temperature controllers and recorder.

In molding a stringer, a layer of nonporous Teflon-coated glass cloth* was placed on each side of the four-ply debulked preform. A layer of Mylar was placed next to each ply

*Armalon 406A-116, Product of E.I. duPont de Nemours & Company.
†Product of Union Carbide Corporation.

of glass cloth. This lay-up was placed on the rubber female mold section, and the mold was slowly closed. Because the stringers were given a post cure, minor variations in press cure schedule were allowed in order to accommodate work schedules. A typical cure schedule is given in Table XIX. The stringer was numbered and machined to its final width of 1.08 inches.

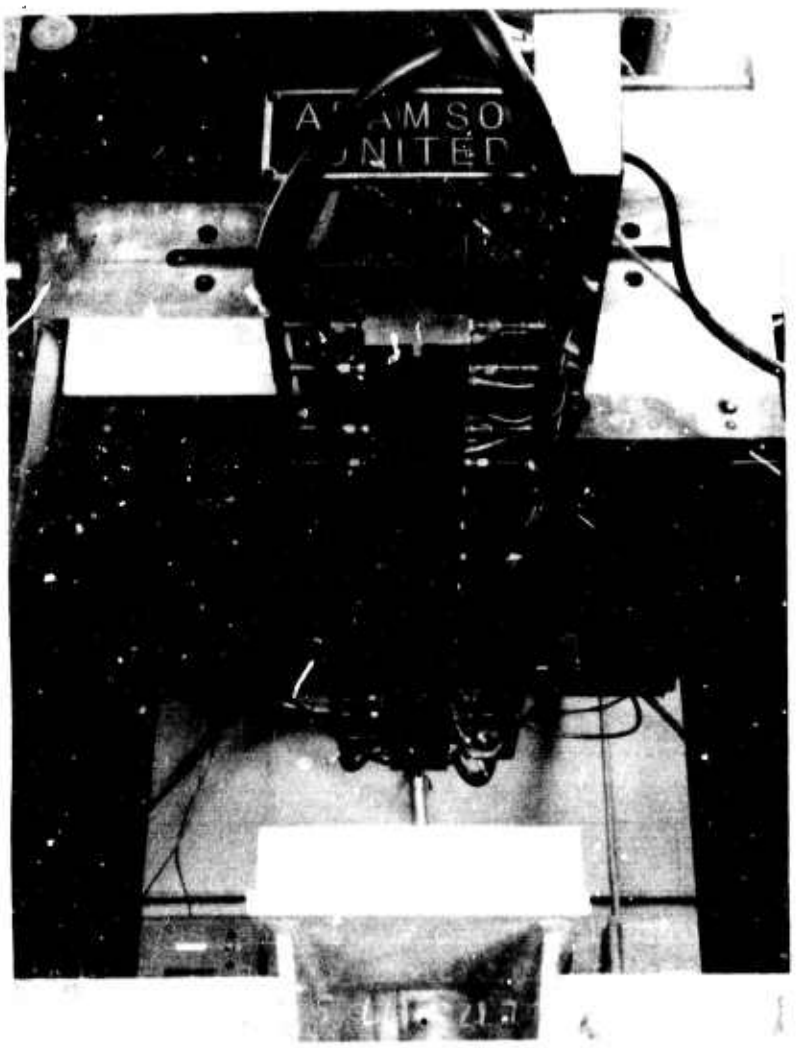

Figure 19. Photograph of Steel Section of 54-Inch Hat-Shaped Stringer Mold.

N-20364

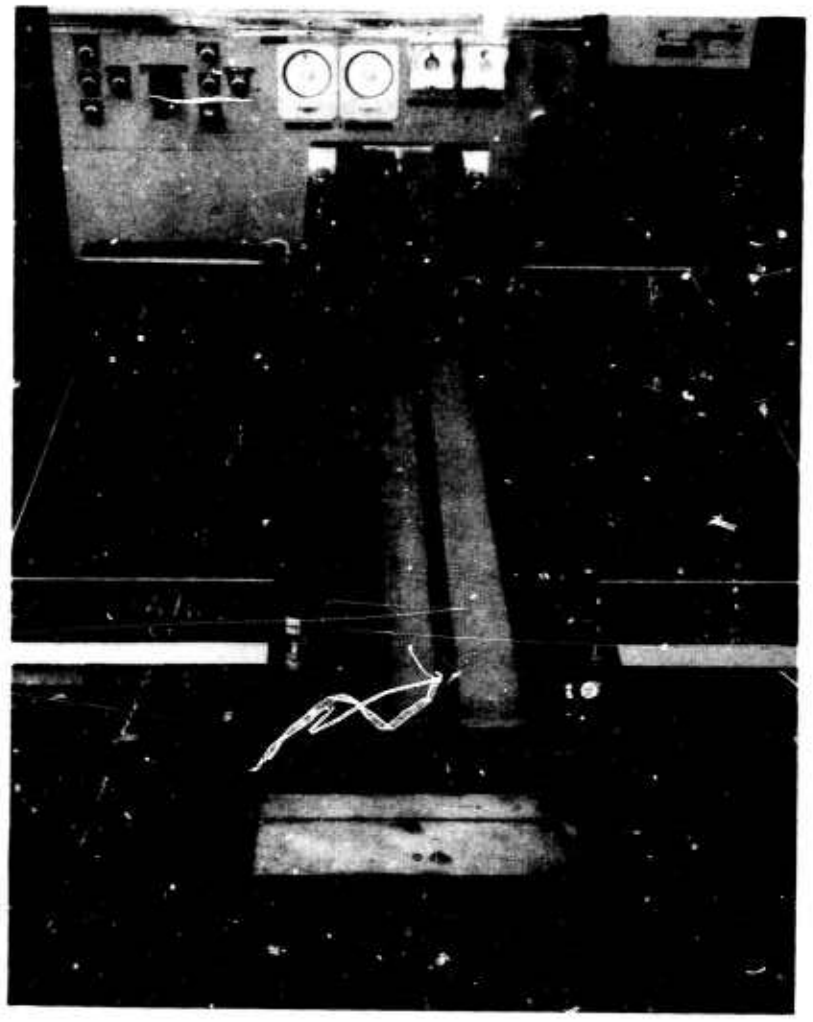

Figure 20. Photograph of Rubber Section in Steel Chase of 54-Inch Hat-Shaped Stringer Mold.

N-20363

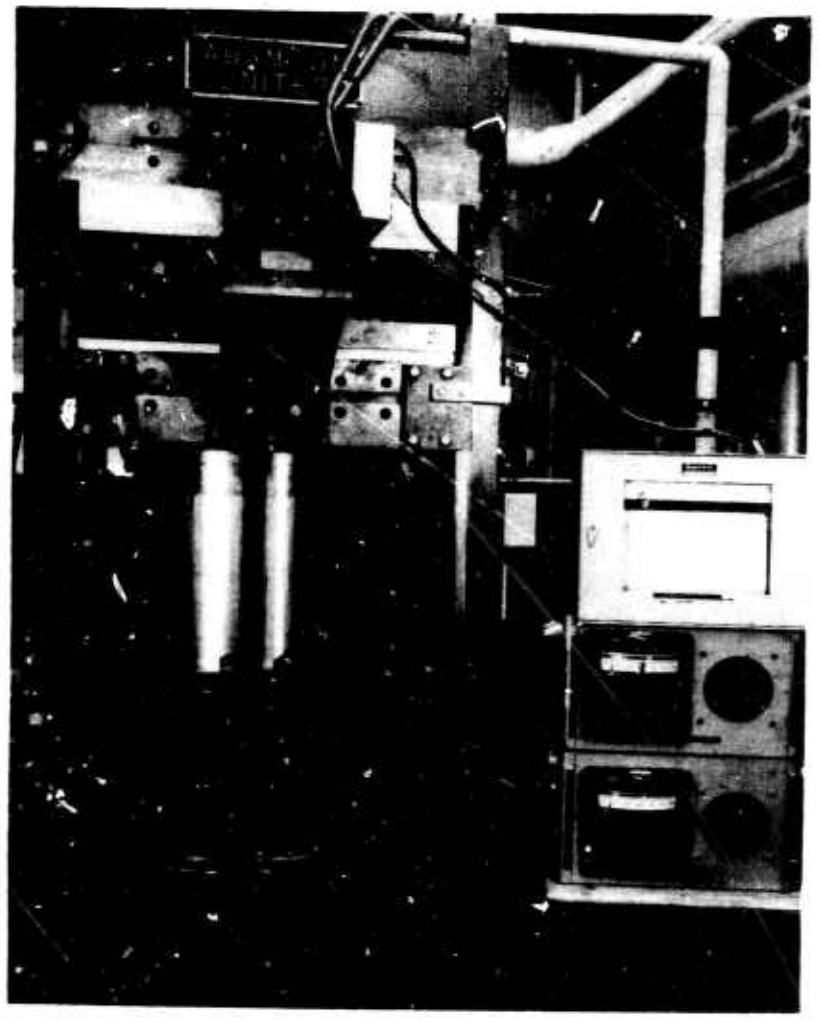

Figure 21. Molding Equipment Used to Form Hat-Shaped Stringers.

N-20362

TABLE XIX

TYPICAL CURE SCHEDULE FOR MOLDING
HAT-SHAPED STRINGERS

Press Cycle at 80 psi pressure	
RT to 240°F (116°C)	in 30 min
Hold at 240°F (116°C)	for 2 hrs
240°F (116°C) to RT	in 20 min
Post Cure Unconstrained	
320°F (160°C) for 6 hrs	

Forty-five stringers were made for possible use on the component. These stringers were given the quality control tests discussed in Section IV D. On the basis of the test results, thirty-one of the forty-five stringers were selected for the component. The test results were also used to select the position at which each stringer was to be placed around the shell. The stringer test results and the selection criteria are given in Section IV D. Fiber properties for the yarn in the stringers are summarized in Section IV E.

C. Fabrication of Balsa-Core Ring Stiffeners

The ring stiffeners, which provide circumferential stability for the fuselage component, consist of a segmented balsa-wood core reinforced with "Thornel" fiber, epoxy composite. The ring design was shown in Figure 149(b) of the Third Annual Report.[3] Most of the composite material for the rings was fabricated with untreated "Thornel" 40 fiber and ERL 2256/MPDA epoxy resin before the decision was made to change to a treated "Thornel" 50 fiber for the skin and stringers. Since the tests of the untreated "Thornel" 40 ring beam elements had shown adequate strength for this material, the untreated "Thornel" 40 fiber was used in all the ring material. Assembly of the ring stiffeners was subcontracted to Lumb Woodworking, Incorporated, a company which has the equipment and capability to machine balsa wood. The inner unidirectional composite ring and the three-ply (0°,±45°) composite shear webs were fabricated by Union Carbide. Figure 22 gives the dimensions of the composite shear webs.

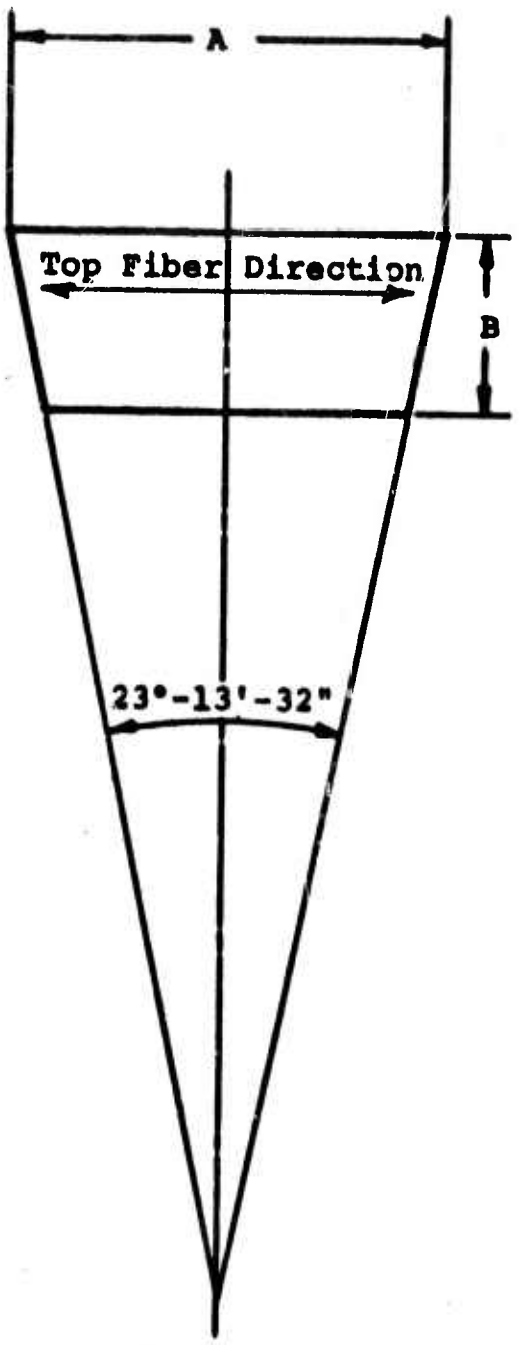

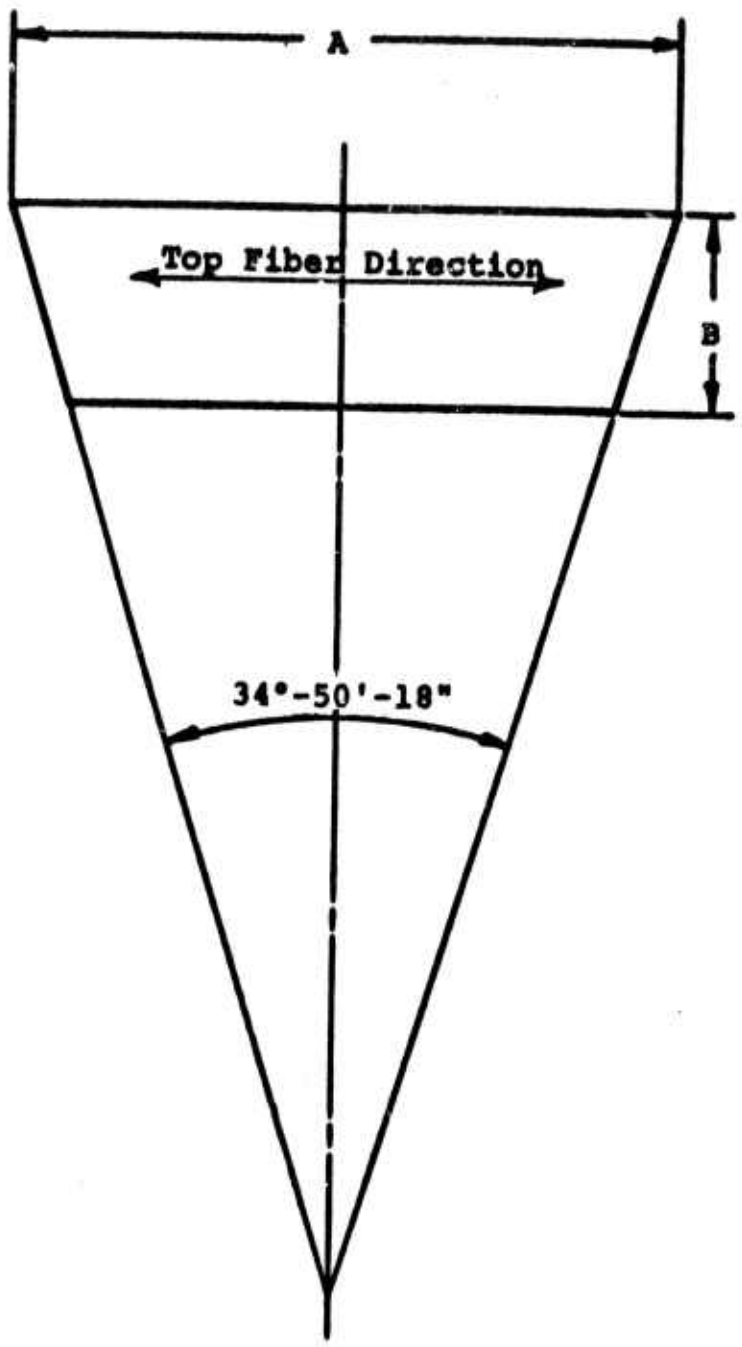

	Double Web			Triple Web		
Ring O.D.	A	B	No. Req'd.	A	B	No. Req'd.
20.5"	4-5/16"	1-11/16"	28	6-19/32"	1-29/32"	2
21.5"	4-17/32"	1-11/16"	28	6-29/32"	1-15/16"	2
22.5"	4-3/4"	1-11/16"	28	7-7/32"	1-31/32"	2
23.5"	4-15/16"	1-23/32"	28	7-17/32"	2"	2

Figure 22. Shear Webs for Ring Stiffeners.

N-21489

Each ring stiffener was fabricated by bonding balsa-wood segments with the grain oriented radially to a unidirectional composite ring. The relatively thin unidirectional ring (0.040 inch thick and 0.650 inch high) was supported on a circular composition board containing an aluminum metal hub, as shown in Figure 23. After the balsa-wood segments were bonded together, the ring assembly was sanded to the specified height of 0.500 inch and machined to the required outside diameter (see Figure 24). Trapezoidal composite shear webs were then bonded to the sides of the balsa-wood core. Wooden clamps, shown in Figure 25, were used to hold the web segments during the bonding operation. The three-ply (0°,±45°) web segments were bonded to the core material so that the zero-degree fibers were on the outer surface of the ring and were perpendicular to the radial direction at the center of the web. After the excess trapezoidal web material was removed by machining, the stringer slots were cut by using a high speed router (see Figure 26). The damaged areas in the core material were repaired with a filled epoxy resin.

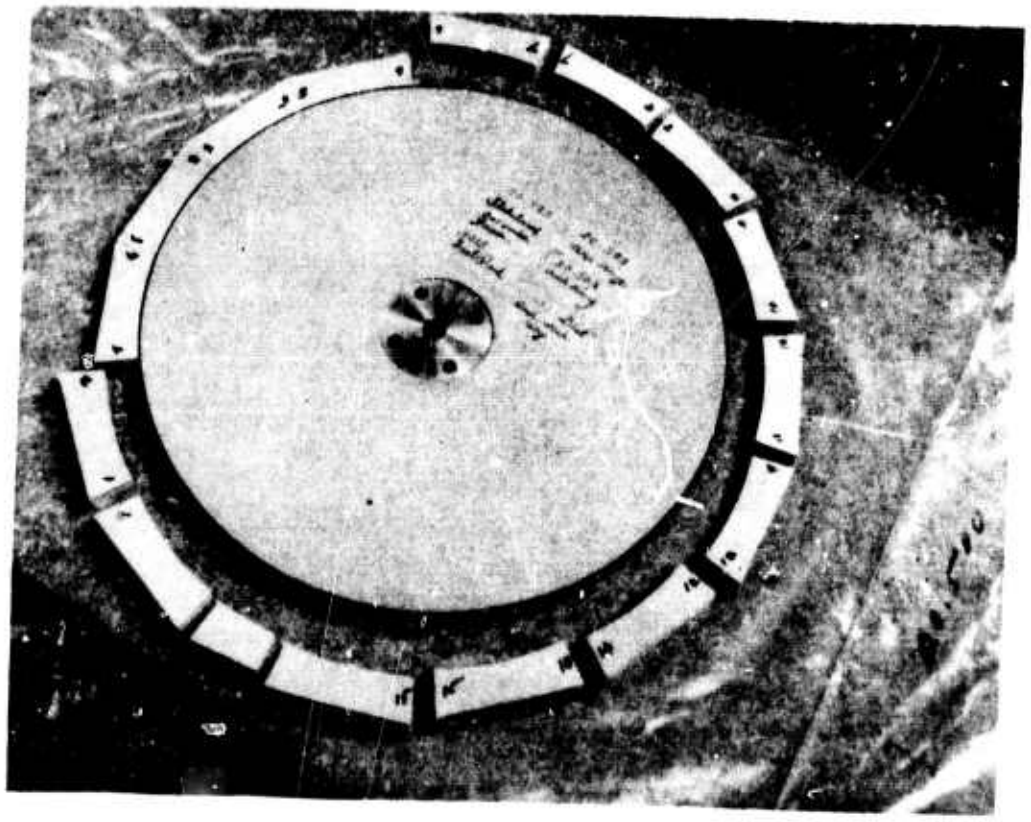

Figure 23. Bonding of Balsa-Wood Core to Unidirectional Composite Ring on Support Disc. N-2185

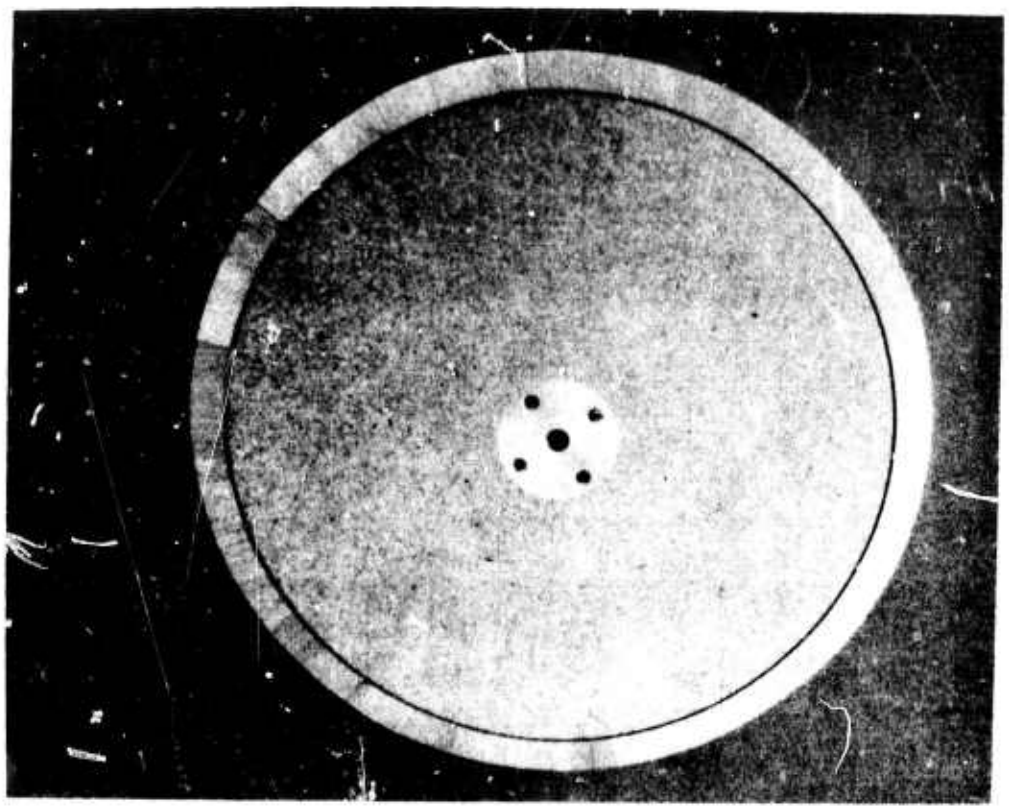

Figure 24. Balsa-Wood Core Segments Machined to Form Circular Ring. N-21486

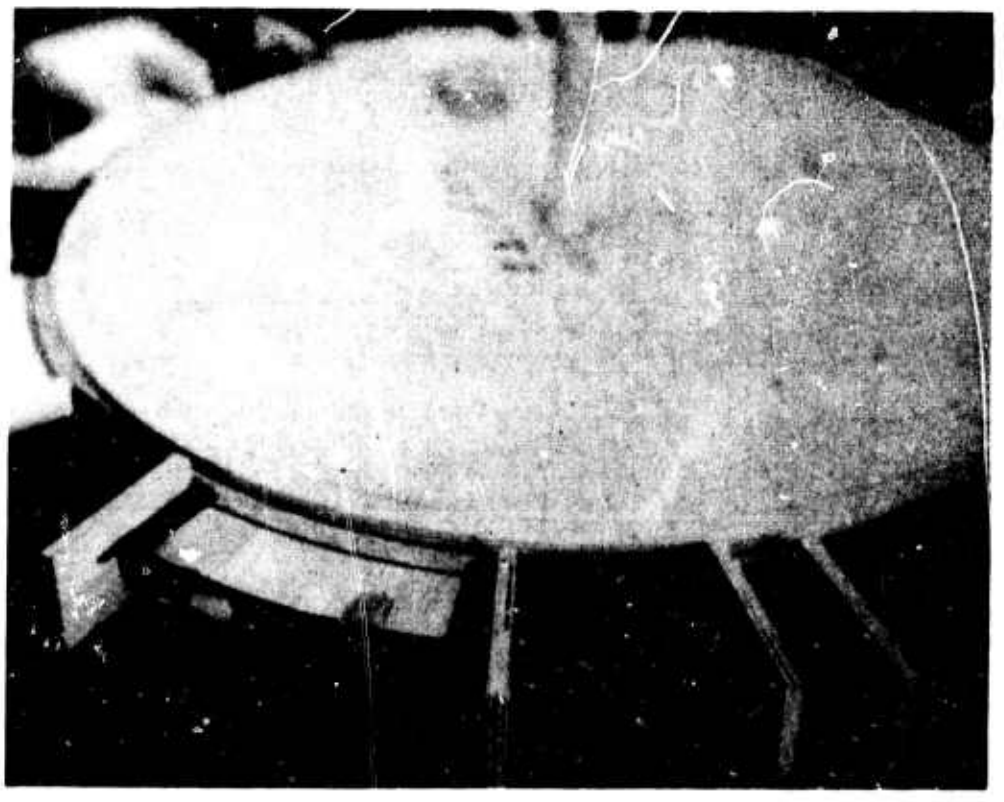

Figure 25. Bonding of Composite Shear Webs to the Balsa-Wood Core. N-20676

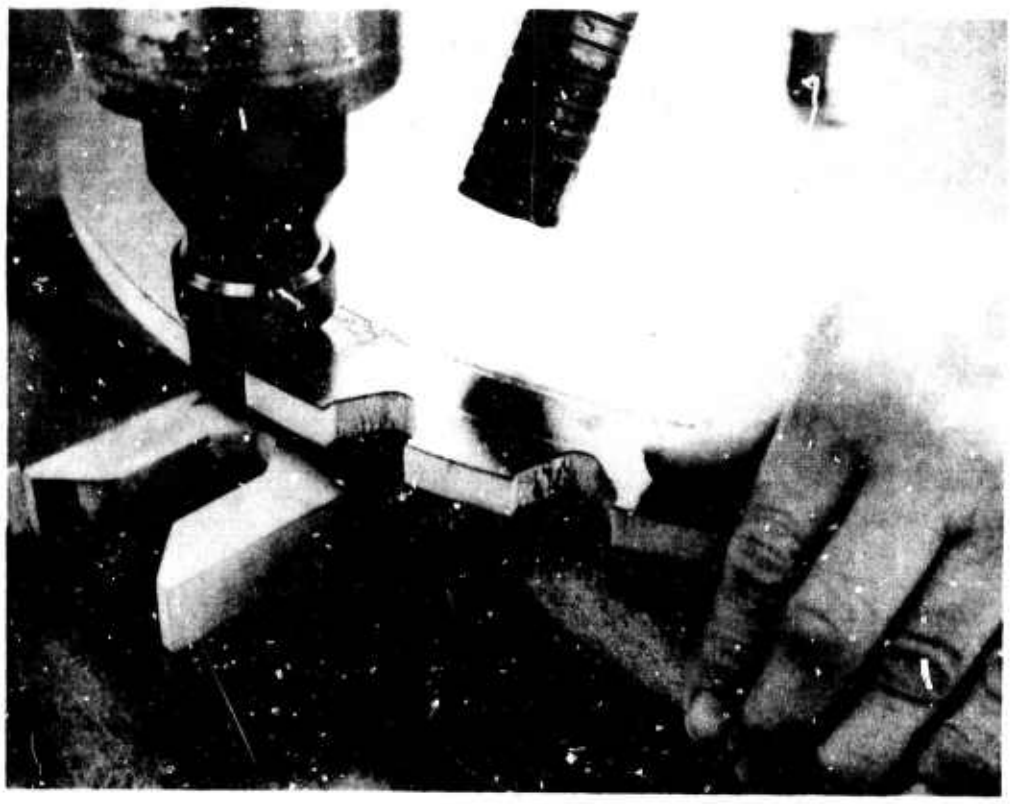

Figure 26. Routing of Stringer Slots. N-20674

Equal spacing of the thirty one stringer slots was accomplished with the aid of the ratchet wheel and pawl fixture shown in Figure 27. The ratchet wheel was bolted to the composition board containing the reinforced balsa-wood core ring and positioned with a steel arbor on the pawl fixture base. The spring-loaded pawl positioned the ratchet wheel for the stringer slot routing operation. The ratchet wheel fixture was designed to machine the equally spaced stringer slots in the four ring stiffeners of different diameters.

After the stringer slots were cut, the ring perimeters were sanded on a 2.4 degree angle to give good contact with the inner surface of the fuselage skin. The areas that were not to be bonded to the skin were sealed with a clear lacquer to minimize water absorption by the porous balsa-wood core. A completed ring stiffener, removed from the composition board support, is shown in Figure 28.

D. Fabrication of Component Skin

The fuselage component skin consisting of four plies oriented at (0° 15° -15° 0°) relative to the cylinder axis, was made with treated Thornel 50 fiber in ERL 2256/MPDA epoxy resin. Fiber properties are given in Section IV E. The skin fabrication procedure was essentially the same as that developed

for fabricating the quarter-scale, one foot long stiffened cylinders. This procedure was described on pages 356-358 of the Third Annual Report.[3] In brief, the procedure was to wet-wind a 90° ply on a plaster mandrel. Each 15° ply was applied by hand in four quarter-sections of prepreg. The outer 90° ply was wet wound.

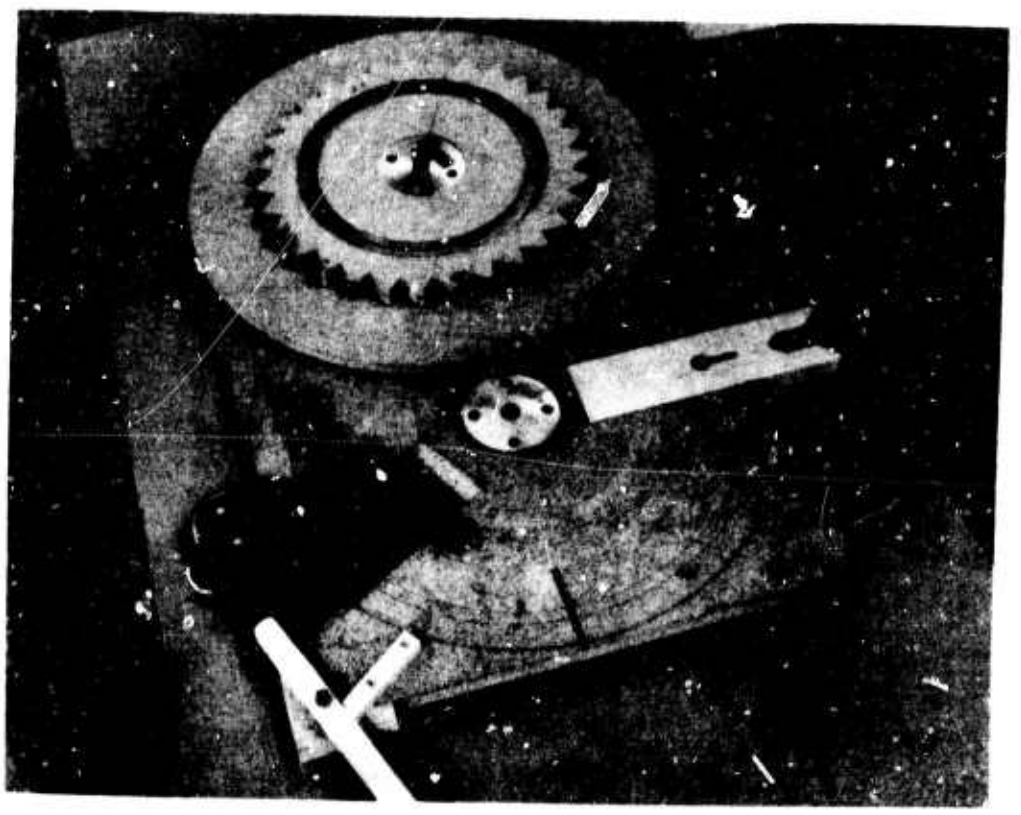

Figure 27. Ratchet Wheel Fixture for Accurately Positioning Ring During Routing of Stringer Slots.

N-21484

A lathe-type filament winding machine was used to wet-wind the 90° plies on a plaster mandrel* (see Section IX K-3 of the Third Annual Report for details of the mandrel dimensions and materials). One coat of polyvinyl alcohol (Plastilease - 512B†) and two coats of carnauba wax were applied to the mandrel to seal the surface and provide a release agent between the mandrel and the skin. Figure 29 shows the mandrel with the indexing discs at each end which were used to position the quarter sections of the 15° plies.

*Fabricated by Mandrels, Incorporated.

†Product of Ram Chemicals Manufacturing Company.

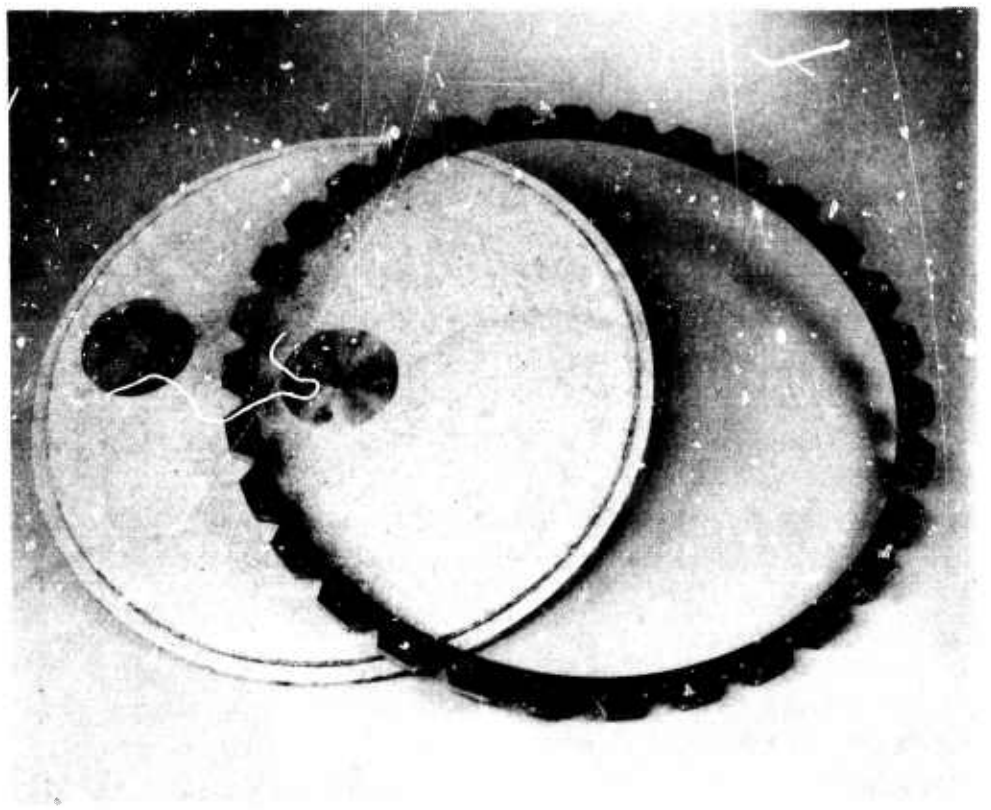

Figure 28. Completed Ring Stiffeners Removed from Support Disc.

N-20575

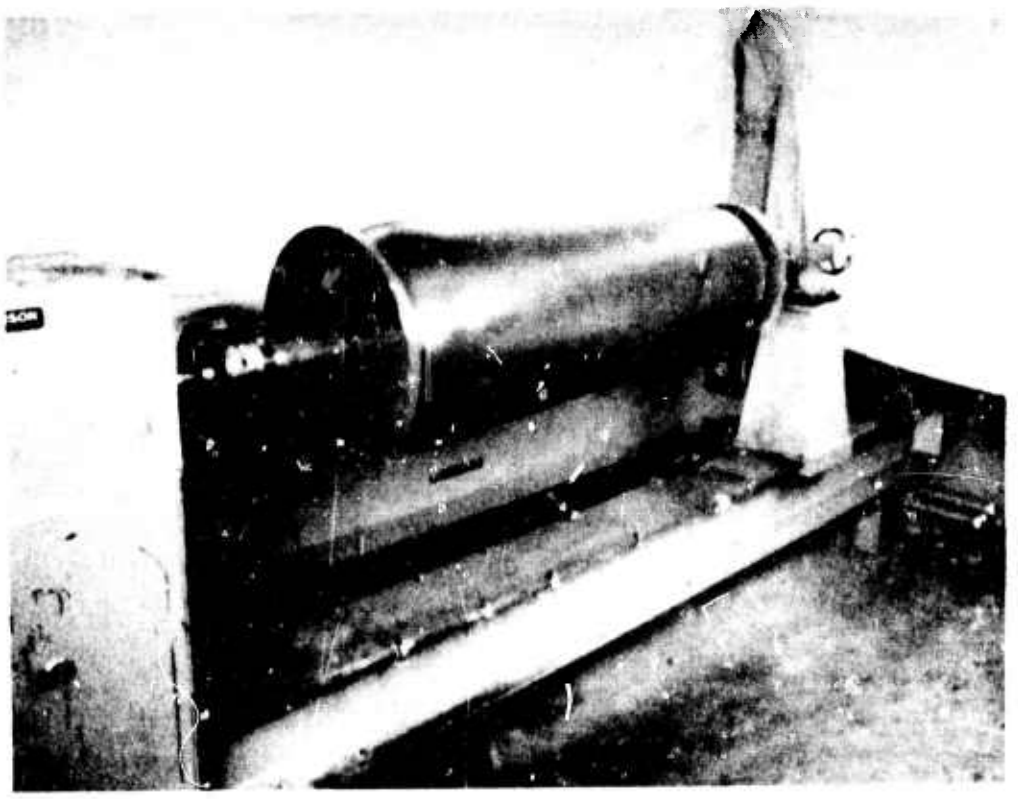

Figure 29. Plaster Mandrel for Winding Component Skin.

N-20680

The shape and dimensions of a 15° ply quarter section were given in Figure 164 and Table XLIII of the Third Annual Report. The taper in the shell necessitated having cut yarns along one edge of the tapered quarter-section panel. The quarter sections used in the component skin were widened by 0.25 inch on the side with the cut yarns (the area GHJI in Figure 164 of Reference 3). The quarter sections were applied to the mandrel so that the continuous fibers at one edge of a section overlapped the cut yarns in the 0.25-inch strip of the adjacent section. This overlap joint helped to hold the cut yarns on the mandrel during fabrication and provided a mechanism for building up stress in the ends of the cut yarns when the component was subjected to external loading. The overlap joint was formed only in the area between the built-up end attachments so that the number of graphite fiber composite plies would not be increased in the end-attachment region.

A Teflon-coated metal template was used as a guide in cutting the quarter sections. The sections were positioned on the mandrel with the aid of a contoured sheet-metal pan. A quarter-section panel of the prepreg material was placed on the pan and brought into contact with the mandrel from beneath. Pressure was applied to the outer surface of the contoured pan while the mandrel was slowly rotated 180° in order to bring the pan to the top position, as shown in Figure 30. At the top position, the pan was removed; the prepreg was then rolled smooth to assure good contact between the fiber layers before the prepreg backing sheet was removed. The proper indexing of quarter-sections of prepreg was assured by the use of pre-located metal guide pins which were positioned on a wooden disc located on each end of the mandrel. Two contoured pans with opposite orientation were required to position both the positive and negative 15° quarter sections. A quarter section positioned on the mandrel surface with the prepreg backing material removed is shown in Figure 31. The prepreg tack was sufficient to hold the quarter sections on the mandrel during fabrication.

The outer 90° ply was wet wound after the positioning of the angle plies was completed. Excess resin was removed from the surface of the outer 90° ply by applying bleeder cloth and light pressure at room temperature. This procedure did not significantly decrease the resin content within the skin, and the final skin resin content and ply thickness were greater than the design goals.

An autoclave of sufficient size to hold the skin and mandrel was not available, so the skin was cured with heat and no external pressure. The bleeder cloth was removed and rod-type heating units were positioned close to the mandrel. The resin was then gelled while the mandrel was slowly rotated by the filament winding machine. After the resin had gelled, the mandrel was placed on a carriage and rolled into a forced-air convection oven.

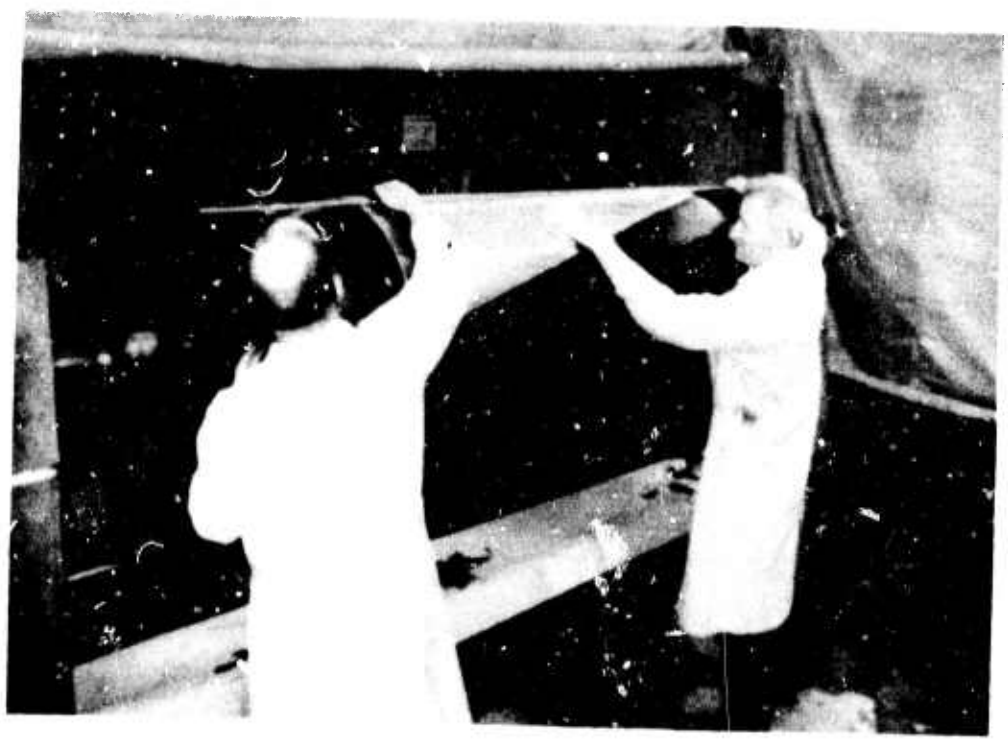

Figure 30. Hand Positioning of a Quarter Section of a 15° Angle Ply.

N-20681

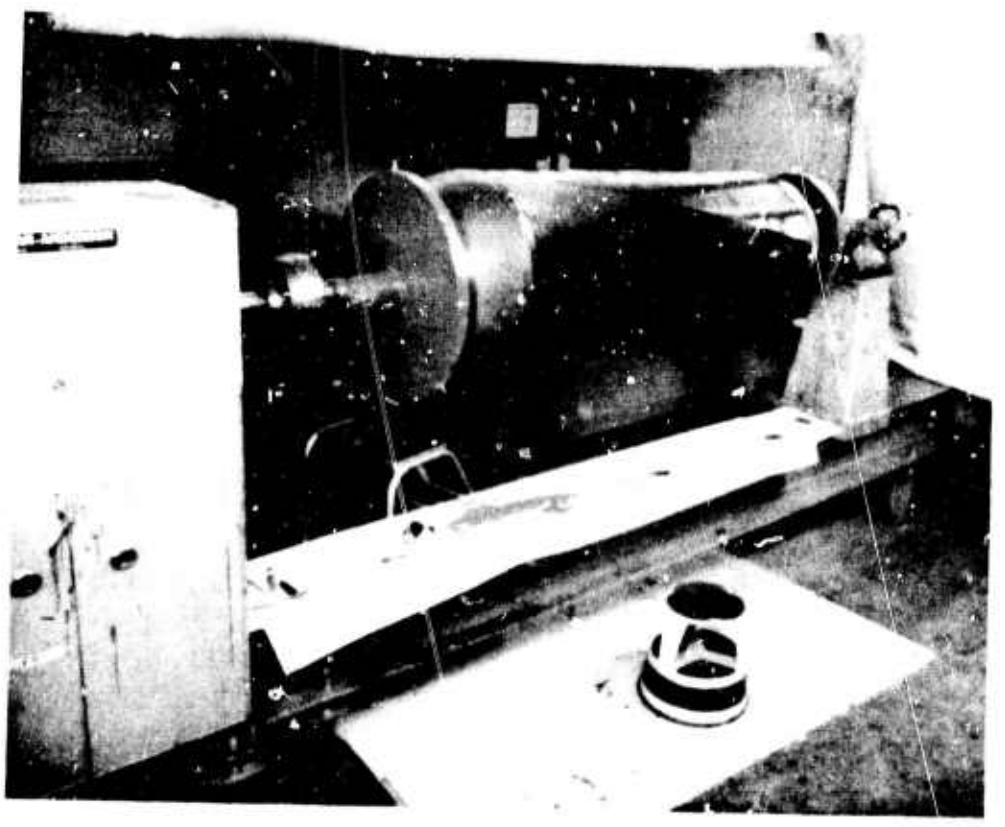

Figure 31. Quarter Section of "Thornel" Prepreg Positioned on Mandrel Surface.

N-20678

To reduce the risk of cracking the heavy plaster mandrel, the temperature in the convection oven was slowly increased and decreased in small incremental steps. Figure 32 shows the air temperature in the convection oven during the cure of the fuselage component skin.

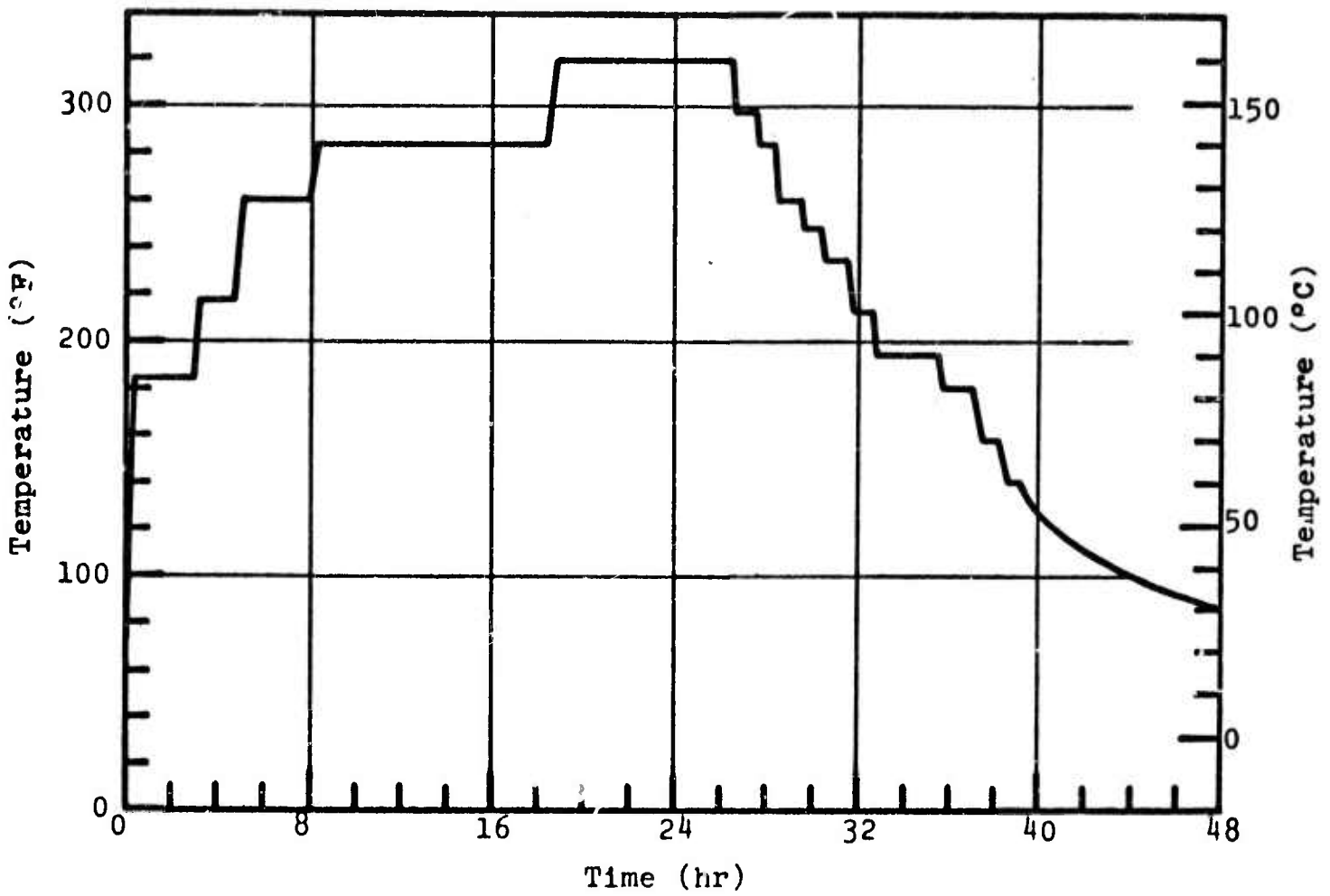

Figure 32. Time-Temperature Cycle for Cure of Component Skin.

E. Bonding of Outer End Attachments

In order to be able to introduce loads into the fuselage component during testing, both ends of the component were built-up with glass fiber reinforced plastic (GRP) laminates and segmented aluminum rings. The design of these end attachments is shown in Figures 149(a) and 149(b) of Reference 3; the design is similar to that used on the end-attachment test panels discussed in Sections IV A and B. The parts of the end attachment on the outside of the skin were added before the skin was removed from the plaster mandrel.

The GRP buildup was formed by wrapping eight layers of Narmco-550 adhesive prepreg* (Style 181 glass cloth) on the ends of the component skin. The skin was lightly sanded and cleaned with ethyl alcohol before the prepreg was applied. The GRP laminate was vacuum bagged and cured in the convection oven with the schedule shown in Table XX (air temperatures are given). Each end was cured separately. After the cure was completed, the GRP laminates were machined to a thickness of 0.050 inch; and the skin was cut to its final length of 48.0 inches. Figure 33 shows the skin and GRP laminate after machining.

TABLE XX

CURE SCHEDULE FOR OUTER GLASS REINFORCED PLASTIC LAMINATE

Buildup at Large End - 12 to 13 psi pressure		
RT to 248°F (120°C)	in	0.7 hrs
Hold at 248°F (120°C)	for	3.5 hrs
Cool to 100°F (38°C)	in	7.5 hrs

Buildup at Small End - 12 to 13 psi pressure		
RT to 257°F (125°C)	in	1.7 hrs
Hold at 259°F (126°C)	for	1.5 hrs
Hold at 273°F (134°C)	for	2.0 hrs
Cool to 100°F (38°C)	in	5.5 hrs

Each aluminum ring was formed from four quarter segments which were fabricated from a tempered 7075 aluminum alloy and supplied to Union Carbide by Bell Aerosystems. The surfaces of the aluminum rings were prepared for bonding by the procedure described in Table XL of Reference 3. Epoxy adhesive EC-2216 (grey)† was used to bond the rings to the GRP laminate. A metal strap was placed over the ring segments in order to obtain good contact between the aluminum and glass laminate surfaces while the adhesive was curing. The aluminum ring segments were accurately positioned by metal pins which were inserted through predrilled pilot holes in the aluminum segments and into the plaster mandrel. So that the aluminum ring segments on the large end would be prevented from moving down the tapered fuselage skin surface, two pins were inserted in each segment at the end of the skin.

*Product of Whittaker Corporation, Narmco Materials Division.

†Product of Minnesota Mining and Manufacturing Company.

Metal bars extending from the segments on the large end to the segments on the small end prevented any longitudinal movements of the rings on the small end. The positioning and bonding of the aluminum segments on the fuselage skin outer surface are shown in Figure 34. In order to avoid any problems that might have been caused by the thermal expansion mismatch between the aluminum rings and the GRP laminate, the EC-2216 adhesive was cured at room temperature for two days.

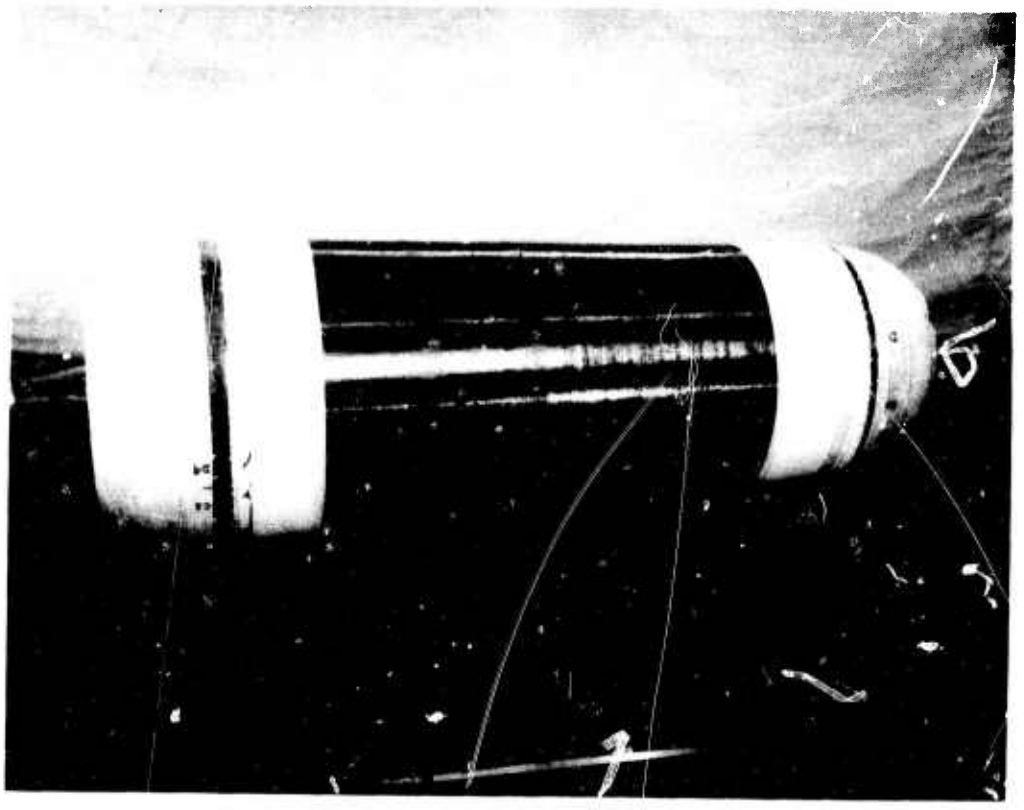

Figure 33. Component Skin After Machining Glass Laminate Reinforced Ends.

N-20366

After the outer end attachments were applied, the plaster mandrel was chipped away to free the component skin. The ends of the mandrel shaft were supported until the shaft could be freed and removed. After the shaft was removed, a contoured plaster cradle supported the skin and remaining plaster. When the plaster was completely chipped away, the skin was cleaned to remove any sealer or release agent adhering to the inner skin surface.

The contoured plaster cradle had been cast earlier by utilizing the mandrel on which the skin was made as a mold. Before casting, material was added to the skin mandrel to simulate

the skin and outer end-attachment buildups. The plaster cradle was supported on a metal carriage, and a rubber blanket was placed between the cradle and the skin. This cradle was used to support the component during the remaining fabrication operations.

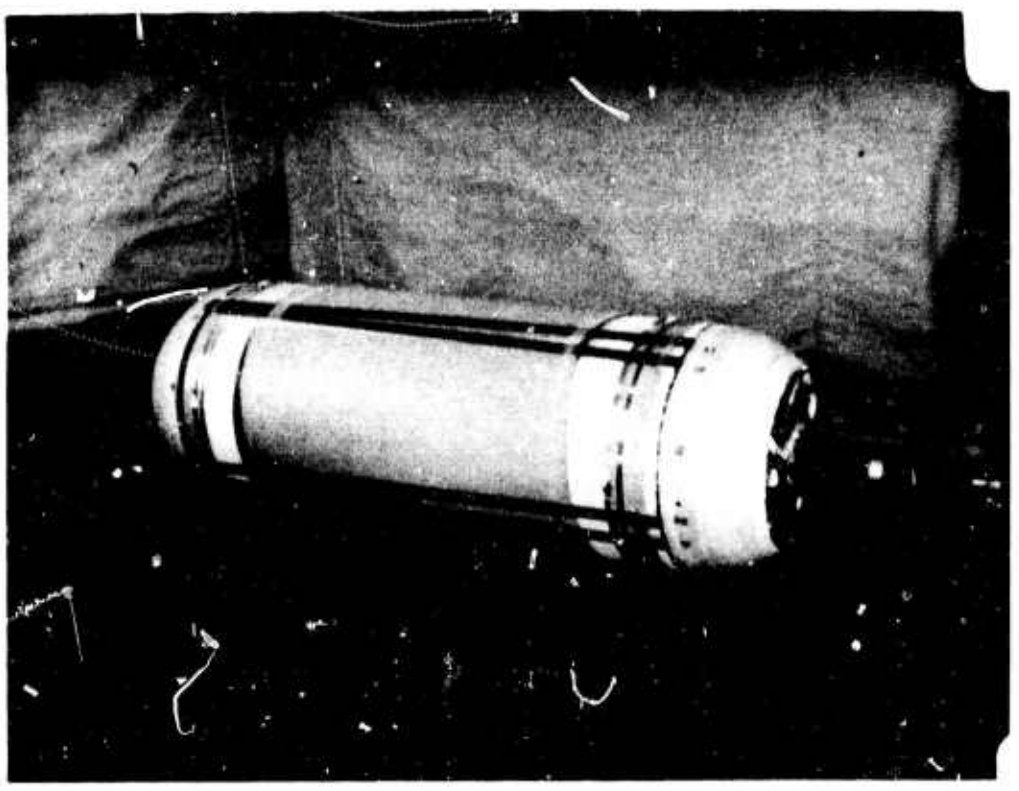

Figure 34. Positioning and Bonding of Aluminum Segments on Component Skin Outer Surface.

N-20679

F. Bonding of Stringers and Rings

1. Stringers

The stringers were bonded to the skin with the fixture shown in Figure 35. The fixture consisted of four movable U-shaped pressure bars positioned by four arc sectors mounted on a central shaft. A drawing of the pressure bar is given in Figure 36. When lowered, the edges of each bar came in contact with the flanges of a stringer and pressed the stringer against the skin during the bonding operation. The pressure bars were held by four slotted sectors; a drawing of a sector is shown in Figure 37. The sectors contained locating pins to position accurately the stringers and set screws to apply force to the pressure bars. In between the bonding operations, the pressure bars were held up by springs.

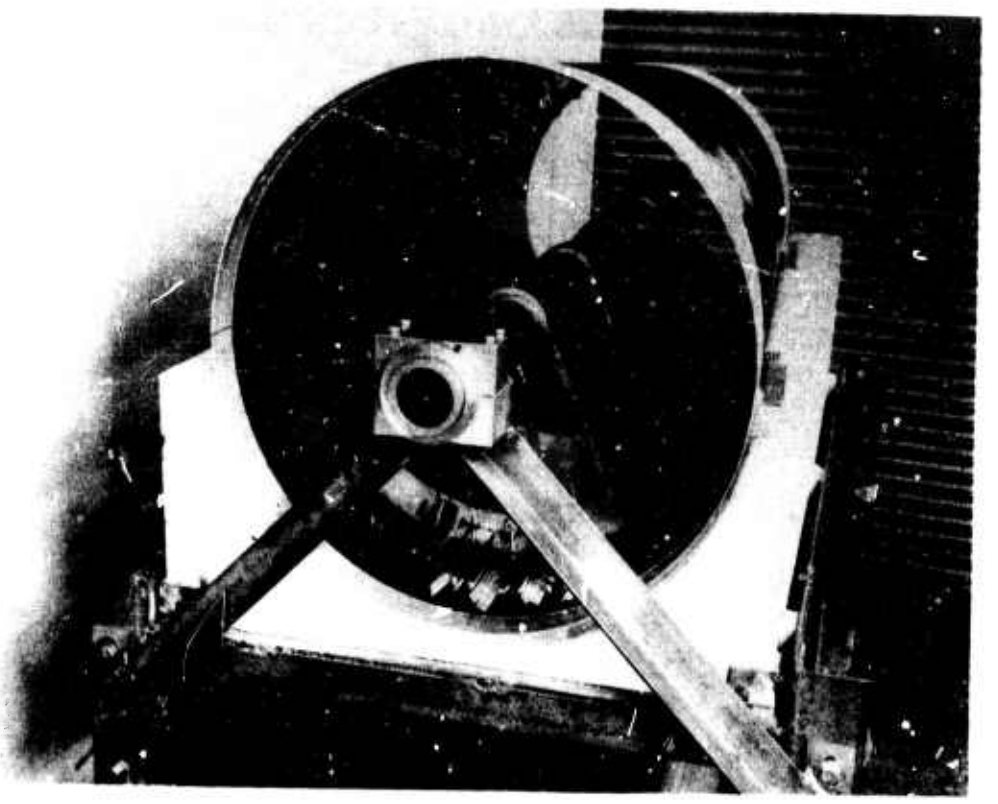

Figure 35. Bonding of Hat-Shaped Stringer to the Component Skin.

N-20353

The bonding surfaces of the skin and stringers were lightly sanded with medium grit sandpaper, cleaned with ethyl alcohol and dried. To facilitate clean-up after the bonding operation, drafting tape was placed on the skin between the stringers, and a layer of Teflon tape having an adhesive backing was used to cover the top of the stringer flanges. The Teflon tape also served to assure a positive release between the pressure bar and stringer after the cure cycle was completed. After a coating of adhesive was applied to the mating surfaces, a stringer was inserted into the pressure bar channel and positioned longitudinally. The locating pins in the sectors positioned the stringers circumferentially and prevented any misalignment when the pressure bars were brought into contact with the top surfaces of the stringer flanges. A minimal amount of force was applied to the pressure bar to cause uniform resin squeeze-out along the stringer flange edges. After a set of stringers was bonded, the pressure bars and locating pins were retracted, and the component skin was then rotated to the position for bonding the next set of stringers.

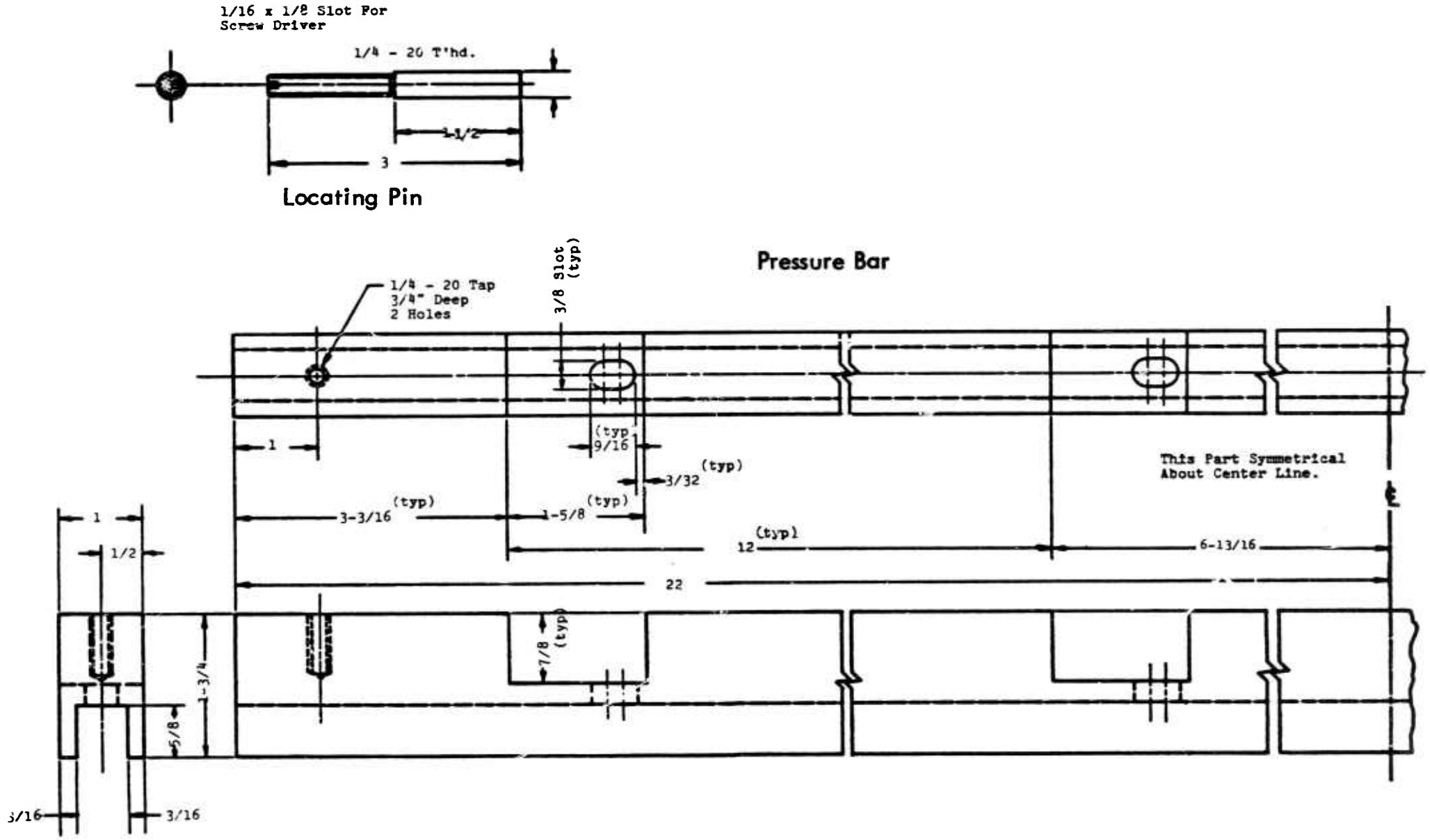

Figure 36. Pressure Bar for Bonding Stringers to the Fuselage Skin.

N-21490

The adhesive used to bond the stringers to the skin consisted of 70 weight percent Araldite 6005* epoxy resin and 30 weight percent ZZLB 0325† hardener. The adhesive was allowed to gel at room temperature for approximately four hours before the structure was placed in the hot-air convection oven. The room-temperature gel period was used to reduce the risk of adhesive flow from the stringer mating surfaces which were necessarily at a slight angle to the horizontal. The thirty-one stringers were bonded in seven sets of four stringers at a time and one set of three stringers. The cure cycle was repeated for each of the eight sets; oven air temperatures and cure times are given in Table XXI.

TABLE XXI

CURE SCHEDULE FOR BONDING STRINGERS AND RINGS TO SKIN

Stringers	
Set 1	RT for ∿4 hrs + 140°F (60°C) for 3.3 hrs
Set 2	RT for ∿4 hrs + 140°F (60°C) for 2.3 hrs
Set 3	RT for ∿4 hrs + 147°F (64°C) for 4.4 hrs
Set 4	RT for ∿4 hrs + 145°F (63°C) for 5.2 hrs
Set 5	RT for ∿4 hrs + 145°F (6 °C) for 5.2 hrs
Set 6	RT for ∿4 hrs + 140°F (60°C) for 3.4 hrs
Set 7	RT for ∿4 hrs + 140°F (60°C) for 1.7 hrs
Set 8	RT for ∿4 hrs + 140°F (60°C) for 4.3 hrs
Rings	
	145°F (63°C) for 7.2 hrs

2. Rings

Because of the taper in the shell, the four ring stiffeners could be inserted from the large end of the component. The shell was not exactly circular; so initially, the rings stopped at a point a few tenths of an inch from their proper location. The rings were hand-fitted to their required position by removing material from selected areas on the outer circumference of the rings. In addition, some of the stringer slots had to be enlarged to maintain proper clearance between the rings and stringers.

*Product of CIBA Corporation, CIBA Products Division.

†Product of Union Carbide Corporation, Chemicals and Plastics Division.

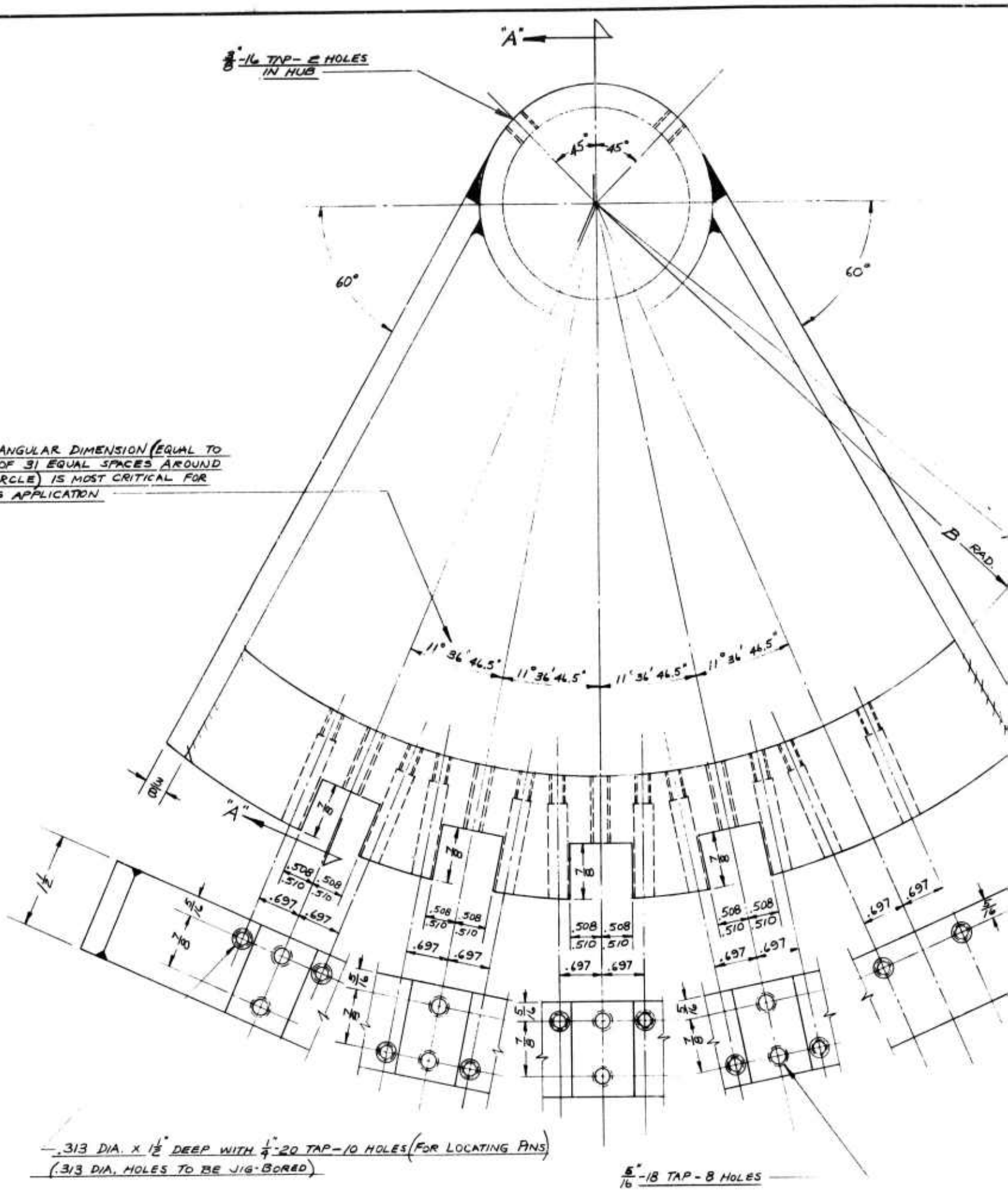

NOTE - WELDED CONSTRUCTION - BEFORE FINISH MACH'G

LOCATING & HOLDING SECTOR
MACHINERY STEEL

Nº REQ'D	A RAD.	B RAD
1	10 15/16"	9"
1	10 7/16"	8 1/2"
1	9 15/16"	8"
1	9 7/16"	7 1/2"

A

NC 440 99

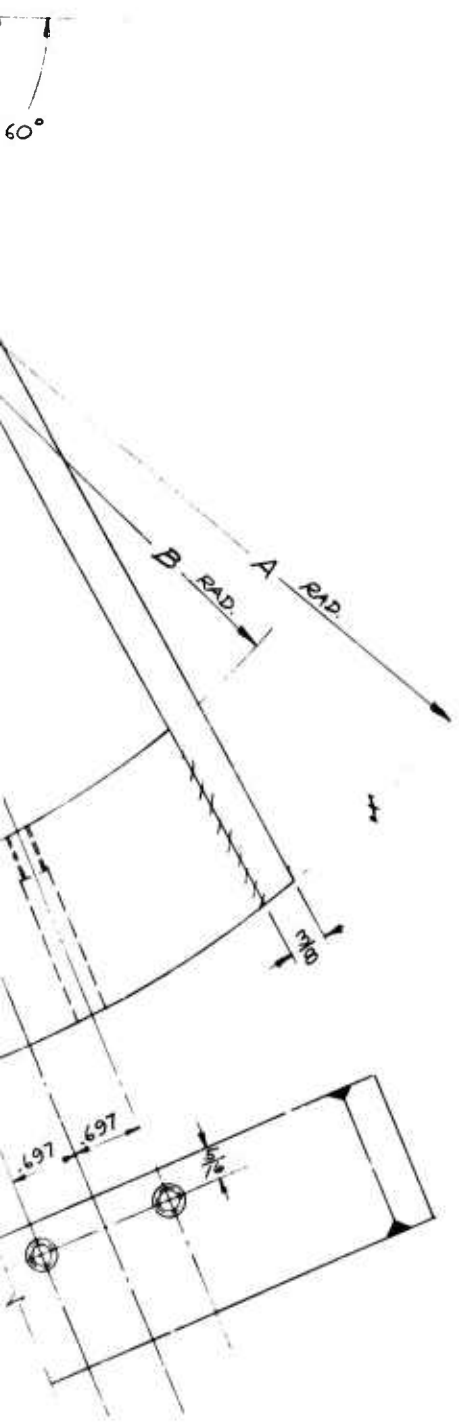

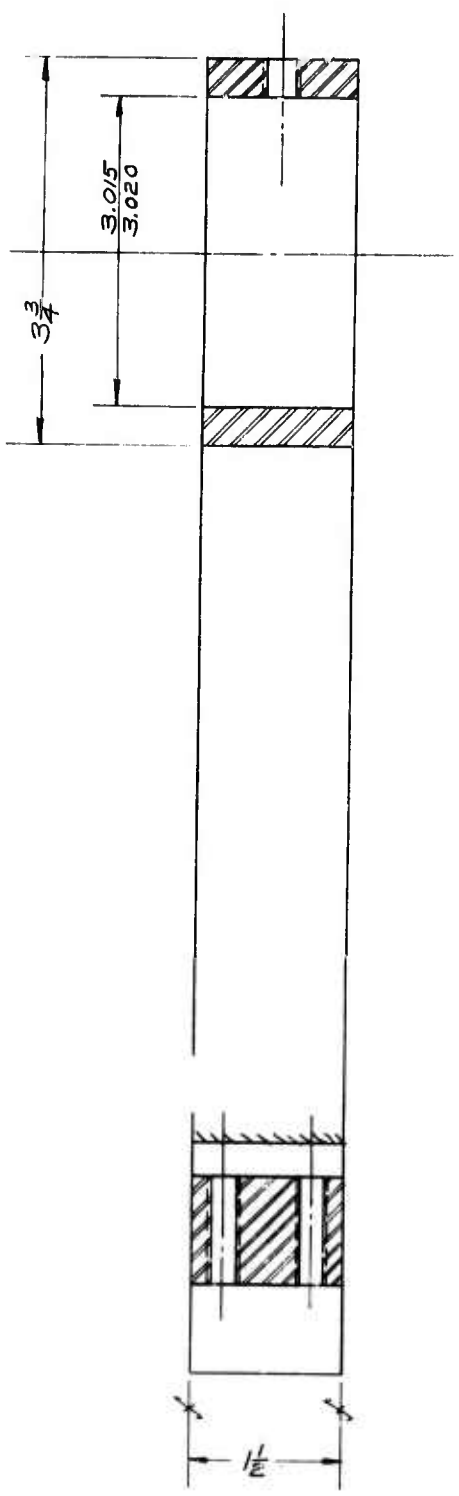

SECTION "A"-"A"

CONSTRUCTION - TO BE STRESS-RELIEVED
E FINISH MACHINING.

Figure 37.

Stringer Bonding Fixture.

REVISIONS				SCALE NONE	ASSEMBLY FIXTURE
NO.	DATE	BY	SUBJECT	DESIGNED R WHITE / DRAWN 5-15-68	-DETAILS-
				CHECKED / APPROVED	
				UNION CARBIDE CORP. CARBON PRODUCTS DIVISION PLANT	RL-334-A1

All four rings were bonded in one operation and cured at the same time (see Table XXI for the curing conditions). The same adhesive, Araldite 6005/HZLB 0325, was used for the rings that had been used for the stringers. A photograph of the component at this stage in the fabrication is shown in Figure 38.

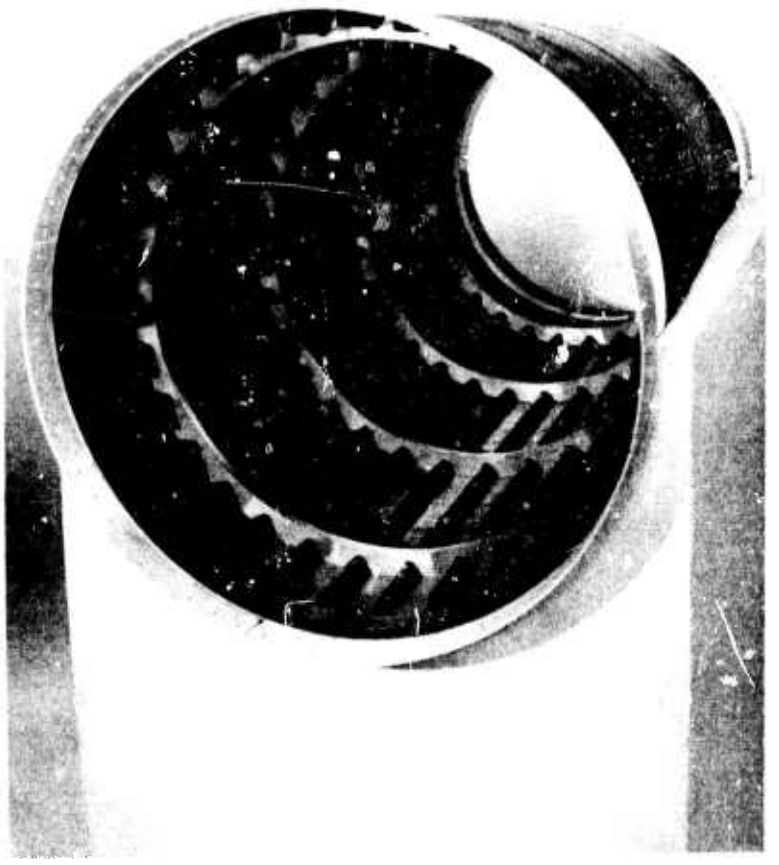

Figure 38. Partially Completed Component.

N-20369

G. Bonding of Inner End Attachments

The glass reinforced plastic (GRP) buildup on the inside of the component was more than 0.4 inch thick. The largest part of this buildup was formed from four pre-molded GRP ring segments. The ring segments were bonded to the skin with five plies of GRP prepreg, and seven plies of GRP prepreg were placed over the segments and the stringer caps.

Each GRP ring segment was fabricated with Narmco 550 adhesive prepreg* (Style 181 glass cloth) laid up on a specially designed steel mold. The tooling was designed to produce ring segments having the inner surface molded to final dimensions and containing the 30° chamfer. Approximately forty rectangular sheets of prepreg were positioned in the steel mold and cured in an autoclave using the manufacturer's recommended schedule. The ring segment blank was machined on its outer surface to a thickness of 0.360 inch, using the steel mold as a turning fixture. After machining the outer surface, the outer edges were trimmed; and the segment was cut to the required chord length. The stringer slots were accurately machined on a milling machine. A photograph of two completed ring segments for the large end is shown in Figure 39.

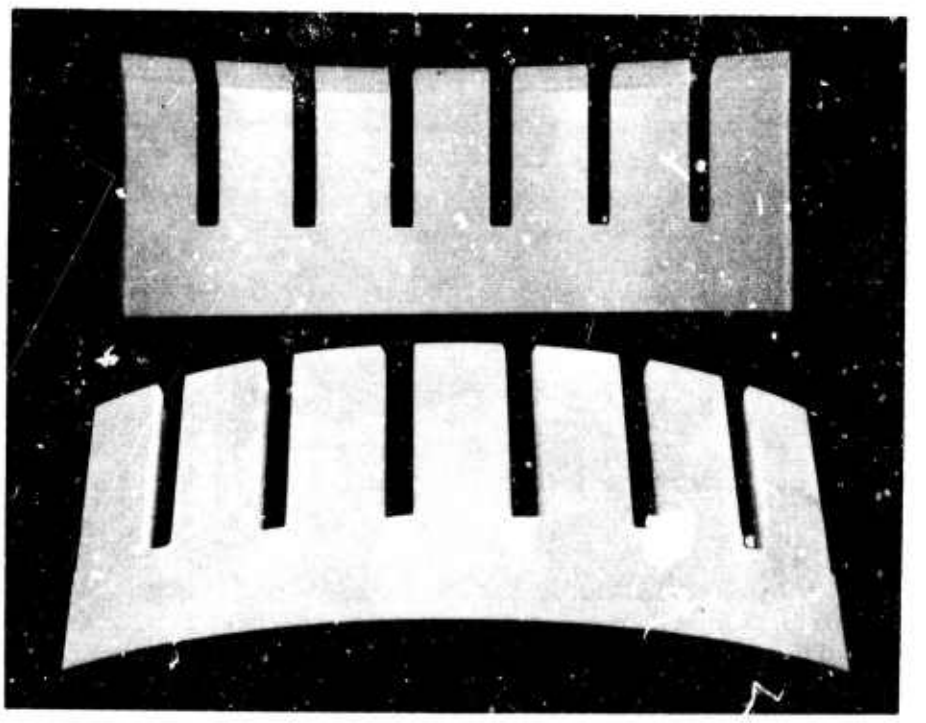

Figure 39. Glass-Reinforced Plastic Ring Segments. Top, Concave Surface Molded to Final Dimensions. Bottom, Machined Convex Surfaces.

N-20371

*Product of Whittaker Corporation, Narmco Materials Division.

Because of the taper in the shell, the slotted GRP segments could not be inserted with a simple longitudinal motion parallel to the skin. At the large end, segments with parallel-sided slots could be inserted by a combined outward radial motion and inward longitudinal motion. In essence, the increase in stringer spacing due to the outward radial motion is compensated by the decrease in stringer spacing due to the inward longitudinal motion. At the small end, this compensation is not possible, and much wider clearances are needed in the stringer slots. In order to minimize the gaps between the stringers and the GRP segments, Bell Aerosystems designed a segment with tapered slots; the amount of taper increased with increasing distance of the slot from the center of the segment. Further discussion of the design is given in Section III A, and a drawing of the tapered-slot segments is given in Figure 1.

The machined GRP ring segments were bonded to the inner surface of the component skin with Narmco 550 adhesive prepreg. Three layers of prepreg were cut with length equal to the circumference of the shell, with width equal to the width of the GRP segments, and with slots such that the fingers extended between, but not on top of, the stringer flanges. Two additional layers were cut with wider fingers which extended to the stringer webs and over the stringer flanges. The five layers were applied with butt joints which were staggered to reduce the possibility of forming a weak fracture path. The four GRP ring segments were positioned over the five prepreg layers, and the assembly was cured in a vacuum bag in the convection oven. A sheet metal protective cover was used on the inner surface of the component to prevent the vacuum bag from pressing on the walls of the stringers and on the balsa-core ring stiffeners. Twelve wooden blocks were placed between the stringers to transfer the load from the conically-shaped metal sheet directly to the skin.

After the GRP ring segments were bonded to the skin, the gaps between the fingers of the segments and the stringers were filled with EC 2216* epoxy adhesive; the adhesive was cured at room temperature. Wherever possible, "Thornel" graphite fibers were forced into the gaps to increase the load transfer capabilities between the end attachment and the stringers.

Seven layers of Narmco 550 adhesive prepreg were used to cover the stringer caps in the end attachment areas. Strips of prepreg 2.75 inches wide were draped over the stringer caps and the parts of the surface of the GRP ring segments which extended between the stringers. The consolidation and curing of the prepreg were accomplished in a vacuum bag in the convection oven.

*Product of Minnesota Mining and Manufacturing Company.

The GRP buildup was cured in four operations: the ring segments at the large end, the stringer overlay at the large end, the ring segments at the small end, and the stringer overlay at the small end. The oven air temperatures and cure times for these operations are given in Table XXII.

TABLE XXII

CURE SCHEDULE FOR INNER
GLASS REINFORCED PLASTIC LAMINATE

Ring Segments at Large End			
	261°F	(127°C)	for 4.7 hrs
	212°F	(100°C)	for 2.4 hrs
	174°F	(79°C)	for 2.0 hrs
Cool to	104°F	(40°C)	in 3.5 hrs
Stringer Overlay at Large End			
	261°F	(127°C)	for 4.0 hrs
	210°F	(99°C)	for 2.1 hrs
	174°F	(79°C)	for 4.7 hrs
Cool to	104°F	(40°C)	in 2.1 hrs
Ring Segments at Small End			
	262°F	(128°C)	for 4.3 hrs
	210°F	(99°C)	for 1.0 hr
	174°F	(79°)	for 1.0 hr
Cool to	104°F	(40°C)	in 2.9 hrs
Stringer Overlay at Small End			
	262°F	(128°C)	for 5.3 hrs
	210°F	(99°C)	for 1.3 hrs
	174°F	(79°C)	for 1.1 hrs
Cool to	104°F	(40°C)	in 3.5 hrs

Except for size, the inner aluminum ring segments were the same as the outer aluminum ring segments discussed in Section V E and were prepared for bonding the same way. The GRP ring surface was lightly sanded and cleaned with ethyl alcohol prior to bonding the aluminum ring segments with EC 2216 adhesive. The bonding surfaces were held with "C" clamps and cured for two days at room temperature.

H. Final Assembly of Component

As a precautionary measure, the adhesively-bonded GRP and aluminum end attachments were also bolted to the component. In the event of an adhesive bond failure during the ultimate strength test of the component, the bolts would transfer load so that the test could be continued. The bolts also served to maintain the adhesive bonds under transverse compression and, thereby, reduced the chance of an adhesive bond failure. The bolt holes were drilled through the aluminum, GRP buildup, and graphite composite skin by using a jig mill. The component was placed on the rotary table of the jig mill, and a wooden support was placed next to the inner aluminum ring to prevent undue stresses during drilling. The bolts were tightened uniformly to 175 in. lb with a torque wrench.

A tapered band of fairing material* approximately 2.75 inches wide was added on top of the outer GRP buildup. The fairing simulated a smooth aerodynamic surface from the outer surface of the aluminum ring to the component skin. The catalyzed resin was applied with a trowel to fill the area, sanded to obtain a smooth surface, and painted black to blend with the "Thornel" composite skin. The fairing material was cured at room temperature.

Figure 40 is a photograph of the completed component taken from the large end. A photograph showing the side of the completed component is given in Figure 41. In this figure, the component is supported in the cradle section of the shipping crate. A protective wooden cover was fitted over the cradle section for shipment to Bell Aerosystems Company.

The thickness of the composite skin was measured at twenty-seven locations on the component. The results are listed in Table XXIII. Because of insufficient resin bleedout, the average skin thickness of 0.056 inch was greater than the design goal of 0.047 inch. A summary of the weights of the individual items and of the total weight of the completed component is given in Table XXIV. The weight of the "Thornel" composite structure (skin, 31 stringers, and 4 balsa-core rings) was 16.12 lb, corresponding to a weight per unit area of 0.70 lb/ft.^{2}

*Black Knight Repair Kit, Product of Woodhill Chemical Sales Corporation.

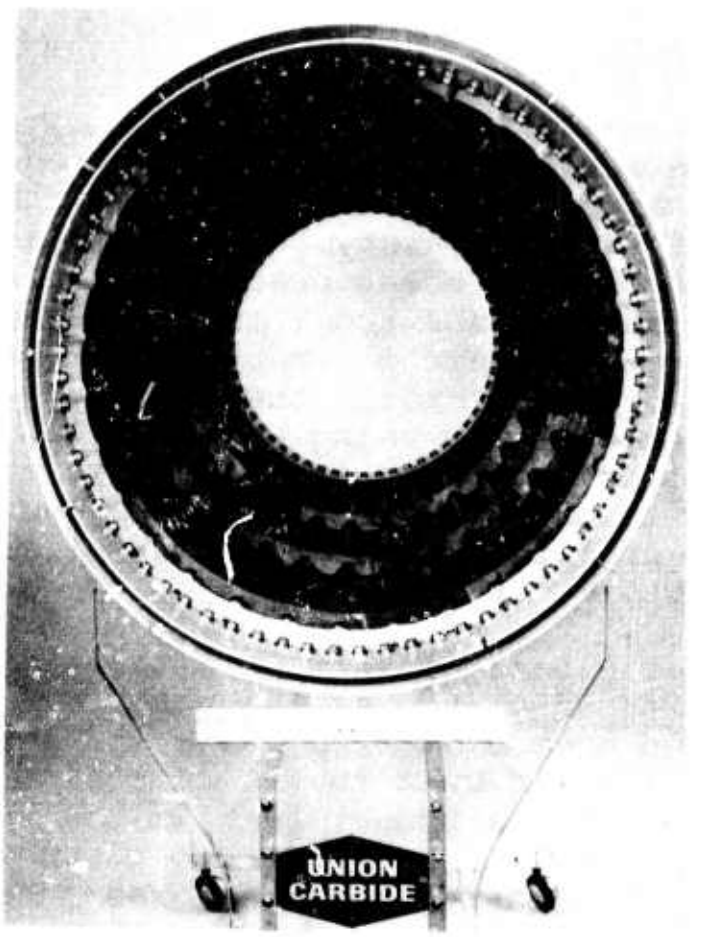

Figure 40. View from Large End of Component.

N-20902

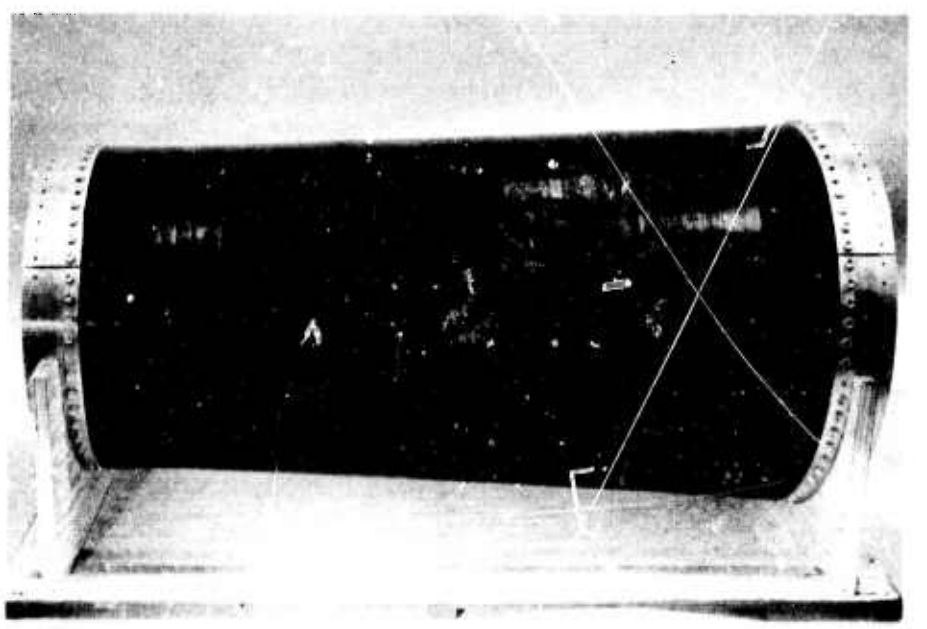

Figure 41. Side View of Component Positioned in Shipping Crate.

N-20905

TABLE XXIII

COMPONENT SKIN THICKNESS

Circumferential Position-Between Stringers Numbered	Longitudinal Position Distance From Large End (in.) 9	12	24	36
1 - 2	--	0.054	0.054	0.058
5 - 6	--	.060	.057	.055
9 - 10	--	.056	.055	.058
12 - 13	0.053	--	--	--
13 - 14	--	.057	.051	.053
16 - 17	.057	--	--	--
17 - 18	--	.057	.054	.055
20 - 21	.056	--	--	--
21 - 22	--	.056	.055	.055
25 - 26	--	.067	.056	.054
29 - 30	--	.061	.055	.055

Skin thickness in inches
Average of all measurements = 0.0561 inch

TABLE XXIV

WEIGHT ANALYSIS OF REPRESENTATIVE FUSELAGE COMPONENT

Item		Weight (lb)
Thornel Composite Structure		16.12
Skin	9.12	
Stringers (31)	5.21	
Ring Stiffeners (4)	1.79	
Aluminum Ring Segments (16)		12.10
Outer Glass-Reinforced Plastic Buildup		2.50
Inner Glass-Reinforced Plastic Buildup		17.74
Fairing Material		1.95
Metal Fasteners		6.96
Assembled Fuselage Component		57.37

SECTION VI

FUSELAGE COMPONENT INSPECTION

The fuselage component was given a brief visual inspection at Bell Aerosystems at the time of delivery from Union Carbide, January 3, 1969. The inspection consisted of overall observations to note any major discrepancies which might have occurred during handling and shipment. None were observed.

The component was stored at Bell in its shipping container until end-ring drilling operations were started on January 13. Drilling was completed on January 28 and, at this time, small areas of craze-cracking were noted on the outer skin surface. On this same date, the component was moved to the instrumentation area for strain gaging. In view of the observed surface defects, it was decided to classify these discrepancies with respect to number, location, and size by carefully inspecting all surfaces under strong lighting and magnifying glasses. This inspection was completed on January 29. While inspecting the internal surfaces, considerable stringer unbonding, minor ring unbonding, and some cracks of the ring-stiffener shear panels were observed.

A. Visual/Mechanical Inspection

(S.L. Cross and D.P. Hanley, Bell Aerosystems)

Visual inspection revealed a total of 9 craze cracks on the outer surface of the skin. Close inspection of these cracks with optical devices did not reveal broken fibers; rather, the damage appeared to be confined to resin crazing. However, "quarter tapping" in the vicinity of some flaws suggested internal delaminations. A photograph of a typical flaw is shown in Figure 42. The principal direction of the most severe cracks was parallel to the hoop wound fibers. The cracks ranged from 1/2 to 7/8 inch in length, with shorter (1/4 to 1/2 inch) branches extending normal to the hoop direction. Several of the skin cracks grew during the two months after they were first detected, either by extending in length (up to 1.5 inch) in their principal direction or by branching.

Six of the nine cracks were located in the area between stringers 18 and 22, located 35 to 40 inches from the large end of the fuselage. The other three cracks were in the vicinity of stringer 31, located 27 to 30 inches from the large end.

Stringer debonding was determined visually and by inserting a 0.003 inch thick aluminum feeler gage between skin and stringers. Approximately 20% of the total length of all stringer

Figure 42 Typical Flaw in Outer Surface of Fuselage Skin.

flanges was debonded to the extent that the feeler gage could be inserted between flanges and skin; 25 of the 31 stringers showed some degree of debonding. Of the 25 debonded stringers, there were 14 cases of debonding in Bay 1 (closest to large diameter end), 14 cases of debonding in Bay 2, and seven cases of debonding in Bay 3. Five stringers were unbonded only in Bay 1, nine unbonded only in Bay 2, and one was unbonded only in Bay 3. Four stringers were unbonded in Bays 1 and 2, one in Bays 2 and 3, and five were at least partially unbonded in Bays 1 and 2, one in Bays 2 and 3, and five were at least partially unbonded in all three bays. No particularly heavy concentration of debonding in any given area could be noted. The nature of the skin-to-stringer debonding is believed to be within the adhesive or at the bond/composite interface; no delaminations of stringers or skin could be noted.

Visual inspection further showed vertical cracks in the ring-stiffener shear panels, in the area over stringer 22, running from the bottom of the stringer cutout to the top of the ring frame. Minor debonding of the ring frame from the skin at the small diameter end was also observed in the general area of stringer 22.

B. Leak Test

(A.A. Pallozzi, Dr. H.F. Volk, and Dr. G.B. Spence, Union Carbide; Dr. K.H. Sayers and D.P. Hanley, Bell Aerosystems)

A further examination of stringer-to-skin debonding was carried out with a helium leak detector, a method which is far more sensitive than the visual/mechanical inspection described in the previous section. The technique was as follows.

A constant flow of helium was introduced into the stringer to be tested while the fuselage was in the horizontal position. The probe was moved slowly along the stringer flat, and the sensitivity of the instrument (scale factor) was adjusted as necessary. Saturation of the inside of the fuselage with helium was not a particular problem; in the beginning, an air fan was used to dissipate helium, but this practice was found unnecessary and discontinued.

As expected, the extreme sensitivity of the helium leak detector indicated a greater degree of debonding than observed by the visual/mechanical tests. In addition to the already identified debonded areas, numerous smaller leaks were found on virtually every stringer. The extent of debonding (as opposed to pin holes) indicated by these small leaks is not clear. The leak rates along all stringer flanges have been recorded and mapped. Helium leak tests will be repeated after repair of the fuselage component.

C. Ultrasonic Measurements
(C.R. Stauffis, Bell Aerosystems)

The need for a nondestructive test became apparent to evaluate the component skin-to-stringer bonds. The ultrasonic immersion through-transmission method was the only known in-house test at Bell capable of evaluating the bonds. However, immersing the component would contaminate stringers, the skin, and the balsa-core ring frames. Therefore a contact ultrasonic test capable of evaluating stringer bonds from the shell skin exterior was required. A contact method was developed using graphite composite end-attachment test specimens and then applied to the fuselage component. This report section describes the contact test method and highlights results of the component examination. Equipment utilized was as follows:

(a) 721 Sperry Reflectoscope

(b) 10-N Pulser Receiver

(c) Fast Transigate

(d) 50B1265, 5 MHz, Pitch and Catch Transducer driven at 2.25 MHz

(e) Glycerin (Couplant)

The transducer employed was originally designed for making thickness measurements of steel or aluminum. However, recent studies were conducted to determine discrimination when the transducer is over one composite thickness, two composites bonded or two composites unbonded. Figure 43 illustrates the three conditions evaluated.

Figure 44 shows a typical cathode ray tube presentation of either the skin or unbonded stringer-to-skin condition. In either case the general characteristics of the trace are the same. Figure 45 shows the response from a bonded stringer and skin combination. Note the signal shift to the right indicating greater thickness. Advantages of this method are: first, the test is portable and secondly, a quantitative determination of a debond condition is obtained. The method has the disadvantage that a defect within the shell skin (such as delamination) would interfere with the test.

In the examination of the fuselage shell, stringers 3, 4, and 5 were evaluated for 36.5 in. of their total length. Areas of bond and unbond were detected. These results show, as expected, debonded lengths greater than those determined from the

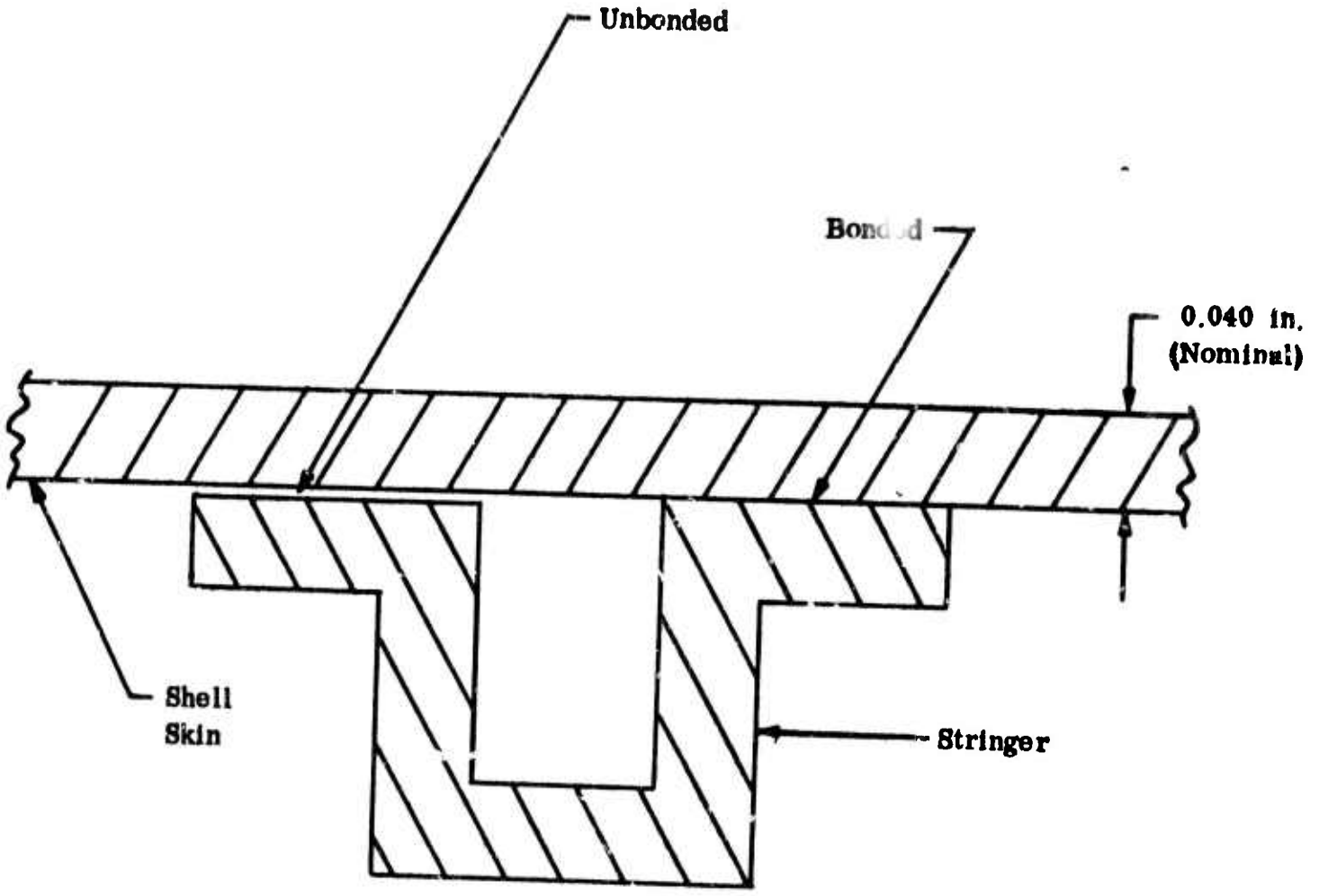

Figure 43. Ultrasonic Discrimination of Shell Skin, Unbonded or Bonded Stringer

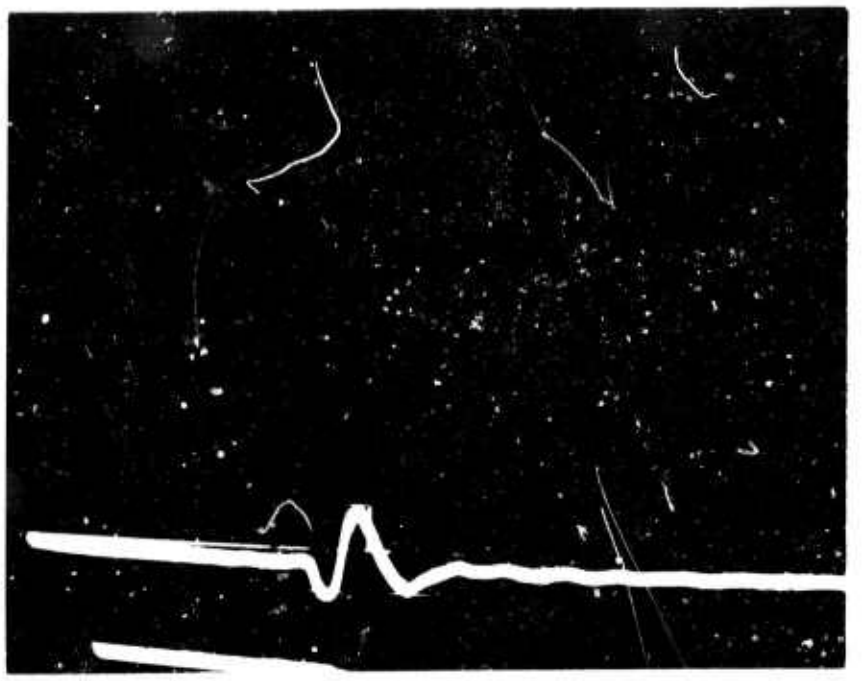

Figure 44. Typical Cathode Ray Tube Presentation of Either the Shell Skin or the Unbonded Stringer-to-Skin Combination.

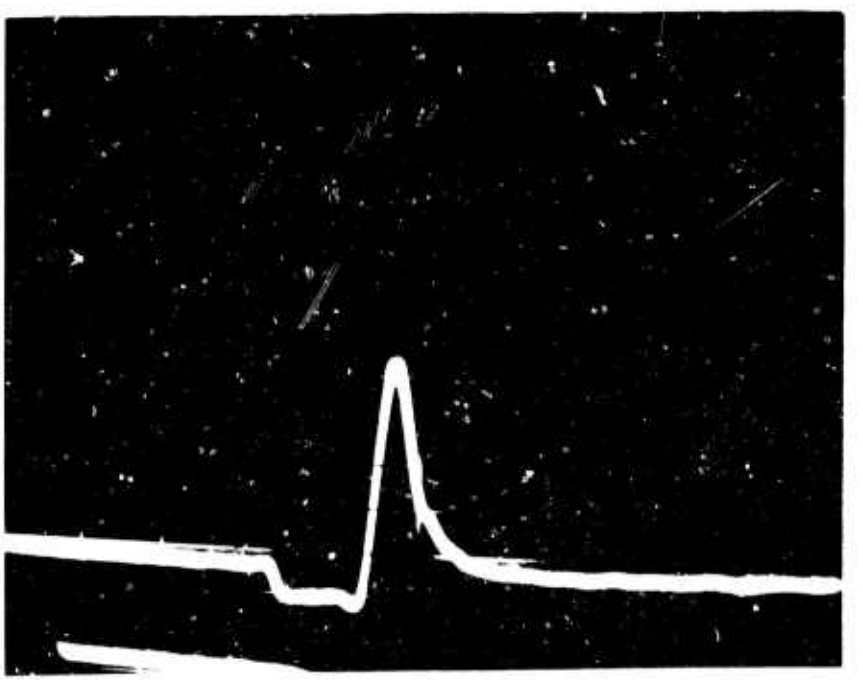

Figure 45. Trace of Response from a Bonded Stringer and Skin in Combination.

visual inspection. The ultrasonic contact test method was used to evaluate the fuselage component repair effectiveness upon completion of work outlined in Section VIII.

D. Acoustic Impact Tests
(Personnel from the AFML and Dr. H.F. Volk, Union Carbide)

An acoustic impact tester, developed by Arvin Systems, Inc., was utilized for further nondestructive testing. The technique consists of an analysis of the vibrations in the test specimen produced by mechanical pulses and has been described in recent AFML reports.(6) The technique was originally developed for the detection of cracks in metallic parts (particularly jet engine components) and later found to be useful as a bond tester. This was the initial application of the equipment to graphite fiber, resin composites. Therefore, interpretation of results required some correlation with results obtained by other techniques and some judgement.

The readings were taken by attaching the probe to the outside of the skin in the areas over the ring stiffeners and between stringers. The measurements over the ring nearest the large diameter (Ring No. 1) were affected by the heavy fiber glass end attachment buildup and gave high readings which are probably not related to debonding. Reproducibility of the measurements was good. Six areas of ring debonding were detected. Ring No. 2 was debonded in the vicinity of stringer 22; ring 3 showed debonding in the area of stringers 18 and 21; ring 4 was found defective between stringers 17 and 19 and stringers 22 and 25. The acoustic impact tests agreed with and refined the results obtained by visual observations; ring 3 could be wiggled by hand in the area where the acoustic tests showed debonding.

Measurements to test the bond between the aluminum end attachment plates and the fiberglass buildup were also performed. Uniform readings were obtained along the entire circumference, and it was concluded that the bonding was sound.

The acoustic impact method was also used in spot checks to detect debonding between stringers and skin; this was accomplished by traversing the probe over the stringer flanges on the inside of the fuselage. The potentially simpler technique of traversing on the outside of the skin over the stringers did not work well, partly because the skin surface was too rough and also due to difficulties in precise positioning of the probe. The results of the acoustic impact test confirm those obtained by other techniques, e.g., visual/mechanical inspection and ultrasonics. However, tests were restricted to spot checks on a few stringers,

since geometric configuration factors (probe somewhat too large, interruption of traverse by the ring stiffeners, difficulties of working on the inside of the fuselage) made the method rather tedious.

SECTION VII

POTENTIAL CAUSES OF FUSELAGE COMPONENT DAMAGE

A. Experimental Investigation

(A. A. Pallozzi, Dr. G. B. Spence, and Dr. H. F. Volk, Union Carbide)

An experimental investigation was conducted to determine the cause(s) of fuselage component damage, particularly with respect to debonding. Numerous stringer reinforced shear and compression panels were made and tested prior to fuselage fabrication, none of which had given any indication of a bonding problem. Even during tests, bond failure was never observed; rather, failure occurred within the stringers or skin panels. The same adhesive system (70 weight percent Araldite 6005 epoxy resin and 30 weight percent (ZZLB-0325 hardener) was used for bonding the stringers to the test panels and the stringers and ring stiffeners to the fuselage component. However, due to the size and complexity of the fuselage component, some details of the fuselage bonding procedure were somewhat different from those used for test panel fabrication. Potential failure causes are also related to the much larger size of the fuselage component (which enhances thermal expansion effects) and to the possible mismatch in curvature between stringer flanges and skin.

1. Effects of Surface Contamination

Masking tape was used during fuselage fabrication to cover the area between stringers in order to expedite subsequent removal of excess adhesive. After the tape had been applied, the skin between the tape strips was lightly sanded, vacuumed, and cleaned by wiping with ethyl alcohol. Thus, the surface could have been contaminated by an alcohol soluble constituent in the masking tape. To test this theory, short (one-inch long) pieces of stringer were bonded to flat plates by a procedure that duplicated the use of masking tape and by a control procedure in which the tape was omitted. After bonding and curing (cure cycle: four hours at room temperature, six hours at 60°C) the top (hat) of the stringer was cut off and the remaining (L-shaped) sections were tested in shear. Shear strength values obtained on stringers bonded by using the tape procedure were 1452, 1054, 2370, and 1000 psi (avg. 1684 psi); the control sample gave values of 1875 and 1560 psi (avg. 1720 psi). Failure occurred in all samples within the stringer or skin material, not at the bond. Contamination from the masking tape was, therefore, ruled out as a possible failure mechanism.

Material leached from the Dixie cups used for blending the two-part adhesive system was also suspected as a possible contaminant. Although Dixie cups had been used throughout the

entire program, the adhesive may have remained in the cups for a longer time period during fuselage bonding, thus increasing the chance of contamination. Shear tests performed on stringers bonded with adhesive that had been stored in the cups for 1-1/2 hours gave values of 1350, 1910, 1570, and 1280 psi (avg. 1520 psi); failure again occurred within the composite rather than in the bond line. Moreover, the shear values obtained with the aged adhesive were reasonably close to the control values of the previous (masking tape) test in which fresh adhesive had been used. Contamination from the Dixie cups was, therefore, also ruled out as a failure cause.

2. Effect of Bond Line Thickness

The stringers used for the fuselage component had curved flanges which approximated the radius of the shell. However, due to the tapered cross section of the shell, the radii of curvature matched exactly only at a point approximately 14 inches (approximately 1/3 of the total length of the component) from the large diameter end. The mismatch in curvature at any other point along the stringer length made it impossible to maintain a constant glue-line thickness, although the differences are quite small (approximately 0.001 inch at the small end, where the effect is greatest). Moreover, the steel fixture employed for pressurizing the stringers during the cure cycle permitted only poor control over the bond-line thickness. Experiments were, therefore, performed to determine the effect of glue-line thickness on the shear strength of the stringer-to-skin bond. Specimens with minimum (approximately 0.001 inch) and with 0.003- and 0.010-inch thick bond lines were tested. Further tests were performed on curved stringers bonded to flat plates. The results, shown in Table XXV, indicated superior performance when a bond approximately 0.003-inch thick was employed.

TABLE XXV

EFFECT OF BOND LINE THICKNESS ON SHEAR STRENGTH OF STRINGER TO SKIN BOND

Flange Shape	Bond Line Thickness (in.)	Shear Strength (psi)
Flat	minimum	1320
Flat	minimum	1760
Flat	0.003	2140
Flat	0.010	1240
Flat	0.010	1760
Curved	minimum	1550
Curved	minimum	2120
Curved	0.003	3040
Curved	0.010	2470
Curved	0.010	1330

However, even the thinnest and thickest bonds had shear strengths well over 1000 psi; moreover, failures in the shear tests again occurred within the composite. For these reasons, it is unlikely that variations in bond line thickness caused the observed component damage.

3. Influence of Cure Temperature on Properties of Adhesive

Three stages of cure temperatures were used during fabrication of the representative fuselage component. The stringers were cured at 70°C during the bond cycle. Since the stringers were bonded in sets of four, those stringers which had been bonded first were exposed to the first cure cycle several times. The component was then subjected to another cure cycle at 100°C for bonding of the ring stiffeners. Finally, the component was heated four times at 130°C (two to three hours each time) to bond the fiberglass ring segments which form a part of the end attachments of the component. Resin embrittlement may have occurred during these cure cycles, causing a decrease in adhesive strength.

Lap shear tests were performed on bonded aluminum sheet samples to determine the effect of cure temperature on lap shear strength. Two samples each were cured for six hours at 60°, 100°, and 130°C, respectively. The test area was one-inch square, with a bond line thickness of three mils. All six samples failed within a narrow load ranging from 1320 to 1380 lbs. Further tests were performed to determine the influence of cure temperature on the mechanical properties of the adhesive resin system. Cast bars were cured for four hours at room temperature, followed by six hours heating at 60°C and four hours each at 100° and 130°C. The results are shown in Table XXVI. Both the tensile strength and the elongation-to-failure were considerably reduced after the samples were heated at the higher cure temperatures. This effect was particularly disturbing in view of the very high thermal expansion coefficient of the resin system ($100 \times 10^{-6}/°C$). However, the same thermal stresses must have been present in the stringer-stiffened test panels in which no debonding was observed. For this reason, thermal stresses in the bond line are not considered to be the principal cause of component damage.

4. Thermal Expansion of Component Parts

The thermal expansion of graphite-fiber, resin-matrix composites is strongly dependent on the fiber lay-up pattern. Each functional part (skin, stringer, ring shear panel) of the fuselage component utilizes different fiber lay-up geometries; the resulting mismatch in thermal expansion will give rise to thermal stresses upon cooling from the cure temperature. This problem was recognized earlier in the program, but the effect was not judged to be

serious (a more comprehensive mathematical treatment is given in Section VII B on Analytical Studies). Nevertheless, in view of the observed stringer-to-skin debonding, the thermal expansion coefficients of the stringers and the skin were redetermined. All measurements were carried out over the range from room temperature to 100°C in a dilatometer by using a traveling microscope. The results are presented in Table XXVII.

TABLE XXVI

MECHANICAL PROPERTIES OF ADHESIVE RESIN SYSTEM

Max Cure Temp. (°C)	Density (g/cc)	Young's Modulus (10^6 psi)	Shear Modulus (10^6 psi)	Tensile Modulus (10^6 psi)	Tensile Strength (10^3 psi)	Elong. to Failure (%)	CTE* (10^{-6}/°C
60°	1.121	0.441	0.169	0.411	8.76	3.57	
		0.425					
100°	1.115	0.397	0.154	0.348	6.90	2.75	101
		0.387	0.156				
130°	1.115	0.396	0.156	0.338	5.57	1.97	100
		0.386	0.153				

*Coefficient of Thermal Expansion

TABLE XXVII

THERMAL EXPANSION COEFFICIENTS OF VARIOUS COMPONENT PARTS

Part	Fiber Lay-Up	Coefficient of Thermal Expansion (10^{-6}/°C) 0° Direction	90° Direction
Skin	90, ±15, 90°	1.9	1.7
Stringer	±10°	-1.8	43.7

5. Other Potential Causes of Component Damage

The experiments discussed in the foregoing paragraphs identified thermal stresses in the bond line and thermal degradation of the adhesive as factors which could have contributed to component damage. However, these conditions also applied for test

panels in which debonding did not occur. The greater length of the component (48 inches vs 8 to 16 inches for test panels) may have aggravated the situation. The extent of debonding, however, indicates that other causes must have contributed to the problem. As mentioned before, all procedural aspects unique to component fabrication are suspect; the steel bonding fixture, in particular, may have caused problems. This fixture, was described in Section V and was shown in Figure 35. Thermal expansion of the V-shaped metal framework during the cure cycle may have raised the pressure bars, in effect relieving the pressure on the stringers during curing. Since the pressure bars were pushing against the stringer flanges, pressure relief may also have caused a slight lateral motion of the stringer flanges at a time when the adhesive was not yet fully cured. Another possibility that cannot be completely ruled out concerns the entrapment of air bubbles in the bond line.

B. Analytical Studies

(Dr. K. H. Sayers and S. L. Cross, Bell Aerosystems)

Thermal stresses and stresses due to radius of curvature mismatches between stringers and the shell skin were suspected as possible causes of the debonding in the fuselage component. Since each part of the shell (skin, stringers, rings, and end attachment buildups) is fabricated separately at elevated temperature, each part will suffer local thermal stresses when cooled to ambient temperature. Subsequent bonding operations in the shell assembly are also performed at elevated temperatures, giving rise to additional stresses because of differences in expansion coefficients. Obviously, in the fuselage shell, the complete thermal or residual stress pattern is very complex. This report section presents the analyses and assumptions made to assess the influence of fabrication stresses.

1. Thermal Stresses

The problem of thermal stresses was recognized in mid-1968 when the most significant effect was judged to be that of skin-to-stringer bonding. Since the stress levels were relatively low, this work was not reported earlier. An analysis of the last compression panel tested (SP-50-1, Section IX G of Reference 3) was made because shell measurements were not then available. The panel was fabricated with the same materials (treated "Thornel" 50) and the same layup patterns as the shell. The thicknesses and fiber contents, however, were somewhat different. Nominal properties of the panel and fuselage shell are given in Table XXVIII, and thermal property data are given in Table XXIX.

TABLE XXVIII

COMPRESSION PANEL AND FUSELAGE COMPONENT PROPERTIES

	Panel			Shell		
	Layup	Fiber Vol. Content (%)	Thickness (in.)	Layup	Fiber Vol. Content (%)	Thickness (in.)
Skin	90,±15,90°	53.0%	0.035	90,±15,90°	~35	0.056
Stringers	±10,∓10°	50.3	0.038	±10,∓10°	~52.5	0.038

TABLE XXIX

THERMAL PROPERTY DATA

$\alpha_{Fiber} = -1.01 \times 10^{-6}/°C$	(Table XXIX, Reference 2)
$\alpha_{Matrix} = 77.0 \times 10^{-6}/°C$	(Table XXXIII, Reference 2)
Bonding Temperature = 160°C	(Table XXXIV, Reference 2)
Ambient Temperature = 20°C	

Note: α = Coefficient of Thermal Expansion

In Table XXX, the stresses in the 1-direction of the skin and stringer plies are small and compressive. The stringer ply shear stresses are approximately 15-20 percent of the ply shear strength. Transverse stresses in the 2-direction of the skin plies are tensile stresses of magnitudes greater than the estimated transverse strength. The transverse stresses were originally discounted for several reasons: (1) no damage was observed in the skin panels after fabrication, (2) it is not known when the composite becomes a structure during cure and what creep and relaxation effect occur, and (3) applicability of the Grezczuk thermoelastic theory is questionable in regard to fiber anisotropy. There is more recent evidence, however, that transverse stresses are in fact a problem since cracks were observed in the component skin. Also, dye penetrant and permeation tests have shown that resin cracking can occur in cured, cross-plied laminates.

From the total composite strains and the known applied temperature change, the overall composite expansion coefficients were computed. Measurement of these coefficients were obtained by Union Carbide for plates having the same layups but somewhat different fiber contents and thicknesses. The data are compared in Table XXXI.

TABLE XXX

PLY THERMAL STRESSES DUE TO FABRICATION

	Layer	σ_1	σ_2	τ_{12}
Skin	90°	-4410	5090	0
	15	-5820	5140	-15
	-15	-5820	5140	15
	90	-4410	5090	0
Stringers	10°	- 345	343	948
	-10	- 345	343	-948
	-10	- 345	343	-948
	10	- 345	343	948

Notes: (a) 1-direction is parallel to fibers.
2-direction is transverse.

(b) Twisting displacements were restrained for the skin; stresses in psi.

TABLE XXXI

THERMAL EXPANSION COEFFICIENTS

		α_x	α_y	α_{xy}
Skin				
	Computed	1.80	-1.39	0
	Measured	1.87	1.66	-
Stringers				
	Computed	-1.05	33.9	0
	Measured	-1.73	43.8	-
Adhesive				
	Measured	100	100	-

Notes: (a) x--direction is 0°
y--direction is 90°

(b) Units are 10^{-6}/°C

The effects of bonding the skin to the stringers were estimated by treating the stiffened panel assembly as a long beam subjected to a uniform temperature change. Computed elastic constants were employed for the skin and stringers. Adhesive modulus was taken as 0.41×10^6 psi (Table XXVI). Bonding temperature was 100°C, and 22°C ambient temperature was assumed. The maximum predicted axial thermal stresses after cool-down were:

Skin:	σ_x = +2500 psi;
Stringer (Cap):	σ_x = -4160 psi; and
Adhesive:	σ_x = +3240 psi.

Although the expansion coefficients of the skin and stringers given in Table XXXI have opposite signs, their low absolute values cause the resulting thermal stresses in these elements to be low. Bond stresses are high compared with the adhesive strength (approximately 5600 psi, Table XXVI). Local transverse stresses will also be present under the stringer flats; the adhesive stress in the transverse direction was found to be equal (approximately 3000 psi) to the axial adhesive stress.

The thermal stress effects do not appear to be severe enough in themselves to cause the stringer-to-skin debonding. However, stresses in the adhesive represent a substantial fraction of the adhesive strength. Other factors probably contributed to the debonding, since no thermal stress damage was observed in any of the test panels. Predicted transverse stresses due to skin fabrication appear significant and may be related to the observed skin cracks. Computed expansion coefficients were found to be in reasonable agreement with measurements. Stresses caused by skin-to-stringer bonding were found to be low, except in the adhesive itself.

In certain other laminates and structural assemblies, thermal stresses may be very significant because of differences in expansion coefficients. Further correlation work and work on bonding techniques designed to reduce thermal stresses are needed.

2. Stringer/Skin Radius of Curvature Mismatch

The stringers in the fuselage shell were designed with a flange radius of curvature equal to that of the shell interior radius midway between ring Frames 1 and 2 (see Figure 46). There were two reasons for having selected this condition: (1) the large end of the shell would be critical in the final (destruct) test and it was desired that the best fit be at this end; and, (2) the stringers could be machined with only a single radius of curvature along their lengths, precluding an exact fit at all

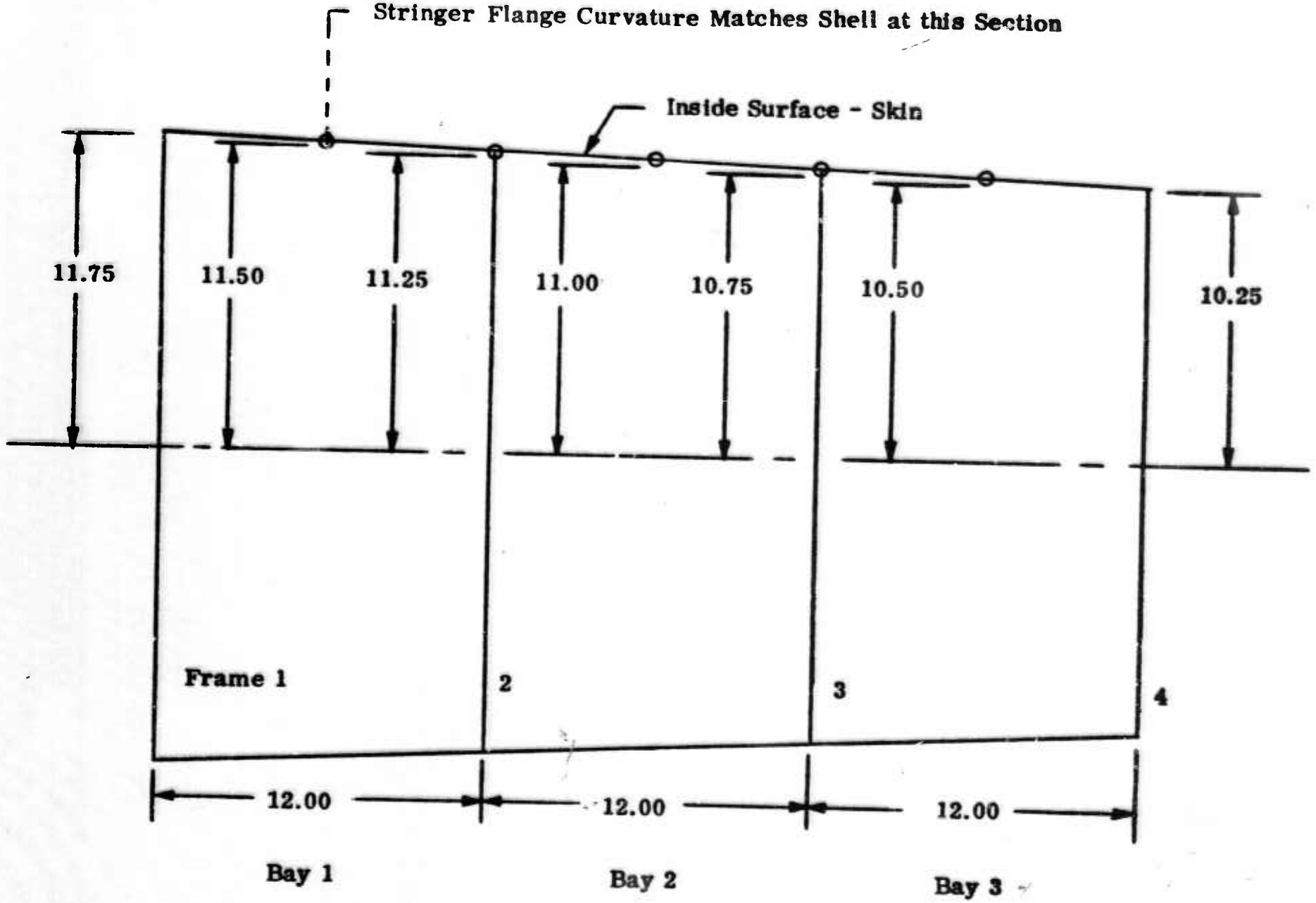

Diameter Tolerances ±0.005

Figure 46. Fuselage Shell Geometry

stations. Consequently, a mismatch occurs in radii of curvature of the stringers flats and the shell I.D. at either end of the component. Figure 47 shows the geometrical mismatches at both ends of the shell. Thermal expansion and/or distortions of the stringers were thought to be small and were not included in the mismatch calculations.

The primary intent of this study was to assess the magnitude of peeling stresses in the adhesive between stringers and skin due to the mismatch conditions. Maximum mismatches were calculated to be 0.0003 in. at the large end of the shell and 0.0009 in. at the small end. The stringer flat was assumed to be a cantilever, and the peel stresses due to a distributed transverse load or bending moment were determined for the more severe 0.0009 in. displacement produced by the bond tooling shown in Figure 35. A bond peel load of 0.434 lb/in. and a bending moment of 0.149 lb/in. were calculated.* Respective estimated ultimate strengths were 15-20 lb/in. or 17-22 in.lb/in. (Section III C-3 and also Reference 7). Thus the peel loads due to curvature mismatch are small and do not seem likely to have contributed significantly to stringer debonding from the shell.

*These values are on the "high side" because of additional flexibility in the stringer fillet which was ignored in calculation.

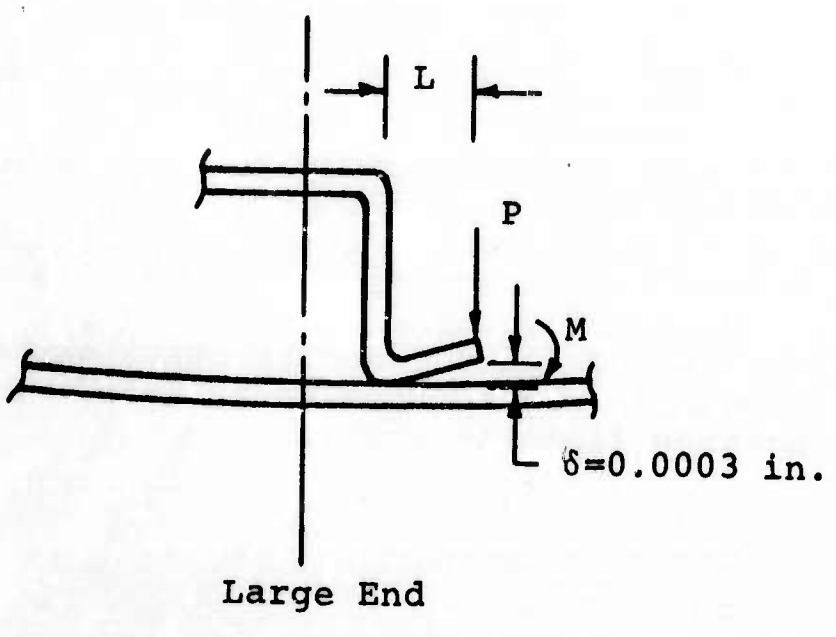

Large End

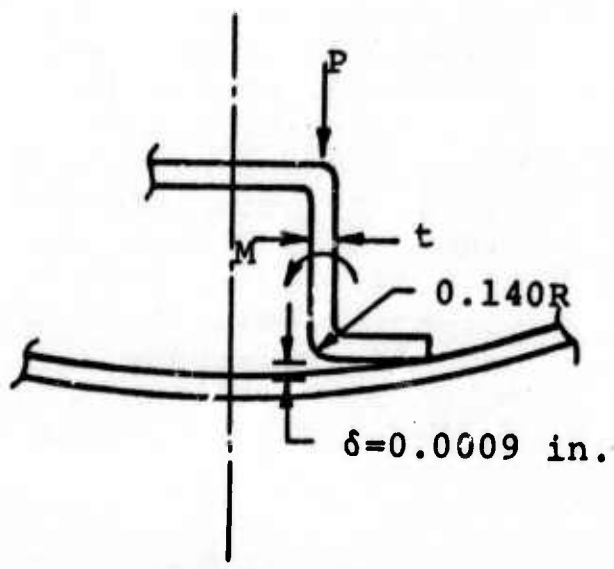

Small End

Distributed Transverse Load

$$P = 3E_2 I\delta L^3$$

$E_2 = 1.18 \times 10^6$ psi

$I/b = t^3/12 = (0.040)^3/12 = 5.33 \times 10^{-6}$ in.^{3}

$\delta = 0.0009$ in.

$L = 0.34$ in.

$P = 0.434$ lb/in.

Distributed Bending Moment

$$M = 3E_2 I\delta/bL^2$$

$= 0.149$ in.lb/in.

Bending Stress

$$\sigma_b = 6M/t^2$$

$= 550$ psi

Figure 47. Stringer/Skin Mismatch.

SECTION VIII

REPAIR OF FUSELAGE COMPONENT

(A. A. Pallozzi, Dr. G. B. Spence, and Dr. H. F. Volk, Union Carbide)

Repair of the observed defects in the representative fuselage component was successfully accomplished. The repair procedures were established by Union Carbide Corporation in close consultation and cooperation with Bell Aerosystems Company. Since thermal stresses probably contributed to the debonding problem, only room temperature curing adhesives were used for the repair work. The stringers were rebonded to the skin by inserting tubular perforated bladders into the stringers cavities, filling the bladder with adhesive, and pressurizing to force the resin to flow into the debonded areas. The ring stiffeners were rebonded to the fuselage shell by draping fiberglass tape prepregged with adhesive over the ring stiffeners, and the craze cracks in the skin were covered with a layer of prepregged fiberglass tape.

A. Evaluation of Adhesives and of Repair Procedures

There was no known prior art for adhesive rebonding of fiber reinforced plastic hat-section stringers to a fiber reinforced plastic shell structure. Experiments were performed to verify the validity and practicality of the proposed repair techniques, to select the proper adhesive systems, and to gain the necessary experimental expertise.

1. Evaluation of Adhesive Systems

Two types of room temperature curing adhesive were required for repair: a low viscosity resin for stringer-to-skin rebonding and a more viscous adhesive for prepregging the fiberglass tapes. Further desirable characteristics for the adhesive included high elongation to failure, good peel and shear strength, and a useful working life of at least 90 minutes. These requirements were met by Scotch-Weld adhesives 2216/clear and 2216/gray.* Both materials are urethane modified epoxies with similar properties in the cured state (30 day cure at room temperature), but the clear adhesive has a much lower viscosity than the gray adhesive.

Shear strength measurements were carried out to evaluate the strength of the stringer/skin bond obtainable with adhesive 2216/clear. The shear test samples consisted of 0.9-inch-long sections of stringers bonded to a flat panel. The stringer

*Products of 3M Company.

cap was cut longitudinally to allow each stringer flange section to be tested separately. The load was applied to the edge of the stringer flange while the flat plate was supported and rigidly held. The shear strength was calculated by dividing the failure load by the bond area. Bond line thickness was 3 mil, and the adhesive was cured for various periods of time under a pressure of 2 psi. The shear strength values obtained after curing for 140 hours were judged quite satisfactory; it was also found that the bond obtained after 20 hours curing time was sufficiently strong for handling. The numerical results are listed in Table XXXII.

TABLE XXXII

SHEAR STRENGTH OF STRINGER/SKIN BOND
(ADHESIVE: SCOTCH-WELD 2216/CLEAR)

Sample No.	Adhesive Cure Time(1) (hrs)	Bond Area ($in.^2$)	Load (lb)	Shear Strength (psi)
29	20	.304	433	1420
29	20	.283	300	1060
30	20	.273	248	910
30	20	.278	350	1260
31	44	.298	562	1880
31	44	.284	452	1590
32	44	.298	370	1240
32	44	.277	500	1810
33	140	.267	522	1960
33	140	.253	440	1740
34	140	.251	630	2510
34	140	.248	732	2950

(1)All samples cured at room temperatures under 2 psi pressure.

Similar shear strength measurements were carried out on samples where the adhering surfaces had been pre-coated with the original adhesive prior to bonding with Scotch-Weld 2216/clear in order to duplicate the condition which existed in the debonded areas of the component. The bond strengths obtained under this condition (see Table XXXIII) were again found to be

satisfactory, particularly when a post-cure at a slightly elevated temperature (50°C) was applied. Thus, it was decided not to remove the old adhesive from the debonded areas of the component, an attempt which would have been difficult at best.

TABLE XXXIII

SHEAR STRENGTH OF STRINGER/SKIN BOND (ADHESIVE 2216/CLEAR, BONDED AREAS PRE-COATED WITH CURED ARALDITE 6005/ZZLB-0325 ADHESIVE

Sample No.	Adhesive Cure Time([1]) (hrs)	Bond Area ($in.^2$)	Load (lb)	Shear Strength (psi)
35	16	.307	385	1250
35	16	.290	405	1400
36	16	.293	318	1080
36	16	.305	330	1080
37	46	.275	348	1260
37	46	.258	318	1230
38	46	.260	253	980
38	46	.290	198	680
39	22([2])	.270	352	1310
39	22([2])	.255	138	540
40	22([2])	.266	289	1100
40	22([2])	.270	292	1090
41	168	.265	500	1940
41	168	.267	451	1740
44	146([3])	.275	520	1920
44	146([3])	.280	451	1740
45	146([3])	.291	800	2710
45	146([3])	.286	740	2590

([1])Samples cured at room temperature under 2 psi pressure.

([2])Additional 24 hrs cure at zero pressure.

([3])Additional 90 hrs cure at zero pressure.

Adhesive 2216/clear was also evaluated in lap shear and in peel tests on specimens prepared according to ASTM methods D 1002-64 and D 1876-61 T, respectively. The influence of the strain rate upon lap shear strength (one-inch wide aluminum adherends) is presented in Table XXXIV. The observed strain rate dependency, also reported by other investigators,[8,9] is a characteristic of a flexible adhesive.

TABLE XXXIV

INFLUENCE OF STRAIN RATE UPON LAP SHEAR STRENGTH OF SCOTCH-WELD 2216/CLEAR

Specimen No.	Cure Schedule	Bond Area ($in.^2$)	Breaking Force (lb)	Strain Rate (in./min)	Lap Shear Strength (psi)	Load Rate (psi/min)
I	Room Temp. Cure	0.518	509	0.002	980	25.5
J	120 hrs @ 2 psi bonding pressure	0.510	400	0.002	780	20.0
A	Room Temp. Cure	0.525	852	0.05	1620	860
B	92 hrs @ 2 psi	0.525	910	0.05	1730	990
C	Room Temp. Cure	0.505	1010	2	2000	16,000
D	92 hrs @ 2 psi	0.510	1018	2	2000	25,400

The peel strength of adhesive 2216/clear is listed in Table XXXV; for comparison, the peel strength (as a function of cure temperature) of the adhesive originally used for assembling the fuselage (Araldite 6005/ZZLB-0325) is listed in Table XXXVI. The data clearly show the dramatic increase in peel strength resulting from use of adhesive 2216/clear.

TABLE XXXV

EFFECT OF CURE SCHEDULE UPON PEEL STRENGTH OF SCOTCH-WELD 2216/CLEAR

Cure Schedule	Peel Strength
Room Temperatures 20 hrs @ 2 psi	7.6 lb/in.
Room Temperatures 20 hrs @ 2 psi	8.9
Room Temperatures 44 hrs @ 2 psi	7.3
Room Temperatures 44 hrs @ 2 psi	5.0
Room Temperatures 120 hrs @ 2 psi	10.6
Room Temperatures 120 hrs @ 2 psi	10.3

TABLE XXXVI

EFFECT OF CURE TEMPERATURE UPON PEEL STRENGTH OF ADHESIVE 6005/0325

Cure Schedule	Peel Strength
Room Temperatures 18 hrs + 4 hrs @ 60° C	2.6 lb/in.
Room Temperatures 18 hrs + 4 hrs @ 60° C	2.1
Room Temperatures 21 hrs + 4 hrs @ 100° C	1.8
Room Temperatures 24 hrs + 4 hrs @ 130° C	1.3
Room Temperatures 24 hrs + 4 hrs @ 130° C	1.4

2. Evaluation of Repair Procedures

The stringers were to be rebonded to the skin by forcing the adhesive to flow through perforated bladders (contained within the stringer cavity) into the debonded areas. The cross-sectional shape of these bladders (tubes) was to conform closely to that of the stringer; thus, removal of the resin filled tube after rebonding would leave little excess adhesive in the stringer cavity. Various materials, including nylon and Teflon, were investigated for use as bladders. Polyethylene (Scotchtite 3025-080*) was finally selected because it is non-reactive with epoxies and because it could be heat-shrunk over a mandrel, a characteristic which facilitated the fabrication of bladders with the proper cross-sectional shape. Practice bonding experiments were conducted by using both aluminum stringers and some of the 14 stringers left over from the fuselage fabrication. These stringers were bonded to a full-size aluminum mock-up of the fuselage shell. In some practice runs, the stringers were simply clamped to the shell by using 3-mil steel wire to provide the necessary gaps. In other practice experiments, the stringers were pre-bonded to the shell with large gaps in the bond area to simulate the condition of the component. These practice experiments establish the feasibility of the repair method. A pressure of 3 psi was found to be sufficient to force the adhesive (2216/clear) into all debonded areas. The experiments also provided confidence that rebonding of each stringer could be accomplished within 30-45 minutes, well within the 90 minutes working life of the adhesive.

*Product of 3M Company.

The insertion of a tubular bladder into the stringer cavity required cut-outs in the fiberglass end attachments on each end of the component, and there was some concern that these cut-outs could affect the load transfer into the component. Consequently, appropriate cut-outs were machined into the fiberglass end attachments of the larger of the two halves of the end attachment compression panel remaining from the test described in Section IV of this report. The broken end of this panel was potted, and the specimen was tested again in compression. Strain gage readings and failure level compared well with those obtained in the previous compression test at Bell; thus, it was concluded that the end-attachment cut-outs would not interfere with the proper loading of the component.

The effectiveness of the fiberglass shear clips used to rebond the ring stiffeners to the fuselage shell was also investigated. Balsa core beam elements, 1 inch long x 1/2 inch wide, were bonded to flat graphite fiber composite plates and tested in tension. Some beam elements were bonded to the plate only with glass cloth strips prepregged with Scotch-Weld adhesive 2216/gray. These fiberglass strips extended 0.75 inch onto the flat plate on either side of the shear beam element; the bonding procedure was essentially the same as that outlined later under repair of the fuselage component. The specimens were cured for one week before testing and failed at an average tensile load of 110 lbs. A second set of beam elements was bonded to the flat plates with Araldite 6005/ZZLB-0325, the adhesive originally used in the fabrication of the component; these specimens failed at an average tensile load of 150 lbs. A third set of beam elements was bonded using both fiberglass strips and Araldite 6005/ZZLB-0325; these samples failed at an average load of 225 lbs. Since the primary function of the ring stiffeners is to prevent ovalling of the component, the ring-to-skin bond is only lightly loaded; thus the bond strength obtained with the fiberglass strips was judged more than adequate.

B. Fuselage Component Repair

1. Stringer to Skin Rebonding

The stringers were rebonded to the fuselage skin with Scotch-Weld 2216/clear adhesive. Groups of four stringers were rebonded on alternate days, commencing on Monday of each week. On each repair day, two stringers were rebonded in the morning, and after the adhesive was permitted to gel for three hours, the remaining two of the group were repaired. The component was positioned in the plaster cradle so that the stringers being rebonded were at the lowest point of the fuselage radius of curvature, a procedure which prevented adhesive runoff.

Three hundred milliliters of adhesive were formulated to repair each stringer, and the blended adhesive was centrifuged for eight minutes to remove entrapped air. The adhesive was forced through the debonded areas from a perforated polyethylene tube inserted into the stringer cavity. A 1/2 inch O.D. piece of plexiglas tubing, six inches long, was attached to one end of the perforated tube and also connected to the adhesive reservoir with a swaglock fitting. Attached to the other end of the perforated tube was a three-foot length of tygon tubing (1/4 inch O.D.), which facilitated inserting and positioning the perforated tubing within the stringer cavity. Also, when adhesive was observed flowing within the tygon tube, that tube was clamped to allow pressure buildup within the perforated tube. A pressure of three psi was applied to the adhesive reservoir. After the adhesive had been forced into the debonded areas, the perforated tube was retracted, leaving very little adhesive within the stringer cavity.

Bond line thickness control was achieved by inserting short sections of three-mil steel wire into the debonded areas between the stringer flanges and the skin. The areas into which a three-mil shim could be inserted were marked on masking tape covering the stringer caps. Also marked on the stringer caps were those areas in which some debonding had been indicated by the helium leak tests. During rebonding, adhesive was observed to flow from all areas into which a 3-mil shim could be inserted, whereas adhesive flow was not generally detected in areas in which debonding was indicated only by helium leak tests.

The excess adhesive which flowed from the debonded areas was contained within a dam formed by the ring stiffeners and was spooned from the dams to facilitate the clean up operation. All interior fuselage surfaces were covered with masking tape. After the excess adhesive was removed, a silicone rubber pad was placed over the stringer and weighted with lead weights to apply two psi contact pressure to the bond line. Repair of each set of two stringers was easily accomplished within the 1.5 hours working life of the adhesive. The lead weights were removed after the adhesive was permitted to cure at room temperature for a minimum of 40 hours. The repair procedure is illustrated in Figure 48, which shows the resin reservoir and pressurization system, the bladder inserted into a stringer cavity, and the lead weights used to exert the necessary bond line pressure.

The rebonding procedure required cut-outs at the stringer ends to permit insertion of the perforated tube into the stringer cavity. These cut-outs were made on a milling machine and, at the large diameter fuselage end, were rectangular, measuring 7/8 inch long by 7/32 inch wide, with the ends chamfered 45°. At the small diameter fuselage end, a circular hole of 9/32 inch diameter was machined at the stringer ends to permit the tygon tubing to extend outside the stringer cavity.

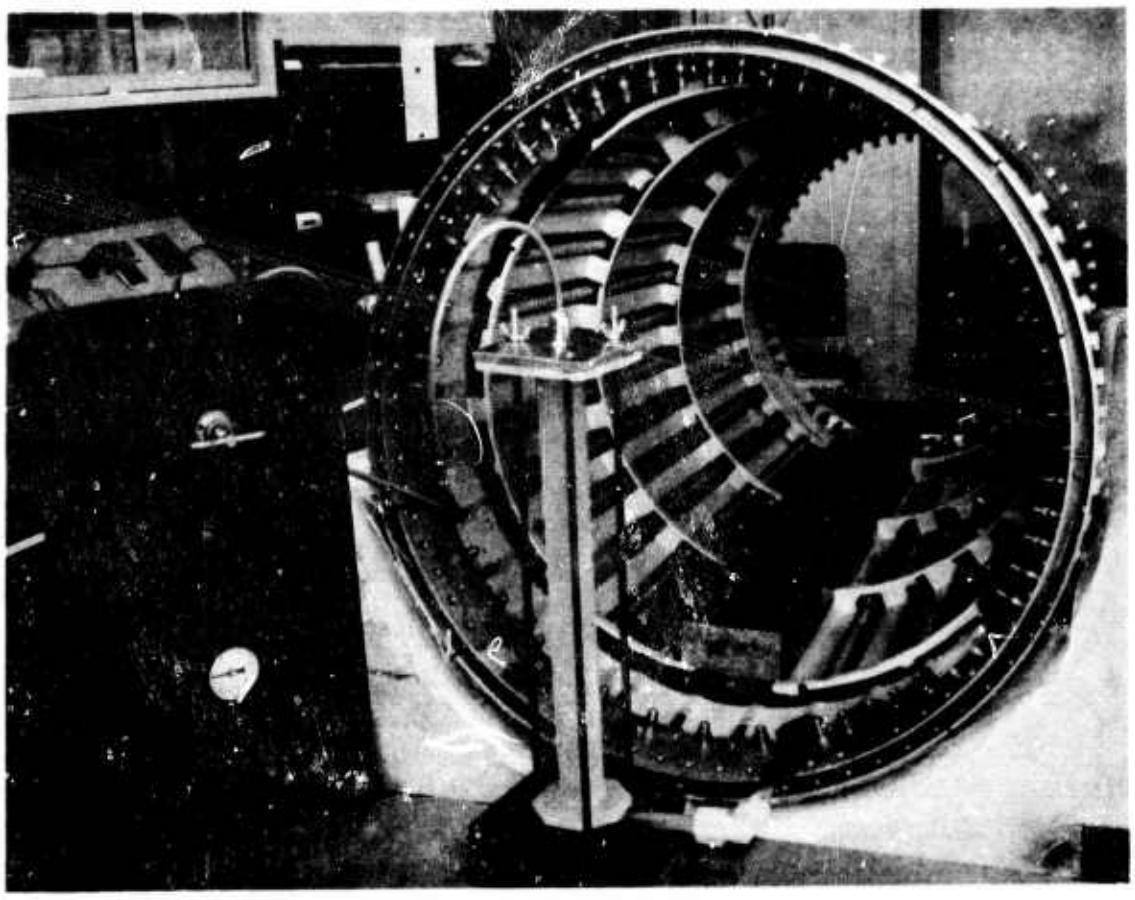

Figure 48. Equipment for Rebonding for Stringers to Skin.

N-22198

After all stringers had been rebonded, the component was heat-cured at 50°C (122°F) for a period of 108 hours to accelerate the final curing of the adhesive system. The thermal stresses resulting from this moderate cure temperature were considered to be small.

The effectiveness of the repair procedure was determined by using both the ultrasonic technique and the helium leak detector described in Section VI of this report. The ultrasonic technique was slightly modified. Instead of looking for a shift in the observed echo, it was found to be more convenient to tune the ultrasonic equipment so that no echo at all was observed for a stringer in the bonded condition. Old panels with debonded stringers and the fuselage itself prior to final repair were checked to verify the ability of this method to detect known debonds. After fuselage repair, all stringers were checked over their entire length and found to be bonded. Similarly, no leaks could be found with the helium leak detector on the repaired component.

2. Bonding of Ring Stiffeners to Skin

Visual inspection and the acoustic impact tests had indicated a few areas in which the ring stiffeners were debonded from the skin, as discussed in Section VI of this report. However, since visual inspection is not fully reliable and the interpretation of the acoustic impact tests required some judgment, it was difficult to decide how many sections of the ring stiffeners should be rebonded. For this reason, and because the adopted repair procedure was fairly straight forward, it was decided (in consultation with Bell Aerosystems) to rebond all four ring stiffeners over their entire length. This task was accomplished by draping fiberglass shear clips over the ring stiffeners in the areas between the stringers.

The shear clips consisted of 4-inches long glass cloth (Style 181) strips cut on a 45° bias and impregnated with Scotch-Weld 2216/gray adhesive. The width of the glass cloth strips was designed to cover the entire skin area between stringers and varied for each ring stiffener. The widths used for the smallest through the largest diameter ring stiffeners were 0.85 inch, 0.95 inch, 0.105 inch, and 0.115 inch, respectively. The adhesive impregnated shear clip was draped over and extended for 3/4 inch on both sides of the ring stiffeners. The adhesive was cured for at least 18 hours at 12-14 psi. The bonding pressure was obtained by placing the component in a vac-bag.

Uniformity of bonding pressure over the shear clip surface was assured by using a formed silicone rubber pad. This pad fitted tightly over the adhesive impregnated glass cloth strip and two strips of porous Teflon coated glass cloth which absorbed the excess adhesive. A spring steel clip was placed over the silicone rubber pad which prevented the pad from spreading when pressure was applied by the vac-bag. The vac-bag was prevented from applying pressure to the stringers by placing a conical shaped sheet metal ring between the ring stiffeners. Wooden blocks placed between alternate stringers supported the sheet metal ring. Because of the limited working life of the adhesive, only one quadrant of the ring stiffeners could be rebonded in a single operation; thus, four separate operations were required to bond all shear clips to the ring stiffeners.

3. Repair of Fuselage Skin

The original visual inspection (Section VI of this report) had revealed nine craze cracks in the outer surface of the skin of the fuselage component. In the intervening period during which repair procedures were established (from January to June 1969), some of these craze cracks had grown in length, and eight additional crazings had developed, indicating residual stresses in the skin.

Although the cracks appeared to be in the resin only (with no evidence of broken fibers), caution dictated that the cracks be repaired by an overlay of fiberglass cloth. Accordingly, patches of glass cloth (Style 181), extending approximately one inch beyond the visible ends of the cracks, were adhesively bonded to the skin with Scotch-Weld 2216/gray adhesive. These patches were bonded at the same time the shear clips were applied to the ring stiffeners and pressure cured during the vacuum bagging operation. Seventeen areas of the fuselage skin, ranging in size from 2 x 3 inches to 4 x 6 inches, were covered with fiberglass in this manner.

4. Nondestructive Inspective

On completion of the repair work, the component was given a careful visual inspection and no further discrepancies were observed. In addition, each and every stringer was checked over its entire length for complete rebonding using both ultrasonic and the helium leak detector methods; both tests confirmed that repair was successfully accomplished. After delivery of the repaired component to Bell, another visual inspection and ultrasonic spot-checks on some stringer flanges confirmed that the component was ready for testing.

5. Weight Analysis of Repaired Component

The weight increase resulting from the various items added to the fuselage are as follows:

Component weight before repair	60.13 lbs
Weight increase from rebonding stringers	1.96 lbs
Weight increase from skin patches, shear, and metal clips	0.68 lbs
Total weight after repair	62.77 lbs
Total weight increase due to repair procedure	2.64 lbs

SECTION IX

FUSELAGE COMPONENT TEST PLAN

This report section presents the revised shell loads based on the material change from untreated "Thornel" 40 to treated "Thornel" 50 fiber, the instrumentation plan for the component, and describes fixturing and test preparations.

A. Revised Shell Loads

(R.A. Elkin and D.P. Hanley, Bell Aerosystems)

As given in the Third Annual Report ([3]), the material from which the fuselage component is to be fabricated has been changed from untreated "Thornel" 40 to treated "Thornel" 50. This change has necessitated a modification of the fuselage component test plan loads reported in Section IX.L of Reference 3. The revised loading plan is shown in Table XXXVII.

At the loads shown for Response Test 1, the maximum bending and shear stresses in the component will be equal to 1/2 the limit stresses for bending and shear. For Test 2, the shear stress will equal 1/2 limit shear. At the loads shown for Test 3 the shear stress will equal 1/2 limit shear and the bending stress will be 10 times the shear stress. This bending stress is ~ 1/3 the limit bending stress. The local frame loading test, No. 4, will result in the frame bending stress equal to 1/2 limit; the 80 lb load given in Table XXXVII for this condition is labeled 'tentative' since this was the load previously calculated for the "Thornel" 40 component. For the destruct test, No. 5, the ultimate stresses in bending and shear should occur almost simultaneously.

The ultimate, yield, and limit loads for the component in tension, compression, shear, and bending are shown in Table XXXVIII. These values are based upon tests of treated "Thornel" 50 stiffened panels. Limit loads have been taken as the lesser of yield or 2/3 ultimate.

B. Instrumentation Plan

(S.L. Cross and K.H. Sayers, Bell Aerosystems)

The instrumentation plan for the fuselage component has been defined. The planned mounting locations of strain gages are given in Figure 49 (Bell Drawing No. 8506-150014). A total of 60 channels will be required. These channels will be fed into the Beckman Data Recording System. Dial gages will also be employed. The strain gages are functionally grouped as given in

TABLE XXXVII

PLANNED LOADING SEQUENCE AND TEST ARRANGEMENT

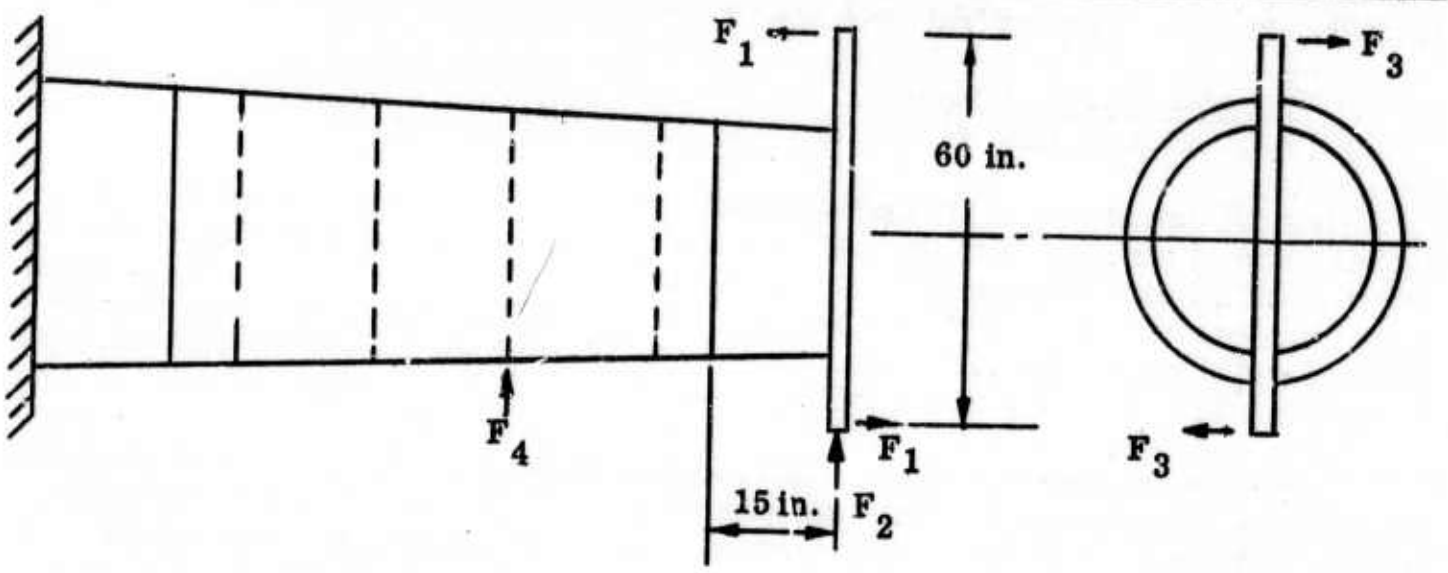

Response Tests	Load, pounds			
	F_1	F_2	F_3	F_4
1. Bending + Shear	4560	2080	—	—
2. Torsion	—	—	710	—
3. Bending + Torsion	2250	—	470	—
4. Local Frame	—	—	—	80 (tent)
Destruct Test				
5. Bending + Shear	6840	13400	—	—

TABLE XXXVIII

ULTIMATE, YIELD, AND LIMIT ALLOWABLES
FOR FUSELAGE COMPONENT (lb/in.)

	Tension	Bending	Compression	Shear
Ultimate	2710 →	2710	3070	416
Yield	2710	2250 ←	2250	129
Limit	1810 →	1810	2050	139

the table above Detail E (Zone A-7) in Figure 49. Gages have been specified as Micro-Measurements Types EA-13-187BB-120 (single elements) and EA-13-250-RA-120 (rosettes). These gages were selected on the basis of past experience and compatibility with the recording system.

C. Fixturing and Test Preparations
(S.L. Cross, Bell Aerosystems)

Fabrication and assembly of support hardware required for mounting the fuselage component have been initiated. Load cylinders have been selected to satisfy the planned response and destruct tests.

Figures 50 (a) and (b) show the general test arrangement. Safety factors in excess of 5.0 have been used in designing the support structure to provide maximum safety and minimum hardware deflection.

A detailed structural test program plan for testing the fuselage component has been outlined and has been reviewed with the Air Force Program Monitor and the Association Program Management.

The test plan document is being finalized and includes pretest preparations, general test arrangement and description, instrumentation, specific test procedures, and special instructions concerning handling, photography, critical gage monitoring and premature failure repair procedures. The pretest preparations involve end ring drilling, instrumentation, and assembly in the test fixture. The general test arrangement treats the overall structural support hardware and dead-weight counterbalance system. Specific test procedures define requirements for completing the response tests and the destruct test along with loading rates and data recording hold times. Delivery of the repaired component to Bell is scheduled for mid-1969.

TABLE SHOWING TYPICAL FRAME

JOINT LOCATION FROM STIFFENER #1	MATERIAL	ANGLE	FRAME #1 R DIA.	FR
J	BALSA	23° 13' 32"	23.500	2
K	BALSA	11° 36' 46"		
L	THORNEL	23° 13' 32"		
M	THORNEL	34° 50' 18"		
N	THORNEL	23° 13' 32"		
O	THORNEL	34° 50' 18"		

TABLE SHOWING FR

FRAME NO.	R DIA	R
1	23.480	2
2	22.480	2
3	21.480	2
4	20.480	2

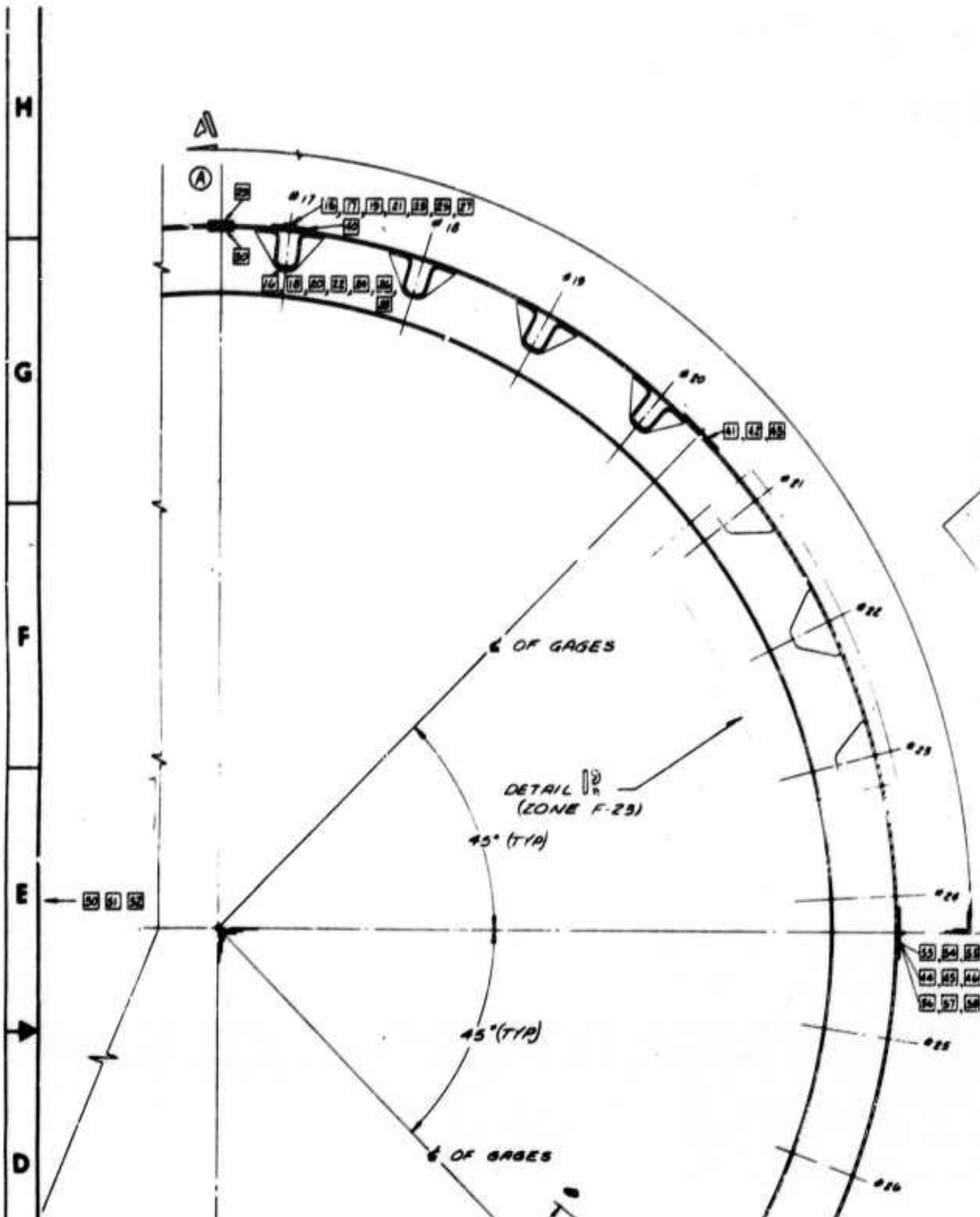

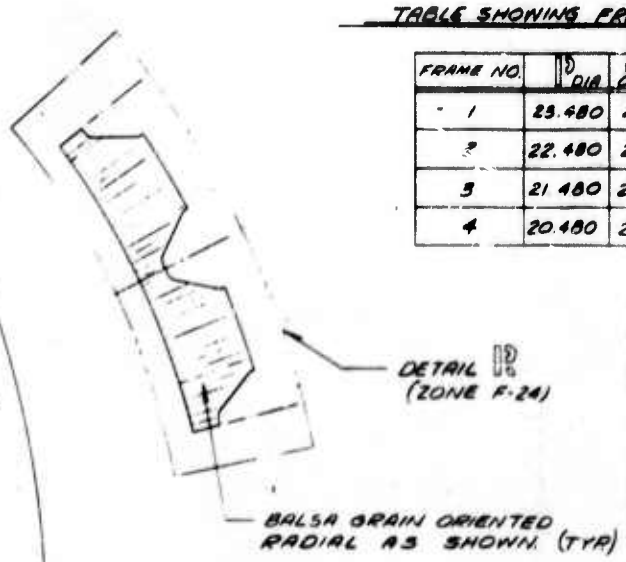

④ 31 REQ'D. EQUALLY SPACED ALONG ENTIRE CIRCUMFERENCE

THESE VIEWS TO SHOW JOINT LOCATION ONLY. (ALL JOINTS TO BE FILLED WITH RESIN).

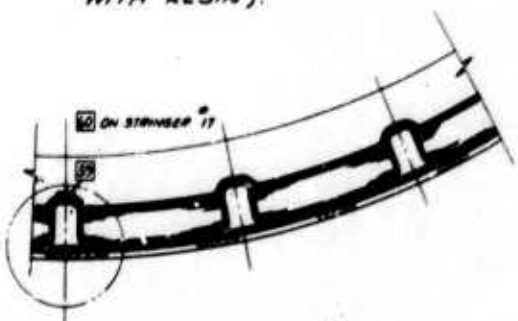

SECTION 13-13

SECTION C-C

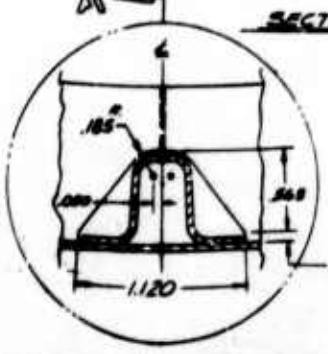

TYP BALSA & SHEAR TIE CUTOUT

.125 x 45° CHAMFER (TYP)

AREA BETWEEN STRINGER & F.G. BUILD-UP TO BE FILLED WITH RESIN PRIOR TO BEING CAPPED WITH AN .010 F.G. LAYUP.

TYPICAL FRAME CONSTRUCTION

ANGLE	FRAME #1 ℄ DIA.	FRAME #2 ℄ DIA.	FRAME #3 ℄ DIA.	FRAME #4 ℄ DIA.	NO. REQ'D.
23°13'32"	23.500	22.500	21.500	20.500	15
°36'46"					1
3°13'32"					14
4°50'18"					1
8°13'32"					14
°50'18"					1

LE SHOWING FRAME DIAMETERS

FRAME NO.	ID DIA	℄ DIA. OF FRAME	OD DIA
1	23.480	23.500	23.520
2	22.480	22.500	22.520
3	21.480	21.500	21.520
4	20.480	20.500	20.520

TAIL ⓓ
ONE F-24)

ORIENTED
SHOWN. (TYP.)

VIEW ⓒ →
(SEE SHEET #2)

℄ SHELL

ALLY
F"RENCE

O

TWEEN STRINGER
WLOUP TO BE
ITH RESIN
D BEING
WITH AN
LAYUP.

Ⓕ SHOWING TYP. ROLL PIN INSTALLATION.

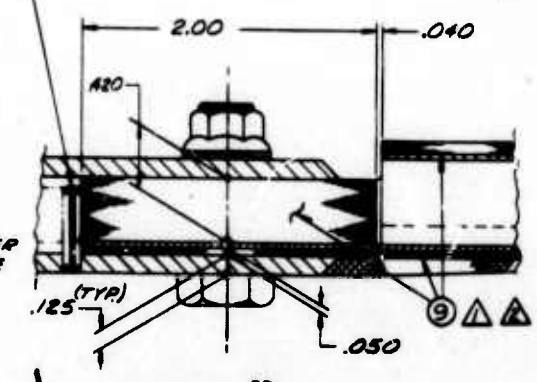

DETAIL ⓓ

B

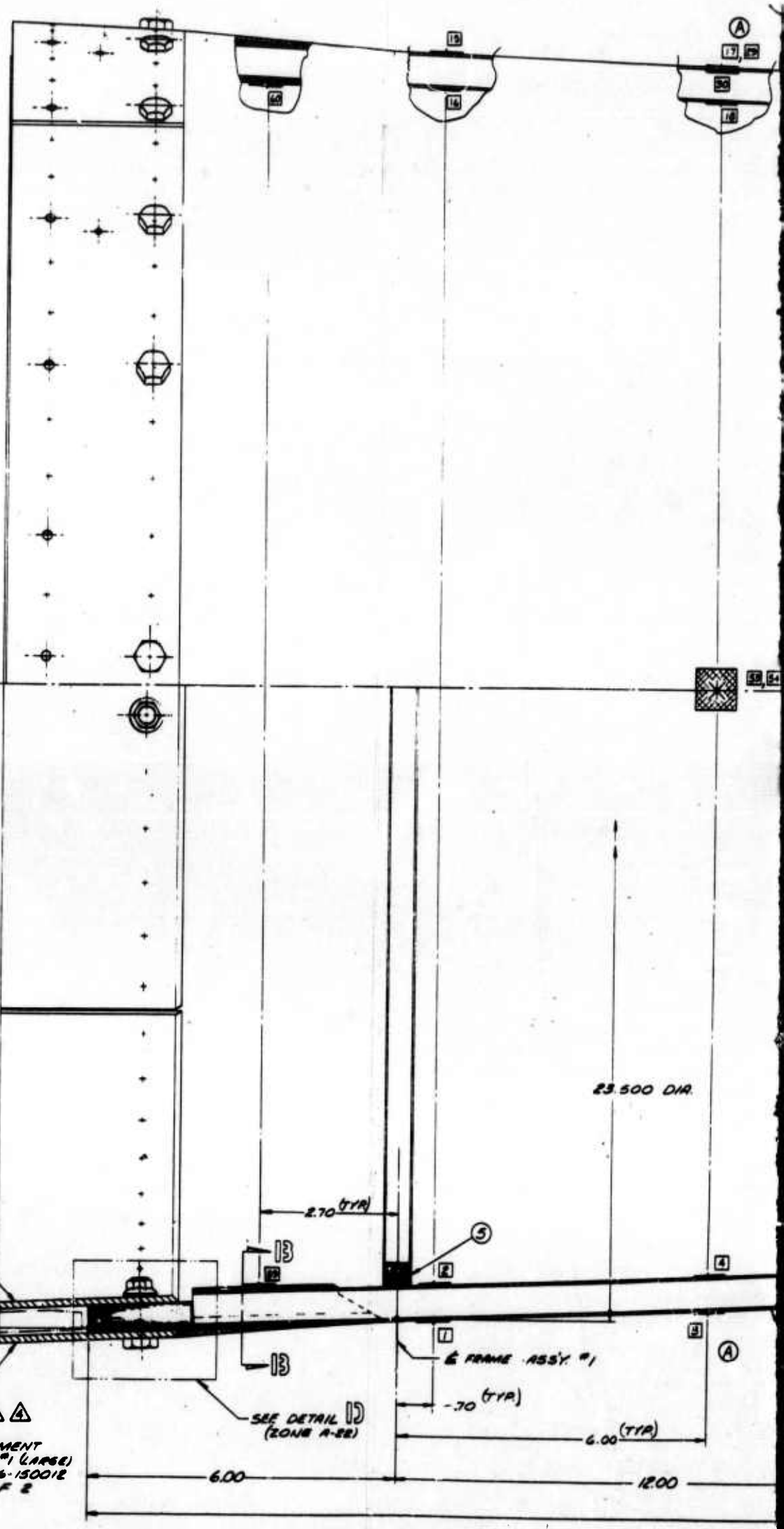

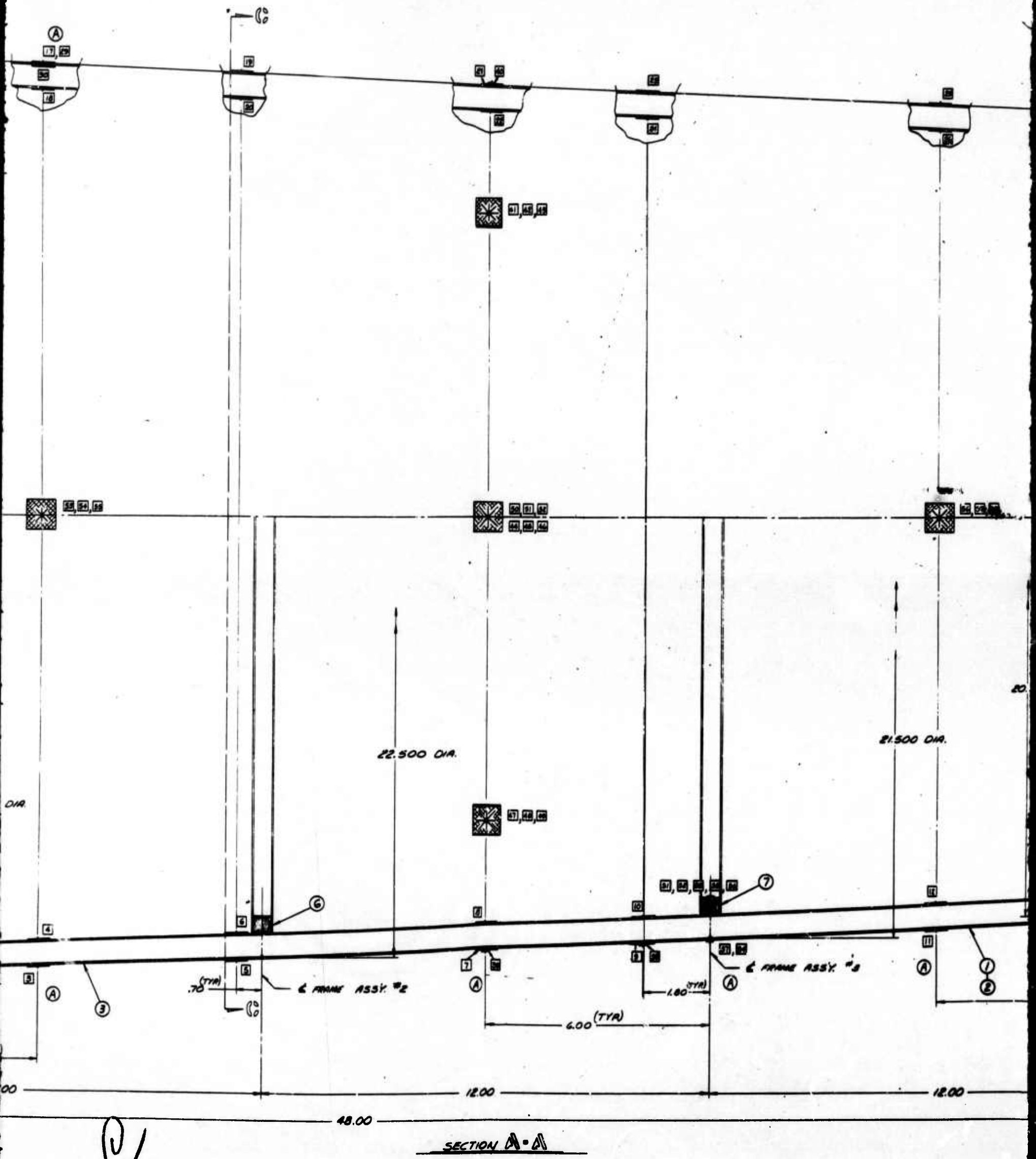
22.500 DIA.
21.500 DIA.
DIA.
6 FRAME ASSY. #2
6 FRAME ASSY. #3
.70 (TYP)
1.80 (TYP)
6.00 (TYP)
12.00
12.00
48.00

SECTION A-A

SEE DETAIL (ZONE A-7)

(REF) END ATTACHMENT FIXTURE NO. #2 (SMALL) DWG. E-8506-150012 SHEET 2 OF 2

← VIEW H (SEE SHEET #2)

20.500 DIA.

20.00 DIA. (INSIDE SHELL)

6.00 (TYP)

6 FRAME ASS'Y. #4

.10 (TYP)

4.5

.448

30°

1.04

.030 (TYP)

.040

.04

.28

.56

5.68 (TOTAL WID

6.00 (REF.)

DTO CONSTANT

DETAIL E 8 X SIZE (ZONE G-

TABLE SH
VARIOUS TH
FIBER ORIEN

ELEMENT	NUMBER OF LAY
SHELL	4
STRINGERS	4
FRAME (CAP)	4
FRAME (SIDE PANELS)	3

● 0° IS ALONG

■ 0° IS ALONG CIRCUMFER

TABL
INSTRU
& AXIS

GAGES
56°1 THRU 56°28
56°29 THRU 56°30
56°31 THRU 56°37
56°38 THRU 56°40
56°41 THRU 56°58
56°59 & 56°60

TABLE SHOWING VARIOUS THORIEL 50 FIBER ORIENTATION

ELEMENT	NUMBER OF LAYERS	AVERAGE FIBER ORIENTATION	
SHELL	4	90°, +15°, -15°, 90°	●
STRINGERS	4	+10°, -10°, -10°, +10°	●
FRAME (CAP)	4	0°	■
FRAME (SIDE PANELS)	3	0°, +45°, -45°	■

● 0° IS ALONG SHELL Ē

■ 0° IS ALONG SHELL CIRCUMFERENTIAL DIRECTION.

TABLE SHOWING INSTRUMENTATION FUNCTION & AXIS OF ORIENTATION

GAGES	ORIENTATION	GAGE FUNCTION
56"1 THRU 56"28	LONGITUDINAL	STRINGER BENDING
56"29 THRU 56"30	LONGITUDINAL	SKIN BUCKLING
56"31 THRU 56"37	CIRCUMFERENTIAL	FRAME STRAINS
56"38 THRU 56"40	CIRCUMFERENTIAL	SKIN STRAINS
56"41 THRU 56"58	BIAXIAL PLUS SHEAR	SKIN STRAIN COMPONENTS
56"59 & 56"60	LONGITUDINAL	FIBERGLASS LOAD TRANSFER

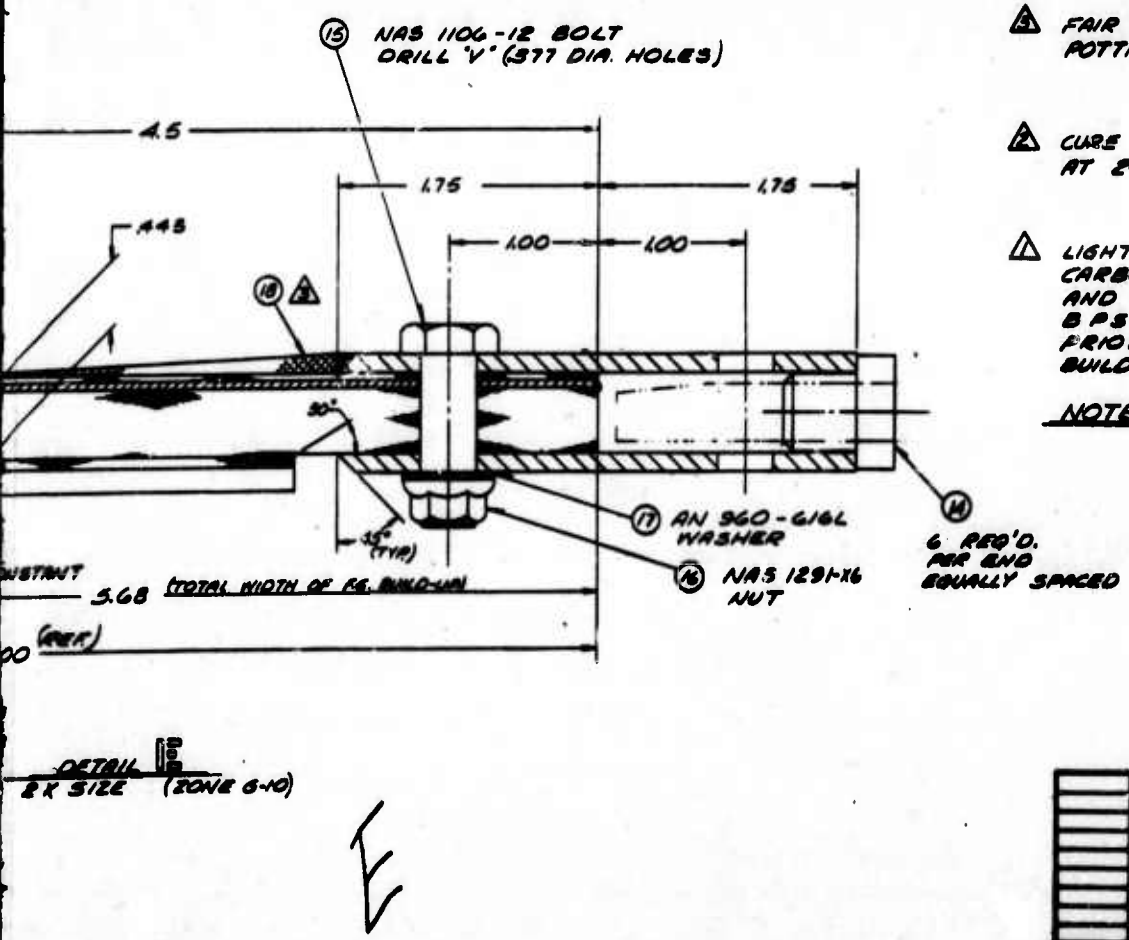

DETAIL E
2X SIZE (ZONE G-10)

(5) DRAPE .070 FIBERGLASS BUILD-UP PLIES - ONE LAYER AT A TIME.

(4) BOND ON ALUM. PLATES WITH EC 2216

(3) FAIR WITH ROOM TEMPERATURE CURING POTTING COMPOUND AFTER ASSEMBLY.

(2) CURE IN PLACE FOR 120 ± 5 MINUTES AT 245 ± 10°F AND 40 P.S.I.

(1) LIGHTLY SAND (300 GRIT) AND DEGREASE CARBON LAMINATE WITH MEK. AND CLEAN AND ACID ETCH ALUMINUM PLATES PER BPS FW 4852, REV D, METHOD II PRIOR TO BONDING TO FIBERGLASS BUILDUP.

NOTES:

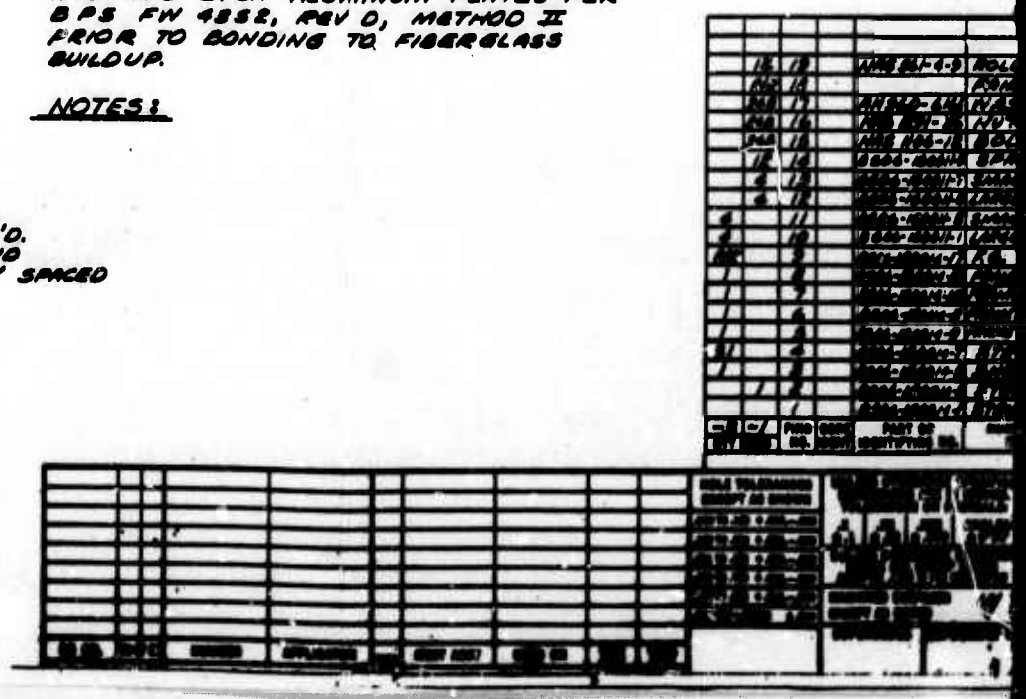

	A	STRAIN GAGES #29 THRU #34 RELOCATED		

H G F E D C B A

5 DRAPE .070 FIBERGLASS BUILD-UP PLIES - ONE LAYER AT A TIME.

4 BOND ON ALUM. PLATES WITH EC 2216

3 FAIR WITH ROOM TEMPERATURE CURING POTTING COMPOUND AFTER ASSEMBLY.

2 CURE IN PLACE FOR 180 ± 5 MINUTES AT 245 ± 10°F AND 40 P.S.I.

1 LIGHTLY SAND (300 GRIT) AND DEGREASE CARBON LAMINATE WITH MEK. AND CLEAN AND ACID ETCH ALUMINUM PLATES PER BPS FN 4852, REV D, METHOD II PRIOR TO BONDING TO FIBERGLASS BUILDUP.

NOTES:

M 6 REQ'D. PER END EQUALLY SPACED

Figure 49.

F

-139-

Shell Instrumentation Locations

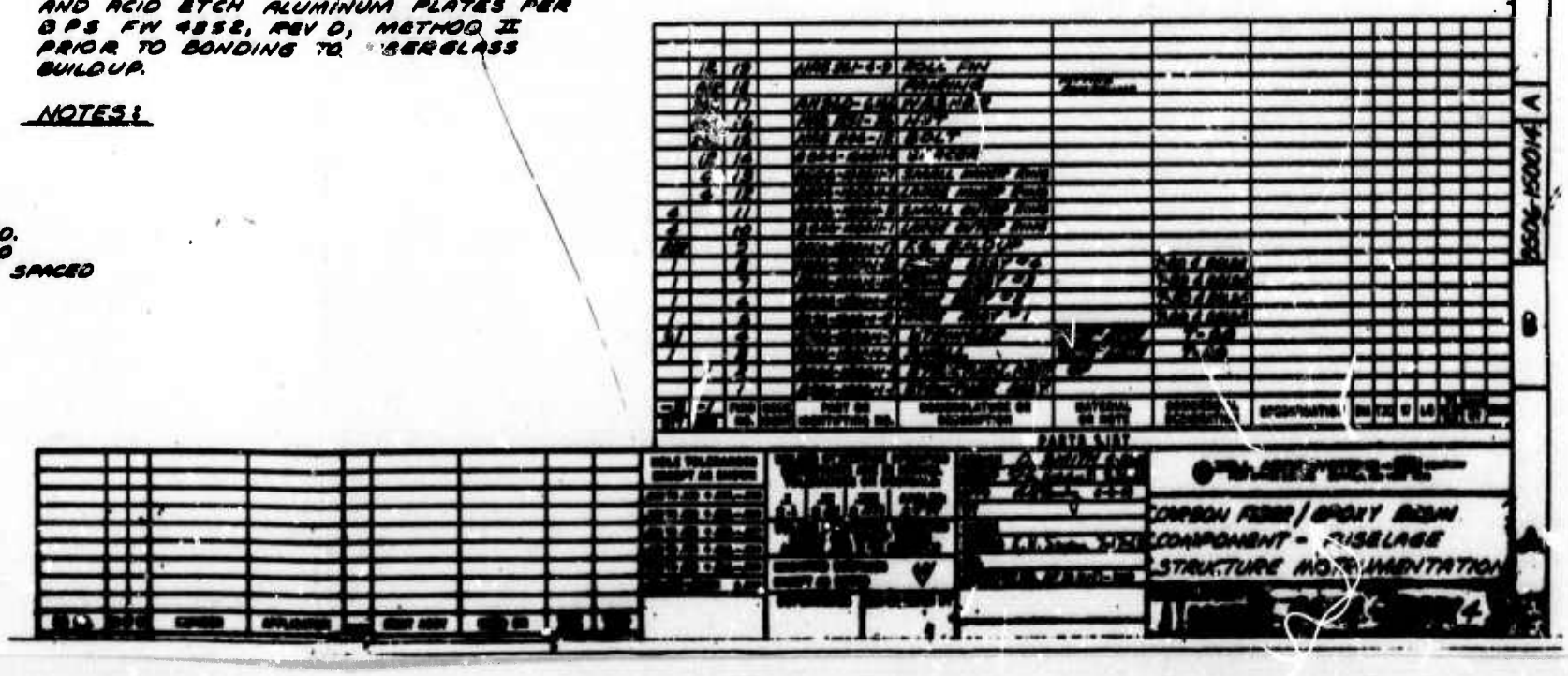

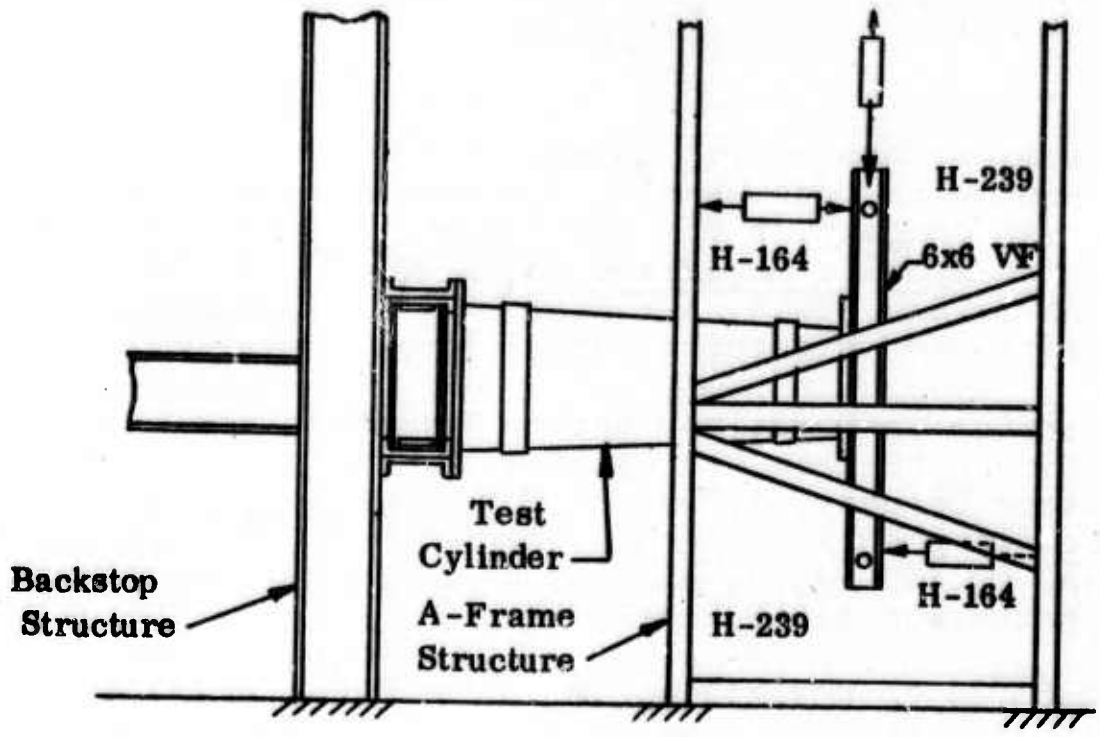

Figure 50(a). Side View Horizontal Test Setup

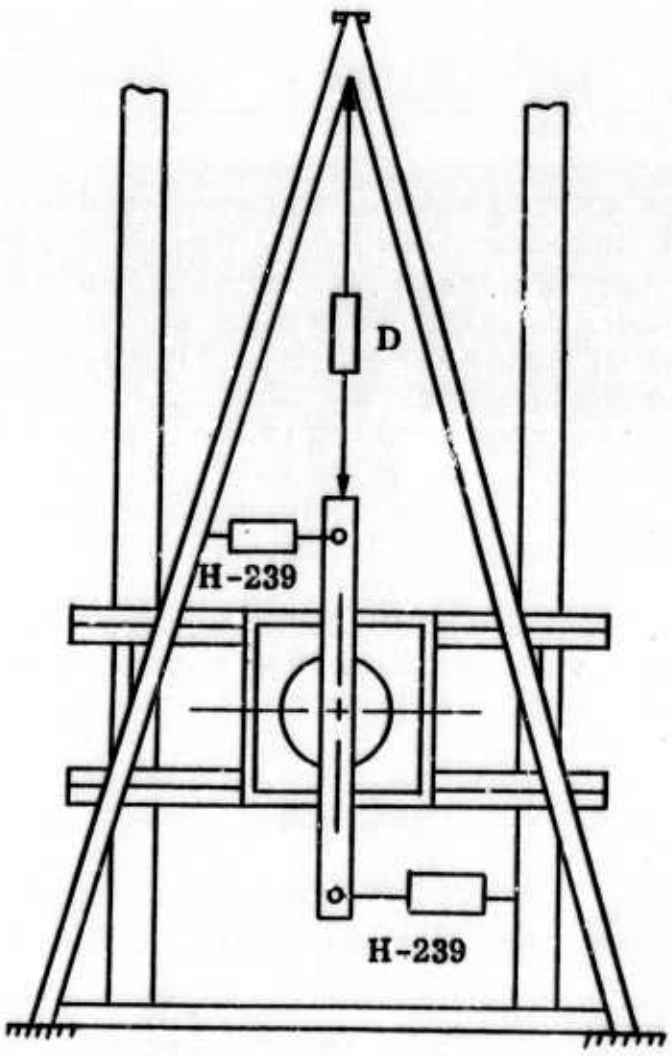

Figure 50 (b). Front View Horizontal Test Setup

REFERENCES

1. Union Carbide Corporation, Carbon Products Division, in Association with Case Western Reserve University and Bell Aerosystems Company, a Textron Company, Integrated Research on Carbon Composite Materials, AFML-TR-66-310 Part I (October 1966) (AF 33(615)-3110, Air Force Materials Laboratory, Wright-Patterson Air Force Base, Ohio).

2. Union Carbide Corporation, Carbon Products Division, in Association with Case Western Reserve University and Bell Aerosystems Company, a Textron Company, Integrated Research on Carbon Composite Materials, AFML-TR-66-310 Part II (December 1967) (AF 33(615)-3110, Air Force Materials Laboratory, Wright-Patterson Air Force Base, Ohio).

3. Union Carbide Corporation, Carbon Products Division, in Association with Case Western Reserve University and Bell Aerosystems Company, a Textron Company, Integrated Research on Carbon Composite Materials, AFML-TR-66-310 Part III (January 1969) (AF 33(615)-3110, Air Force Materials Laboratory, Wright-Patterson Air Force Base, Ohio).

4. D. L. Block, Influence of Ring Stiffeners on Instability or Orthotropic Cylinders in Axial Compression, NASA TN-D-2482, (October 1964).

5. Union Carbide Corporation, Carbon Products Division: Technical Information Bulletin No. 465-209-BI, "A Strand Test Method for Determining Tensile Strength and Young's Modulus of High Modulus Graphite Fibers"; Technical Information Bulletin No. 465-210-BI, "Determining the Density of Carbon and Graphite Yarn by Liquid Displacement"; and Technical Information Bulletin No. 465-208-BI, "Torsional Shear Test Method". Available from Union Carbide Corporation, Carbon Products Division, Advanced Materials Department, 270 Park Avenue, New York, New York 10017.

6. R. Schroeer, "Research on Exploratory Development of Nondestructive Methods for Crack Detection," AFML-TR-67-867, Part I, August 1967; and Part II, November 1968.

7. O. Ljungstrom, "Bonded Aircraft Structures," Aero Research Conference, Duxford, Cambridge, 1957; CIBA(ARL), Duxford.

8. R. E. Wittman, "Effect of Rate Loading on Shear Strength of Adhesive Bonded Lap Joints," WADC Tech. Report 54-153, December 1954.

9. R. Braune, et.al., "Effects of Rate of Loading on Shear Stress of Resin Adhesives, SPE Journal, Volume 16, May 1960.

UNCLASSIFIED

Security Classification

DOCUMENT CONTROL DATA - R & D

(Security classification of title, body of abstract and indexing annotation must be entered when the overall report is classified)

1. ORIGINATING ACTIVITY (Corporate author)

Union Carbide Corporation
Case Western Reserve University
Bell Aerosystems Company

2a. REPORT SECURITY CLASSIFICATION

Unclassified

2b. GROUP

3. REPORT TITLE

INTEGRATED RESEARCH ON CARBON COMPOSITE MATERIALS, Part IV
Volume III-Structural Component Development

4. DESCRIPTIVE NOTES (Type of report and inclusive dates)

Summary Technical Report July 1968 to June 1969

5. AUTHOR(S) (First name, middle initial, last name)

Union Carbide Corporation, Carbon Products Division, in Association with Case Western Reserve University and Bell Aerosystems Company, a Textron Company

6. REPORT DATE	7a. TOTAL NO. OF PAGES	7b. NO. OF REFS
July 1970	142	9

8a. CONTRACT OR GRANT NO.	9a. ORIGINATOR'S REPORT NUMBER(S)
AF 33(615)-3110	
b. PROJECT NO. ARPA Order No. 719	
c. Program Code 5D10	9b. OTHER REPORT NO(S) (Any other numbers that may be assigned this report) AFML-TR-66-310, Part IV, Volume III
d.	

10. DISTRIBUTION STATEMENT This document is subject to special export controls and each transmittal to foreign governments or foreign nationals may be made only with prior approval of the Nonmetallic Materials Division, MAN, Air Force Materials Laboratory, Wright-Patterson Air Force Base, Ohio 45433.

11. SUPPLEMENTARY NOTES	12. SPONSORING MILITARY ACTIVITY
	Air Force Materials Laboratory Wright-Patterson AFB, Ohio

13. ABSTRACT

The final design of the representative fuselage component was determined, and the component was fabricated with treated "Thornel" 50 graphite-fiber, ERL 2256 epoxy matrix composites. The structure consists of a tapered cylindrical skin, 48 inches long with end diameters of 24 inches and 20 inches; the fiber lay-up orientation of the skin is (90°, ±15°,90°). The skin is stiffened by 31 longitudinal stringers having (+10°,-10°,-10°,+10°) fiber orientation and by three segmented ring stiffeners consisting of a balsa wood core reinforced with panels of (0°,±45°) orientation. The fuselage component structure was analyzed by the discrete element method; stresses, displacements, and margin of safety predictions were obtained for various loading conditions. Prior to component fabrication, several treated "Thornel" 50 panels were fabricated and tested in tension and compression; failure levels were well above design requirements. The 90° layers of the skin were constructed by wet-winding and the inner 15° layers by hand lay-up of pre-pregged sheet. The stringers and the ring stiffener panels were molded from pre-pregged sheet. Stringers and the ring stiffener panels were adhesively bonded to the component skin. Both ends of the component were reinforced with a lay-up of fiberglass tape and bonded to segmented aluminum rings for attachment of the component to the test stand. The NDT inspection of the component revealed defects consisting primarily of partial debonding of the stringers and ring-stiffeners from the skin. Extensive analysis indicated that the debonding very likely resulted from thermal degradation of the adhesive and from thermal stresses incurred during the final cure of the end attachments Novel repair techniques for composite structures were established, and the component was successfully repaired. Detailed plans for the various response tests and the final destruct test of the component are also presented.

DD FORM 1 NOV 68 1473 (PAGE 1)

S/N 0101-807-6811

Unclassified

Security Classification

A-31408

14. KEY WORDS	LINK A		LINK B		LINK C	
	ROLE	WT	ROLE	WT	ROLE	WT
Carbon						
Graphite						
Fibers						
Graphite Fibers						
Composites						
Plastic Matrix						
Metal Matrix						
Properties						
Analysis						
Synthesis						
Mechanical Properties						